ABSTRACT

Title of Dissertation:	ELECTROCHEMICAL PROTECTION OF LITHIUM METAL ANODE IN LITHIUM-SULFUR BATTERIES AND BEYOND
	Yang Wang, Doctor of Philosophy, 2020
Dissertation directed by:	Professor Sang Bok Lee, Department of Chemistry and Biochemistry

With the growing demand of advanced energy storage devices that have high energy density and high power density to power electric vehicles and electrical grid, scientists and engineers are exploring technologies beyond conventional Li-ion batteries which have transformed the industry in the past thirty years. Li-S batteries have much higher energy density than Li-ion batteries and are gaining momentum. However, the intrinsic issues of Li-S batteries require a comprehensive systematic study of the protection of Li metal anodes to put them into practical applications. In the first study of this dissertation, we investigated using conventional electrolyte of Li-S batteries that includes 1,3-dioxolane to electrochemically pretreat Li metal anodes. We concluded that the electrochemical pretreatment of Li metal anodes generated an organic-inorganic artificial solid electrolyte interface (ASEI) layer that greatly enhanced the battery performance of the Li-S batteries. The properties of this ASEI can be tuned by

manipulating the current density and cycle number of the electrochemical pretreatment. In the second study, we studied the comprehensive development and surface protection of $Li_{10}GeP_2S_{12}$ (LGPS) material as solid-state electrolyte, which has ionic conductivity comparable to liquid electrolytes, potentially for solid-state Li-S batteries. Lithium phosphorus oxynitride (LiPON) was coated onto LGPS pellets by atomic layer deposition (ALD). It demonstrated great compatibility with LGPS and extends the electrochemical stability window. The third study explored the potential of transferring this electrochemical pretreatment method to the protection of other metal anodes, particularly Mg. The study discovered the surprising catalytic capability of Mg^{2+} in the polymerization of solvent 1,3-dioxolane (DOL). A layer with poly-DOL component was also found to grow on the surface of Mg metal anodes as a result of the electrochemical pretreatment, and the overpotential of Mg-Mg symmetric cells cycling dropped with the growth of the layer. Future studies are required to test the effectiveness of this method in Mg batteries. Overall, these studies can help to understand the surface chemistry of the electrochemically pretreated Li metal anodes, provide guidelines on the improvement of Li-S batteries and contribute to the development of solid-state Li-S batteries and multivalent metal anode batteries.

ELECTROCHEMICAL PROTECTION OF LITHIUM METAL ANODE IN LITHIUM-SULFUR BATTERIES AND BEYOND

by

Yang Wang

Dissertation submitted to the Faculty of the Graduate School of the
University of Maryland, College Park, in partial fulfillment
of the requirements for the degree of
Doctor of Philosophy
2020

Advisory Committee:

Professor Sang Bok Lee, Chair
Professor Neil Blough
Professor John Cumings
Professor Efrain Rodriguez
Professor Gary Rubloff

Dedication

I dedicate this to my parents, who have offered me unconditional love and support throughout the years.

Acknowledgements

I would like to thank my advisor Dr. Sang Bok Lee for his continuous guidance and support throughout my PhD study. He taught us the importance of dedication and self-motivation which are the reasons that I am here.

I would like to thank my past and current group members. Dr. Junkai Hu, Dr. Eleanor Gillette, Dr. Jaehee Song, Dr. Nikki Schneck, Dr. Nam Kim, Dr. Emily Sahadeo, Hakeem Henry, Darrin Liau, Jisoo Shin, Brandon Johnston, Shoukang Hong and George Caceres. Special thanks to Emily who joined the group with me together and went through everything in graduate school, whom I have collaborated and coauthored on several projects, and not to say her help on editing and revising all the manuscripts throughout the years. Special thanks to Nam who is the first mentor after I joined the group, who has shouldered the responsibilities as the most senior grad student in the group since his 3rd year and offered all kinds of helps and advice throughout the years.

I would like to thank Dr. Rubloff and everyone in his group who have been collaborating closely with our group for all the comments, recommendations and opportunities given over the years. I would like to thank Dr. Keith Gregorczyk, Dr. Alex Kozen, Dr. Chuan-Fu Lin, Dr. Malachi Noked, Dr. Marshall Schroeder, Dr. Alex Pearse, Dr. Chanyuan Liu, Dr. Davey Stuart, Dr. Angelique Jarry, Emily Hitz, Blake Nuwayhid, Haotian Wang, Victoria Ferrari and Sam Klueter. Special thanks to Dr. Alex Kozen, Dr. Chuan-Fu Lin, Dr. Malachi Noked and Dr. Marshall Schroeder, who have been my mentors, coworkers and friends and whom I collaborated with over the years. The help they provided and the influence they had over me are beyond research.

I would like to thank John Hoerauf of University of Maryland and Binh Hoang of

Catholic University of America for the time and effort they have put into our collaborations.

I would also like to thank my committee members, Dr. Sang Bok Lee, Dr. Gary Rubloff, Dr. Efrain Rodriguez, Dr. Neil Blough, and Dr. John Cumings for their time and considerations to be part of my dissertation defense.

I would like to thank Prof. Natalia White at the Department of Chemistry & Biochemistry, who has been the instructor of all my TA assignments over the years. It was a real pleasure and honor to work with her and I am beyond grateful for her support and help to me.

I would like to thank the UMD Nanocenter and the staff members at Fablab, AIMLab and SAC, John Abrahams, Mark Lecates, Dr. Jiancun Rao, Dr. Sz-Chian Liou, Dr. Wen-An Chiou, Dr. Elizabeth Lathrop and Dr. Karen Gaskell, as well as director of Mass Spectroscopy Facility Dr. Yue Li who gave me tremendous help and assistance to my research.

Table of Contents

This Table of Contents is automatically generated by MS Word, linked to the Heading formats used within the Chapter text.

List of Tables

List of Figures

List of Abbreviations

ACC – Activated Carbon Cloth

ALD – Atomic Layer Deposition

ASEI – Artificial Solid Electrolyte Interphase

CE – Coulombic Efficiency

CPE – Constant Phase Element

CV – Cyclic Voltammetry

DME – 1,2-Dimethoxyethane

DOL – 1,3-Dioxolane

EDS – Energy Dispersive X-ray Spectroscopy

EIS – Electrochemical Impedance Spectroscopy

FIB – Focused Ion Beam

FWHM - Full Width at Half Maximum

HVC – High Voltage Cathode

LiOtBu – Lithium tert-butoxide

LPE – Lithium Protected by Elastomer

LiPON – Lithium Phosphorus Oxynitride

LiTFSI – Lithium bis(trifluoromethanesulfonyl)imide

LGPS – $Li_{10}GeP_2S_{12}$

MALDI – Matrix-Assisted Laser Desorption/Ionization

Mg(TFSI)2 – Magnesium bis(trifluoromethanesulfonyl)imide

MS – Mass Spectroscopy

MIEC – Mixed Ion-Electron Conductors

NaSICON – Sodium Super Ionic Conductor

PC – Propylene Carbonate

PDMS – Polydimethylsiloxane

PEO – Polyethylene Oxide

PFA – Perfluoroalkoxy Alkane

PVDF-HFP – Poly(vinylidene fluoride-co-hexafluoropropylene)

RH – Relative Humidity

SCCM – Standard Cubic Centimeters Per Minute

SEI – Solid Electrolyte Interphase

SEM – Scanning Electron Microscopy

SSE – Solid-State Electrolyte

TEGDME – Tetraethylene Glycol Dimethyl Ether

TMP – Trimethylphosphate

TOF – Time of Flight

UHV – Ultrahigh Vacuum

XPS – X-ray Photoelectron Spectroscopy

1. Li-S Batteries: Technology beyond Li-ion Batteries

Some content discussed in this chapter has been published on Journal of Materials Science, 2019, 54, 3671–3693 and ACS Applied Materials & Interfaces, 2018, 10, 29, 24554-24563. Dr. Emily Sahadeo contributed to the writing of introduction of Mg anode protection.

1.1 Background

With the depletion of fossil fuels and the increasingly dire situation with regard to air pollution and climate change, academia, industries and governments have been searching for renewable energy sources to match up to the world's growing demand of energy. Designing and developing energy storage devices that have high energy density, power density, long lifespan and safety is one of the most crucial missions to accomplish the goal of powering through the 21st century.

In 1991, Sony Corp. commercialized the first lithium-ion (Li-ion) batteries by using graphite as anodes and the layered-structured $LiCoO_2$ cathodes discovered by Goodenough.[4, 6-9] It has since transformed the industries of energy storage devices and portable devices like electronics and small appliances thanks to its elimination of battery memory effect, long lifespan and large energy density than prior rechargeable batteries. As of today, Tesla, Inc. and other electric vehicle manufacturers are using lithium-manganese-cobalt-oxide (LiNMC) and $LiFePO_4$ (LFP) cathodes as part of the battery packs in their electric vehicles. However, even the state-of-the-art Li-ion batteries so far cannot deliver enough energy and power to approach those generated from combustion of gasoline and diesel in automobile markets.[7] Therefore, energy storage devices beyond Li-ion batteries are required.[7, 8]

1.2 Lithium-Sulfur (Li-S) Batteries

1.2.1 Mechanism of Energy Storage in Batteries

Electrochemical storage of energy involves the conversion of electrical energy to chemical energy or vice versa driven by electrochemical reactions in a battery when it is connected to an external circuit. A battery is made of three components, the cathode, the anode and the electrolyte. The electrolyte is a medium that allows the transport of ions but not electrons between the two electrodes. The cathode is where the reduction reaction happens, and the anode is where the oxidation reaction happens. Cathode and anode can switch when the battery is under charging or discharging status.[10, 11] In the example of a conventional Li-ion batteries, when the battery is being charged, the electrons go from positive to negative in the external circuit while Li^+ ions deintercalate and transport from $LiCoO_2$ electrode to graphite electrode, in which graphite is intercalated. When the battery is being discharged, Li^+ ions deintercalate and transport from graphite to $LiCoO_2$ and the electrons go from negative to positive in the external circuit which powers the electronic device it is connected to.[12] Generally, the discussion of cathodes and anodes is based on the discharging state of the batteries.

There generally are three basic metrics to evaluate the performance of a battery. One is energy density E, which is defined as the amount of energy a battery can hold. It is commonly shown in the form of gravimetric (Wh/g), volumetric (Wh/L) and areal (Wh cm^{-2}). It can be calculated as shown in Equation 1.1

$$E = C \times V$$

Equation 1.1

where C is the specific capacity of the cell and V is the potential of the cell. The potential of the cell is calculated as shown in Equation 1.2

$$V = V_c - V_a$$

Equation 1.2

where V_c is the voltage of the cathode and V_a is the voltage of the anode. The theoretical capacity of an electrode can be calculated as shown in Equation 1.3,

$$C = \frac{xF}{MW} = \frac{26800x}{MW} \quad mAh\ g^{-1}$$

Equation 1.3

where x is the number of electrons transferred during charging or discharging, F is the Faradic constant and MW is the molecular weight of the electrode material. The capacity of the cell is calculated as shown in Equation 1.4

$$^1/_C = {}^1/_{C_c} + {}^1/_{C_a}$$

Equation 1.4

where C_c is the specific capacity of cathode and C_a is the specific capacity of anode. It can be seen from Equation 1.4 that the electrode with the lowest specific capacity would restrict the ceiling of the specific capacity of the entire battery. Therefore, in order to increase the energy density of a full-cell battery, the specific capacities of both cathode and anode must be improved. Power density is defined as how fast a battery can discharge certain amount of energy or be charged back full at certain discharge and charge current densities. It is commonly shown in the form of gravimetric W/kg, volumetric W/L and aerial energy density Wh/cm^2. Lifespan is defined as the total amount of cycle numbers a battery can run before its capacity drops below an acceptable percentage of the initial capacity, usually

80%. All three metrics are very important to the practical application of the battery, but for most current battery materials, there has to be a trade-off. Depending on the applications of the batteries, certain metrics would be prioritized.[10, 11]

1.2.2 Principles of Lithium-Sulfur Batteries

One of the lithium-based battery systems that stands out and has great potential to be the next breakthrough after Li-ion batteries is Li-S batteries system. Li-S batteries use Li metal as anodes and elemental sulfur, which is usually incorporated with carbon materials, as cathodes. The sulfur cathode has a theoretical specific capacity of 1675 mA h g^{-1} and specific energy density of 2500 W h kg^{-1}.[4, 7, 9] Its specific capacity is around ten times larger than conventional cathodes of Li-ion batteries. Lithium metal, which has the highest specific capacity (3860 mA h g^{-1}) and lowest electrochemical potential (-3.04 V vs. SHE) among metal anodes,compared to 372 mA h g^{-1} for graphite anodes, is also regarded as the key to achieving high energy density energy storage.[4, 7, 9, 13] Sulfur also has the advantages of low-cost and high abundance.[4, 6, 14] However, the Li-S batteries system is facing its own issues with regard to intrinsic properties and practical applications and those challenges must be fully addressed before it can go into wider commercialization.

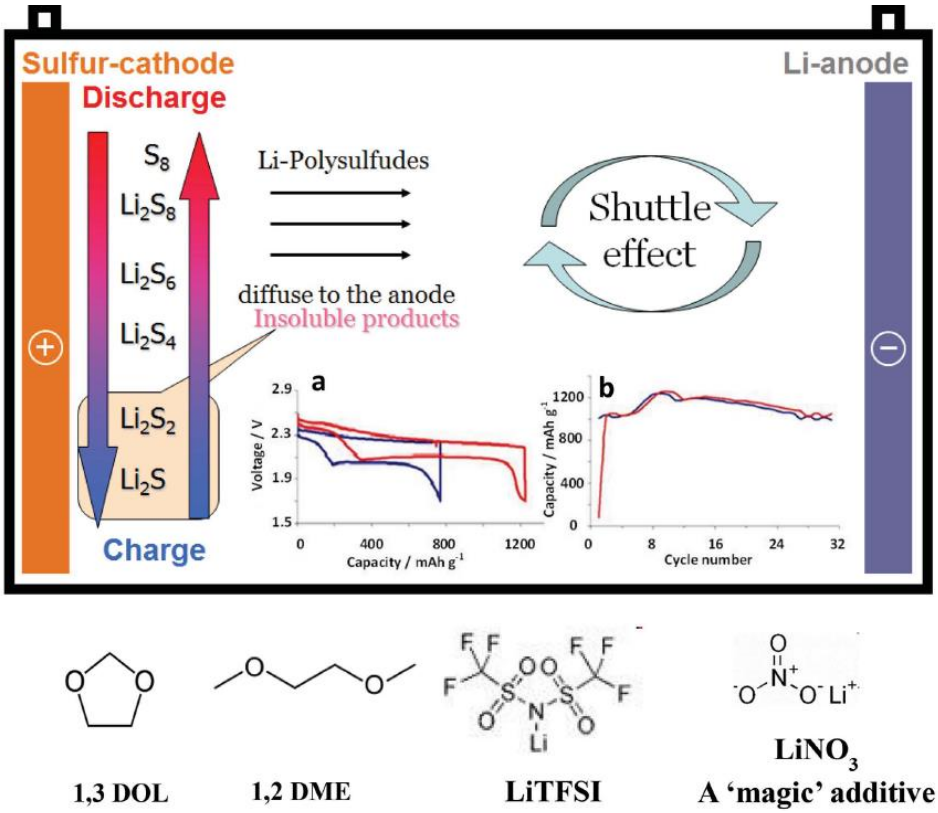

Figure 1-1 Electrochemistry and cycling results of a Li-S battery. **a)** Typical voltage profiles of Li–S cells measured in the DOL/DME (1:1 ratio) with 10 wt% LiTFSI electrolyte solution without $LiNO_3$ (blue curve) and with 2 wt% $LiNO_3$ (red curve) and **b)** charge-discharge capacity vs. cycle number measured in DOL/DME (1:1 ratio) with 10 wt% LiTFSI and 2 wt% $LiNO_3$. Reproduced with permission.[6]

Figure 1-1 demonstrates the basic electrochemistry of the Li-S batteries during electrochemical cycling. During the discharging process, S in the cathode, usually in the form of S_8, is reduced and dissolved into the electrolyte as long chain polysulfides S_6^{2-}.[6] The long chain polysulfides migrate to the Li metal anode side due to electrical fields and are further reduced to shorter chain polysulfides S_x^{2-} until they become final products Li_2S_2 and Li_2S which are insoluble. During the charging process, Li_2S_2 and Li_2S are re-oxidized to shorter chain polysulfides and diffuse back to the cathode side until they are fully oxidized back and redeposit in the form of elemental sulfur. The diffusion of polysulfides in between cathode and anode is called shuttle reactions or shuttle effect. The discharge

curve of Li-S batteries shows two distinct plateaus around 2.3 V and 2.1 V vs. Li^+/Li which correspond to the phase change of continuous reduction of polysulfides.[1, 6, 7, 14, 15]

The shuttle reactions result in multiple issues of Li-S batteries. The Li_2S_2 and Li_2S final products on the anode side are insoluble and ionically insulating which cannot be fully oxidized back to polysulfides.[4, 14] On one hand, this always leads to low Coulombic efficiency of the battery, which describes the ratio of total amount of charge released from a battery to the total amount of charge put in the battery, and continuous loss of active material on the cathode side.[4, 14] On the other hand, the generation of those sulfide products can consume Li metal and build up on its surface which eventually becomes a thick passivation layer that shuts down the reactions.[1, 15] The degradation of the anode due to shuttle reactions is usually severe.[6, 14]

In addition to shuttle reactions, S cathode and Li anode have their own issues. For S cathodes, one stiff challenge is that elemental sulfur is not electronically conductive. As a result, conductive materials such as carbon must be added to make C/S composite electrodes.[7, 14] Generally, it is preferred that the carbon material serving as substrate should be able to contain as much sulfur as possible but it is important to find the optimal sulfur loading since incorporating carbon materials means the active material loading would drop. But meanwhile, high sulfur loading would result in overall low electronic conductivity of the cathode and poor performance, even battery failure. The architecture of such composite electrode is also crucial because it needs to have a large surface area to allow as much contact as possible between S and the electrolyte and a large network to conduct electrons to as much S as possible. The carbon material used as substrate must also be mechanically robust due to the huge volume change results from the dissolution and deposition of sulfur

during discharging and charging processes respectively. The cathode often fails when the carbon structure breaks down[4, 6].

As for Li metal anodes, besides the unique challenges brought by shuttle reactions, the general issues of using a Li metal anode still persist. First, during electrochemical cycling, the stripping and plating of Li metal always leads to the formation of Li dendrites when the current density hits a threshold. Those dendrites not only can cause waste of Li metal anodes by creating "dead Li" which is electrochemically inactive, but also can pierce through separators and cause short-circuit of the cell which can lead to fire and other safety hazards. In addition, Li metal reacts with most organic solvents to generate solid electrolyte interface (SEI) layer on the surface, and the side reactions consume electrolytes which eventually decreases the lifespan of the batteries and lowers the Coulombic efficiency.[9, 13, 15] Last, the theoretically infinite volume change during the Li plating/stripping process further aggravates the interfacial instability and causes the failure of the anodes.[9, 13, 15] However, the reactions between Li metal and the electrolytes and the resulted the SEI layers can be tuned to optimize the performance of the batteries. Such Li metal anode protection strategy will be discussed in detail in the later chapters.

1.3 Enhancing the Li-S Batteries

1.3.1 The Electrolytes of Li-S Batteries and the Solid Electrolyte Interphase

The most fundamental work that has been done to enhance the performance of Li-S batteries is by optimizing the electrolytes. Electrolyte decomposes on the surface of Li metal and generate a layer called solid electrolyte interphase (SEI).[4, 16, 17] SEI has always

been a double-edged sword in battery systems. An optimal SEI layer can serve as a successful passivation layer to block further reaction between the electrolyte and the electrodes, most importantly the anode, while retaining good or acceptable ionic conductivity. A bad SEI, which is mostly the case, either completely passivates the surface and blocks the transport of ions or is unstable and the side reactions and growth of dendrites would continue or even be accelerated by the SEI. Modifying the electrolyte components can generate a stable passivation layer upon cycling, which can reduce further side reactions between electrolyte and the anode and also minimize the generation of electrochemical hotspots that trigger the growth of dendrites.[16-18]

In comparison to Li-ion batteries system which generally uses carbonate solvents for electrolytes, the Li-S batteries system uses ethers, including both cyclic ethers and short-chain or glycerol ethers.[4, 16] This is due to polysulfides anions are nucleophilic and can attack the unsaturated bonds mainly carbonyl groups in conventional carbonate electrolytes and results in irreversible reactions. Ethers, on the other hand are compatible with polysulfides.[4, 16, 19, 20]

The most conventional electrolyte used in Li-S batteries system is lithium bis(trifluoromethanesulfonyl)imide (LiTFSI) as salt, 1,2-dimethoxyethane (DME) and 1.3-dioxolane (DOL) as co-solvents and $LiNO_3$ as additive.[7, 16, 21] The salt and co-solvents combination is compatible with both S cathodes and Li anodes within the operating voltage window of Li-S batteries, generally 1.4 V – 2.8 V vs Li^+/Li. Compared to DME, DOL has larger viscosity and is less polarized which results in lower solubility of polysulfides in the electrolyte.[4, 21] However, such properties also come at a cost of Li^+ ionic conductivity and the utilization of sulfur active material.[21, 22] Therefore, a combination of DOL and DME as

cosolvents of the Li-S electrolytes is a good balance between ionic conductivity of the electrolyte and the deterrence of shuttle reactions.[21] The DOL solvent is able to electrochemically polymerize on the surface of Li metal anodes to form a preferable SEI layer with elastomeric component with improved mechanical properties that is able to accommodate the volume change of Li during cycling, suppress the growth of Li dendrites and retain good Li^+ ion conductivity.[1, 16, 23] These unique properties of DOL will be further discussed in detail in latter chapters. According to research done by Mikhaylik et al., $LiNO_3$ can oxidize Li metal and solvent molecules to form a passivation layer onto the surface to protect the anode from further erosion by components of electrolyte. It strongly limits the shuttle reactions and, in some cases, even double the capacity of S cathodes due to the mitigation of the shuttle effect.[24-27] However, with only DOL as solvent and $LiNO_3$ as additive the improvement of Li-S cycling is still limited. When the cycling current is beyond a threshold, this SEI layer cannot maintain its uniformity and good mechanical property, thus causing fast capacity decay (< 150 mAh g^{-1}, after 100 cycles) or Li dendrites formation at high power.[4, 28]

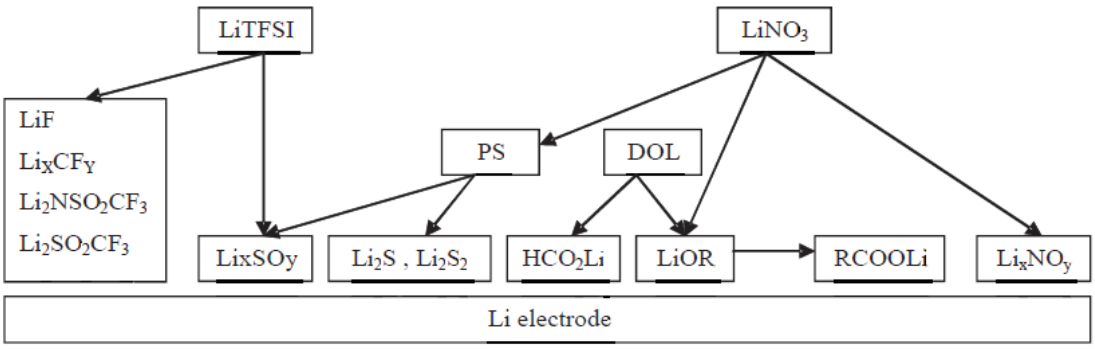

Figure 1-2 A schematic representation of the contribution of the various components in DOL/LiTFSI/Li_2S_6 /$LiNO_3$ solutions to the surface chemistry of Li electrodes. Reproduced with permission.[4]

As a result of the various electrochemical reactions and electrolyte system involved, the SEI layer on the surface of Li metal anode is very complex and the nuanced surface chemistry remains to be investigated. Figure 1-2 shows the diverse components of SEI on the surface of Li metal anodes and their origins.[4] It can be categorized as a composite layer consisting of inorganic and organic components. The inorganic layer is made up of decomposed salt and those products of decomposition are important for the transport of Li^+, coordination of the stripping and plating of Li and are generally imbedded below the organic layer. The elastomeric organic layer which mainly consists of poly-DOL can suppress the growth of dendrites and accommodate drastic volume change of Li during cycling. Deciphering the fine structure of the SEI and tuning each part to maximize its protective function and ionic conductivity would be crucial to any Li metal anode study.[4, 16, 29, 30]

1.3.2 The Enhancement of Cathodes

Based on the issues the sulfur cathodes are facing, the enhancement of S cathodes have been commonly approached by a) confining the polysulfides within the carbon material substrates to prevent dissolution and b) building a stronger carbon structure that can withstand the volume change and store as much sulfur as possible without sacrificing the electronic conductivity too much.

Applying a coating layer on the surface of C/S composite cathodes is one of the most studied subjects.[31, 32] Li-permeable metal oxides, sulfides and halides such as TiO_2[33], ZnS[34], LiBr[35] and LiI[36] have been used as protective layers. Several conductive polymers[37-39] such as PEDOT[40], polypyrrole[41] and polyaniline[42] have been applied via physical, chemical and electrochemical coating methods.

Another successful method that has been used so far to improve the sulfur cathodes is heteroatom doping, mainly by electron-rich nitrogen[43, 44] and electron-deficient boron[45, 46] on the carbon substrates. By doping those atoms, the electronic conductivity of the entire electrode is greatly improved. Due to the affinity between the heteroatoms and polysulfides anions, the dissolution of polysulfides is also mitigated.[47, 48]

An important approach toward containing sulfur and confining polysulfides is by engineering the architecture of carbon materials. Organized microporous[49] and mesoporous carbon[50, 51] gained a lot of attention by having a large surface area and organized structure to increase the electron conducting network and confine sulfur and polysulfides within the pores. In addition, carbon nanotubes[52], porous nanofibers[53], hollow carbon spheres[54] and graphene[55] are also promising host materials for sulfur.

Other methods, including polysulfides-trapping interlayers in between the cathode and the separators[56], novel sulfur hosts beyond carbon[57] and polysulfides-blocking separators[58, 59] have all been reported. All those methods contribute immensely to the overall enhancement of S cathodes, but many will have troubles to realize their practical application and commercialization due to high toxic materials deployed, and materials and/or processes used being too costly and not widely available.

1.3.3 The Enhancement of Anodes

Compared to sulfur cathodes, there has been less work done on the Li metal anodes side due to the complexity and difficulty of the issues. The efforts to enhance the Li metal anodes can be summarized as a) suppressing the formation and growth of dendrites, b) accommodating and constraining the volume change, c) stabilizing and optimizing the surface SEI layer.[9, 60] Such improvement would have universal benefits on all battery

systems that use Li metal as anodes, such as Li-air or Li-oxygen batteries and high voltage cathode (HVC) Li-ion batteries. As for Li-S batteries, if there can be a mechanism on the anode side that can block the polysulfides from reacting and converting to the forms of insoluble and insulating Li_2S and Li_2S_2, the continuous consumption of electrolyte and cathode active material would be mitigated thus the shuttle effect itself would not be the most detrimental issue.

In the liquid electrolyte system, novel 3D Li host structures have been fabricated and built to shield Li from parasitic reactions, suppress dendrite growth and accommodate volume change.[61] Applying designed protective layers to the surface of Li anodes is another widely used strategy. There has been a lot of research done on electrolyte modification to optimize the properties of the SEI formed on Li metals.[1, 62-80] Among all the methods employed, applying protective layers stands out because of its feasibility, variety, controllability, and the capability to address multiple issues with this single strategy. This dissertation is dedicated to the systematic study of the electrochemical fabrication of the artificial SEI (ASEI) layer to protect the Li metal anodes. A more thorough review of the work that has been done on the protective layers on Li metal anodes will be discussed in latter chapter.

1.4 Beyond Conventional Li-S Batteries: Solid-State Li-S Batteries and Multivalent Metal Anodes

1.4.1 Solid-State Li-S Batteries

In order to solve the dendrite growth problem of Li metal anodes and the associated safety hazards, and to resolve the polysulfides dissolution issue of sulfur cathodes once and for all, researchers are turning to a brand-new solid-state electrolyte and battery system as the

future for utilizing Li metal.[62, 81, 82] It was calculated that if the shear modulus of the separator/electrolyte is larger than 6 G Pa, then the dendrite problem of Li metal could be solved.[83] Promisingly, the mechanical strength of most solid-state electrolytes can meet this standard. By replacing liquid electrolyte with solid electrolyte, the issue of the flammability of the organic solvents is also mitigated.

The most important component of the solid-state batteries system is the solid-state electrolytes (SSE). Generally, solid-state electrolytes for Li-S batteries can be divided into two categories, inorganic solid-state electrolyte and polymer solid state electrolyte. Inorganic SSEs include NaSICON-type and garnet-type materials.[84-86] For polymer solid-state electrolytes, polyethylene oxide (PEO) is the most widely used and commercialized. However, the ionic conductivity of dry polymer solid electrolyte is too low for practical applications.[87] Composite polymer SSEs consisting of inorganic and polymeric materials are made to solve this problem.[82]

The research on solid-state electrolyte and solid-state Li-S batteries is gaining growing attention and momentum. However, there is still a long way to go before it can be commercialized. First, most solid-state electrolytes have lower ionic conductivity at room temperature, which makes them unable to meet the demand of high-power batteries for electric vehicles. Second, solid-state electrolytes and Li metal usually have poor contact which results in low wettability of the electrodes and high charge transfer and interfacial impedance at the interface. Third, solid-state electrolytes must be fully compatible with Li metal and both chemically and electrochemically stable under the operation conditions of the batteries. Unfortunately, some polymer and inorganic materials for solid-state electrolytes are not thermodynamically stable against Li metal and/or undergo phase

change during cycling. It is crucial to further investigate those issues and find ideal candidates for solid-state Li-S batteries. At the same time, the study of solid-state electrolytes also provides valuable insight into how to design and apply ideal protection layers for Li metal anodes in liquid-electrolyte Li-S batteries, which will still be the major practical application of Li-S batteries in the near future.

In this dissertation, we studied using sulfide-type solid-state electrolyte $Li_{12}GeP_2S_{10}$ (LGPS) in solid-state Li-S batteries, by applying ALD-coated LiPON as ASEI layer on LGPS, which can extend its electrochemical stability window and greatly enhance its stability against Li metal. LGPS has Li^+ conductivity comparable to conventional liquid electrolyte. By protecting LGPS with ALD-coated LiPON material, it has shown much superior electrochemical cycling stability. The detailed study will be discussed in latter chapters.

1.4.2 Multivalent Metal Anodes: Rechargeable Mg Batteries

Li-powered rechargeable electronic devices have been the tales of tremendous success in both the business world and academia. However, researchers and industry insiders are increasingly inclined to move beyond Li metal toward more novel technologies. One reason is the reserve of lithium is relatively low on earth compared to many other metals that can serve as anodes of energy storage devices. Another reason is many countries that have the largest deposit of lithium in earth's crust are developing and geopolitically unstable countries. Mining lithium in these regions always comes with serious moral and logistical issues. Last but not the least, the metallurgy and recycling of Li metal, and the waste and pollution generated during the processes are also a huge concern. Therefore, it

becomes more and more appealing to move beyond Li metal system towards more sustainable ones.

Multivalent metal anodes, which mostly have been focused on zinc, magnesium, aluminum, and calcium due to their much greater abundance than lithium and the high charge capacities due to the extra charges the ions carry. Most of those multivalent metal anodes are still very early even in terms of scientific studies. Among them, magnesium-sulfur (Mg-S) batteries are a promising technology due to the high theoretical capacity of sulfur cathodes and the abundance and high volumetric capacity (3,832 mAh cm^{-3}) of Mg metal anodes. While Mg has a higher reduction potential (-2.37 V) relative to Li (-3.04 V), magnesium deposits in a non-dendritic morphology in electrolytes compatible with the Mg anode, making it inherently safer than the dendritic deposits typical of Li metal. Creating a Mg-S battery can enable a cost-effective system with a high theoretical energy density (3200 Wh L^{-1} and 1700 Wh kg^{-1}).[88, 89] Although promising, issues mentioned earlier, such as polysulfide shutting, which persist in Li-S batteries largely remain in Mg-S systems. However, Mg metal has a more complex problem involving the potential for passivation film formation at the Mg anode surface that would block electrochemical activity.[89-93] In this dissertation, we delved into the study of applying the methodology of electrochemical protection methodology of lithium metal to magnesium metal. There is still a long way to go on this route, but the early results we have obtained so far contain important information on the unique challenges Mg metal anodes are facing and where the possible breakthroughs lie. It will be discussed in a latter chapter.

1.5 Objectives of This Dissertation

In this dissertation, electrochemical protection of Li metal anodes is systematically studied to understand the surface chemistry of the ASEI layer and its impact on the electrochemical performance of the Li metal in Li-S batteries system. Conventional and well-defined electrolyte and S cathode materials are used to focus on the study of anode. The main goals of this dissertation are:

(1) Use electrochemical method to fabricate an ASEI serving as the protective layer on Li metal anodes.

(2) Study and understand the surface chemistry and electrochemical impact of this ASEI and provide further guidance on the optimization of the ASEI layer and Li-S batteries system

(3) Develop the electrochemical methodology and apply it to solid-state batteries and Mg batteries systems.

In Chapter 2, the electrochemical protection of Li metal anodes in the liquid electrolyte Li-S batteries system is studied which satisfies the first two objectives of the dissertation. In Chapter 3, the development of solid-state electrolyte LGPS and the application of ALD-coated LiPON on LGPS in the solid-state Li-S batteries system are studied. In Chapter 4, the electrochemical protection of Mg metal anodes is studied, and the up-to-date results are discussed. These two chapters meet the third objective of the dissertation. In the final chapter, the summaries of these studies and the prospects are discussed.

2. Electrochemical Protection of Li Metal Anodes in Liquid Electrolytes

The work discussed in this chapter has been published in ACS Appl. Mater. Interfaces. 2018, 10, 29, 24554-24563 and Journal of Materials Science. 2019, 54, 3671–3693.

2.1 Introduction

2.1.1 ASEI Layers for Li Metal Anodes

Among all the methods employed to protect Li metal anodes, applying protective layers stands out because of its feasibility, variety, controllability, and the capability to address multiple issues with this single strategy. An ideal protection layer, also known as an artificial SEI (ASEI) layer must meet the following criteria. First, the layer should be chemically and electrochemically stable against Li metal and the electrolytes in the desired operating environment, current densities, and voltage window.[63] Second, the layer must be mechanically strong enough to suppress the growth of dendrites.[62] Third, the layer must be flexible enough to accommodate the huge volume change during cycling. Being too rigid can cause cracks on the layer that create local hot spots and dendritic formation which lead to disastrously fast decay of the battery. The layer is desired to be conformal and uniform to prevent uncovered hot spots.[94] Fourth, ideally the layer shall be electrically insulating, yet have excellent ion conductivity to selectively conduct Li^+ or other metal cations.[9, 60, 62] There has been tremendous work done in the field of designing and optimizing ASEI as protective layer, and herein the following examples of the different types of ASEI layers and methods of fabrication are discussed.

The first type is inorganic materials, which have long been used as coating materials for electrodes, separators, and current collectors of batteries because of the variety of materials and fabrication methods to choose from. Inorganic materials are also favored for formation of protection layers due to their robust mechanical strength, some with good conductivity, and the feasibility for fabrication and modification.[63] Metal oxides are also widely used as coating layers because of their high chemical stability which could withstand the corrosion from the electrolyte.[95, 96] Kozen et al. used plasma-assisted atomic layer deposition (ALD) to deposit a 14-nm thick Al_2O_3 layer on the surface of Li metal anodes which demonstrated the capability to prevent Li corrosion in atmosphere, organic solvents, and polysulfide electrolytes.[97] In addition to metal oxides, LiF has gained tremendous attention due to its electrochemical stability in a wide electrochemical window and its capability to regulate surface tension, despite its low ionic conductivity.[71, 98-101] Moreover, Li_3PS_4[102-105], Li_3N[106], SiO_2[107], MoS_2[108], and L_2S_3[109] mixed ionic and electronic conductor (MIEC) thin films[110] are other inorganic materials which have been employed as protective layers recently. Though inorganic materials are effective in suppression of dendrite growth due to their high modulus and ability to mitigate side reactions with the electrolytes thanks to their electrochemical stability[111], the rigid structures develop cracks or pinholes and these defects could create local hotspots that facilitate severe growth of dendrites which often leads to the failure of the protective layers and the anodes. In addition, by preventing the electrolyte from accessing the Li surface, it also results in poor interfacial ion transport and sometimes sacrifices the Li ion conductivity.[111]

Another type of material that has been extensively studied and used for protection layers is polymers.[112-117] Major advantages that polymer materials have over inorganic materials

are elasticity and self-healing properties of the materials.[62] These characteristics make them promising for accommodating the volume change and suppressing the growth of dendrites during battery cycling. By modifying the surface functional groups and adjusting the degree of cross-linking of the polymers, the protective layers can further facilitate smooth plating/stripping of Li on the surface of anodes and enable solely Li^+ transport.[111] Liu et al. developed an adaptive "solid-liquid" interfacial protective layer consisting of cross-linked polydimethylsiloxane (PDMS). The protective layer greatly inherited the flowability of material, enabling it to act as a stable and conformal interface between the Li anodes and electrolytes regardless of the charging or discharging state of the batteries.[118] The viscoelasticity of the polymer materials makes them a favorite as the protective layers for Li metals. However, the electrochemical stability of the polymeric layers and their compatibility with Li metal and the components of the electrolyte with a large voltage window and high cycling current densities are still in question. While they are more successful in accommodating the drastic volume change of the Li metal anodes during cycling, the lack of rigidness of some polymeric SEI layers may not be able to control the growth of dendrites in long-term cycling of the cells.[111]

Inorganic and polymeric materials both have their advantages and drawbacks when it comes to protecting Li metal anodes from side reactions with electrolytes and the growth of dendrites. Therefore, combining the advantages of both to fabricate composite or hybrid artificial SEI layers to balance their mechanical rigidity and flexibility is a promising strategy for Li anode protection.[119-124] Xu et al. designed "soft-rigid" protective layer by hybridizing copolymer poly(vinylidene-*co*-hexafluoropropylene) (PVDF-HFP) and embedding LiF particles in the copolymer. Therefore, the layer was able to manage a

smooth deposition of Li, attributed to LiF, while also accommodating volume change and the growth of dendrites due to the soft and sticky nature of the copolymer.[125] Composite protective layers may be the most desirable ones for Li metal batteries with liquid electrolytes because they incorporate the favorable properties of both inorganic and polymeric materials, while compensating for their respective disadvantages when used alone as protective layers. However, further improvement of techniques for applying the ASEI layers are needed to make the practical application of composite protective layers more feasible.

2.1.2 1,3-Dioxolane and the Electrochemical Protection of Li Metal Anodes

Regarding composite protective layers, one group that cannot be ignored is the one naturally grown on the surface of Li anodes during electrochemical cycling of Li-S batteries. One solvent used in conventional electrolytes for Li-S batteries, 1,3-dioxolane or DOL, is known for its ability to polymerize and electropolymerize. Aurbach et el. reported that during electrochemical cycling of Li-S cells, DOL can electropolymerize to form an elastomeric layer that is able to both accommodate the volume change and suppress dendrite growth, as shown in Figure 2-1.[1] Additionally, the additive $LiNO_3$ and dissolved polysulfides can form an inorganic component of the SEI layer. This inorganic layer combined with the naturally formed DOL layer enables the Li anodes in Li-S batteries to have a much better conditioned SEI layer than Li anodes in conventional systems with carbonate solvents. Even though the *in situ* formed SEI layer in Li-S batteries is unable to fully protect the Li metal from shuttle effects or dendrite growth, it has given valuable ideas to several research groups to take advantage of DOL and use it to create much more

optimized artificial SEI layers.[29, 126-128] Cheng et al. took advantage of the synergic effect between polysulfides and $LiNO_3$ to form a conformal and stable passivation layer by electrochemically charging then discharging the Li metal anodes for one cycle in a conventional Li-S electrolyte with both $LiNO_3$ and Li_2S_5 as additives. The *ex situ* formed artificial SEI is smooth, conformal and compatible with both conventional electrolyte for Li-S batteries and carbonate electrolyte for Li-ion batteries.[129] Because of the electrochemical polymerization property and its conventionality in Li-S electrolyte, it is highly desired to be used as the building bricks of a protective layer without introducing more chemicals in an already complex electrolyte system.

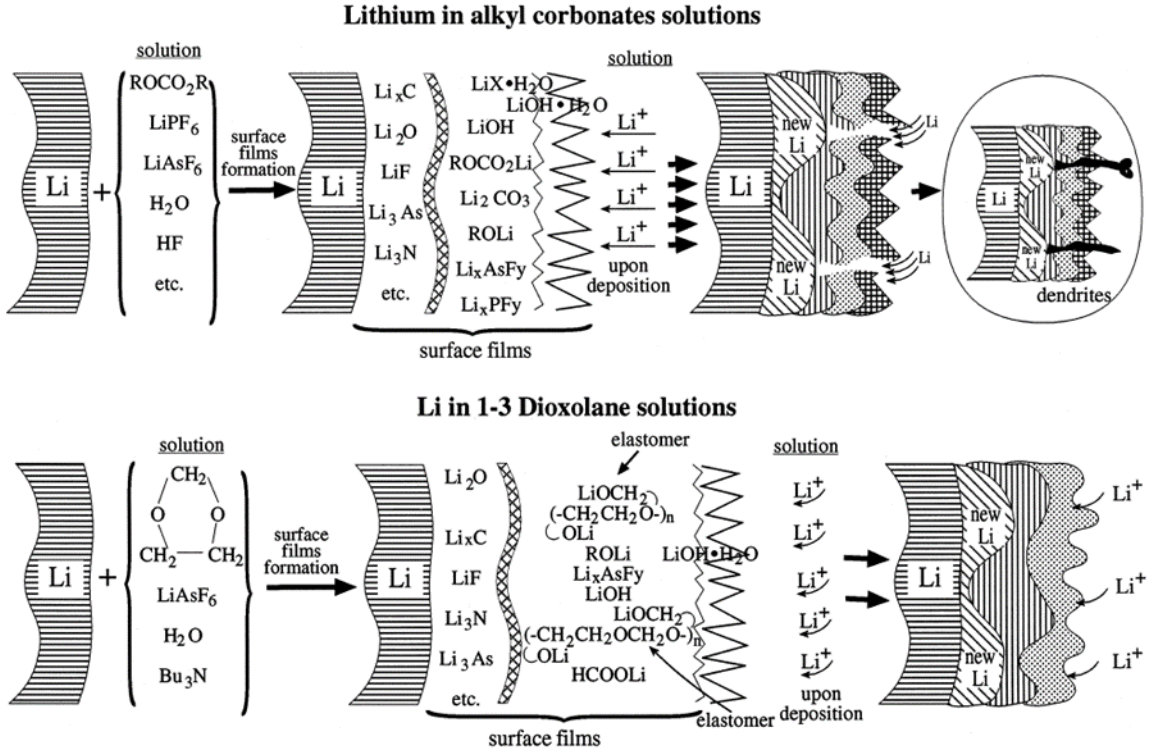

Figure 2-1 A schematic illustration of surface film formation on lithium electrodes in alkyl carbonates and in 1,3-dioxolane solutions. Reproduced with permission.[1]

In addition, electrochemical protection method has the advantages of fine tuning the conditions of how the ASEI layer is grown. By manipulating the current density and

electrochemical cycling time along with adjusting the electrolyte used for the fabrication of ASEI layer, the properties of the layer can be tuned to yield the enhanced performance of the Li metal anodes. It also has cost-effective benefits compared to many physical and chemical methods that require complex and expensive processes and chemicals.

2.1.3 Objectives of This Project

In this chapter, our research focuses on controlling the electropolymerization of DOL to electrochemically pretreat the Li metal anodes to grow well-defined SEI layer that serves as a good protection layer of Li metal that possesses good mechanical properties for high power cycling. We systematically studied the effects of electrochemical pretreatment under various conditions (e.g. current density, the cycling number and total time). Additionally, we identified the chemical variations of the artificial SEIs grown under different conditions, which allows us to connect the chemical composition of the SEIs and the electrochemical performance to the pretreatment conditions. The Li anodes protected by the controlled elastomer (LPE) demonstrated much better Li-S battery performance compared to the cells that have untreated pristine Li with uncontrolled formation of SEI, in terms of specific capacity, rate capability and Li dendrites formation. Therefore, this controlled ASEI layer in Li-S system can better accommodate the volume change and suppress dendrites growth during electrochemical cycling, which may as a result greatly expand its cycle life and alleviate the safety risk. We also conducted extensive characterizations and testing to study the surface chemistry and morphology of the layer, to understand how parameters of electrochemical pretreatment affected its properties which ultimately determined the battery performance of the Li metal anodes.

2.2 Experimental Methods

2.2.1 Fabrication of Sulfur Cathodes

In order to study the electrochemically protected Li metal anodes, we controlled the sulfur cathodes we used in the project so it would not be the limiting factor. We chose to use a well-defined carbon/sulfur composite cathode, activated carbon cloth (ACC)/S. ACC is made by weaving activated carbon fibers into cloth and it is easy to cut this cloth into small disks to serve as the carbon substrate to store sulfur and improve electronic conductivity due to the high surface area and large amount of micropores and mesopores on the carbon fibers. Another important benefit of using ACC is it can be used as a freestanding current collector with incorporated sulfur. This saves a lot of efforts of using binder and making cathode slurries. Elemental sulfur has a melting point at 115 ºC and at 155 ºC, it has the lowest viscosity. Due to capillary effect, the melted elemental sulfur can easily diffuse into the micropores and mesopores of ACC and be impregnated inside after it freezes.

Based on such properties, activated carbon cloth (ACC-507-15(c), Kynol) pieces with 9.5 mm diameter were cut and vacuum heated at 200 ºC for 24 h first to remove moisture. Then they were mixed with weighed elemental sulfur in the glove box under Ar atmosphere. A special cell shown in Figure 2-2 with a Cu gasket to block air from coming in was made for fabrication of the composite electrodes. Sulfur was weighed and placed in the bottom with ACC on top. The cell was sealed in the glove box then transferred to an oven set at 155 ºC for 12 hours to have the sulfur fully incorporated in ACC. After fabrication, the cell was disassembled, and the electrodes were put into a vacuum oven heated at 200 ºC for an hour to remove sulfur on the outer surface of ACC fibers. The sulfur loading is

calculated as 25 % of the total weight. The areal loading of sulfur is 2.116 mg cm^{-2}. The cathodes were dried at 120 ºC for 30 minutes every time before using.

Figure 2-2 Special cell to make ACC/S composite electrodes.

2.2.2 Electrochemical Pretreatment

The 9.5 mm in diameter Li metal anodes were punched from 0.75 mm thick Li ribbon (Sigma-Aldrich) stored inside an Ar filled glovebox (MBraun LabStar 20) and pressed onto 304 stainless steel spacers (15.5 mm diameter x 0.2 mm). Those Li metal anodes were assembled into symmetric coin cells (CR2032, MTI Corp) with a Celgard separator and 80 µL of 0.35 M LiTFSI (Lithium bis(trifluoromethane)sulfonamide, Sigma-Aldrich) in DME (1,2-dimethoxyethane, Sigma-Aldrich):DOL (1,3-dioxolane, Sigma-Aldrich) (1:1, v/v) electrolyte with 1% w/w $LiNO_3$ (Alfa Aesar) as additive. During pretreatment, these symmetric coin cells were cycled for different discharge/charge cycles (i.e. 25, 50, 100 and 200, annotated as LPE-25, LPE-50, LPE-100 and LPE-200 respectively) of 1 h per discharge or charge process at a low current density of 0.03 mA cm^{-2} to form the polymeric SEI layer.

Separately, symmetric coin cells were also cycled at a higher current density of 0.3 mA cm^{-2} to study the effect of pretreatment current density on the formation of the polymeric layer and the subsequent battery performance, which were annotated as LPE-50-x10.

After the Li metal anode pretreatment, the coin cells were disassembled, and the anodes were removed in glove box. Those anodes were washed with DME then vacuum dried for 30 min in a vacuum transfer chamber loaded directly from the glove box. Later the pretreated anodes were separately stored in dry packs inside the glove box. Li metal anodes freshly cut from Li ribbon without any pretreatments were used as control for all characterizations and electrochemical testing which were annotated as LPE-0.

2.2.3 Characterizations

The pretreated Li anode samples and untreated control samples were transferred via an air-tight glove bag with dry nitrogen atmosphere to an XPS system for surface chemical analysis. The samples were exposed to the dry nitrogen atmosphere for less than 1 minute. XPS data were collected on a Kratos axis 165 X-ray photoelectron spectrometer operating in hybrid mode, using monochromatic Al Ka x-rays (240 W). Charge neutralization was required to minimize sample charging, the working pressure of the instrument was 5 x 10^{-8} Torr or better throughout data collection. Survey spectra and high-resolution spectra were collected with pass energies of 160 eV and 40 eV respectively. Peak fitting was done using Casa XPS software after application of a Shirley background, using peaks with a 30 % Lorentzian, 70% Gaussian product function. All peaks within a region were fixed to have peaks of equal FWHM (full width at half maximum), the spin-orbit split components of the S 2p were fixed to have spin-orbit splitting of 1.18 eV and area ratios of 2:1 for the 3/2, 1/2 components respectively, the O-C-O, RCOOLi and CO_3^{2-} were fixed to have

separations of 1.0, 2.0, 3.4 eV separation from the R-C-O peak. All spectra were calibrated to the C-C/C-H peak at 285.0 eV.

The samples for focused-ion beam (FIB) - scanning electron microscopy (SEM) and energy-dispersive X-ray spectroscopy (EDS) characterizations were sealed in glove bag with Ar atmosphere in the glove box. The glove bag was not opened until the samples were ready to be loaded onto an SEM stage, which ensured minimal (<30 s) air exposure. The Li anode samples underwent FIB cross-sectioning by using 30 kV Ga^+ ion beam. The angle between the electron beam and the ion bean is 55°. A 10 µm (length) by 6 µm (width) trench was milled with 6 nA current for 5 min and then the cross-section was polished with lower current step by step and finished with 50 pA. Finally, the surface and cross-section of the samples were imaged using a Tescan XEIA Plasma FIB/SEM. EDS mapping of the cross-sections of the samples were performed using Tescan XEIA Plasma FIB/SEM. And to investigate the effect of polymeric layer on dendrite growth, we employed SEM imaging to observe the surface morphology of Li anode samples post-cycling.

2.2.4 Electrochemical Testing

The pretreated and untreated control Li anode samples were paired with ACC/S electrodes to make full cells. The coin cells were assembled using a Celgard separator and 100 µL 0.35 M LiTFSI in DME:DOL (1:1, v/v) with 1% w/w $LiNO_3$ and sealed in glove box. The sulfur loading to electrolyte ratio is 7.7:1, m/m. The assembled cells were then galvanostatically discharged and charged on an Arbin BT2000 Battery Test Station at different C-rates at 0.1 C (~0.3 mA cm^{-2}), 0.5 C (1.5 mA cm^{-2}) and 1.0 C (3 mA cm^{-2}) from 1.6 V to 2.6 V vs Li^+/Li. Cyclic Voltammetry (CV, Bio-Logic MPG-2) was performed with 0.25 mV/s scan rate scanning from 1.6 V to 2.6 V vs Li^+/Li.

The assembled Li-S full-cells were also tested on the Bistat for electrochemical impedance spectroscopy (EIS) measurements (Bio-Logic VSP). The EIS was measured from 500 kHz to 10 mHz with an AC amplitude of 10 mV. EIS was measured before cells were galvanostatically cycled at 0.5 C from 1.6 V to 2.6 V vs Li^+/Li. Then additional EIS was measured after 10 cycles and 50 cycles.

2.3 Results and Discussion

2.3.1 Formation of Elastomeric ASEI and Symmetric Cell Profile Study

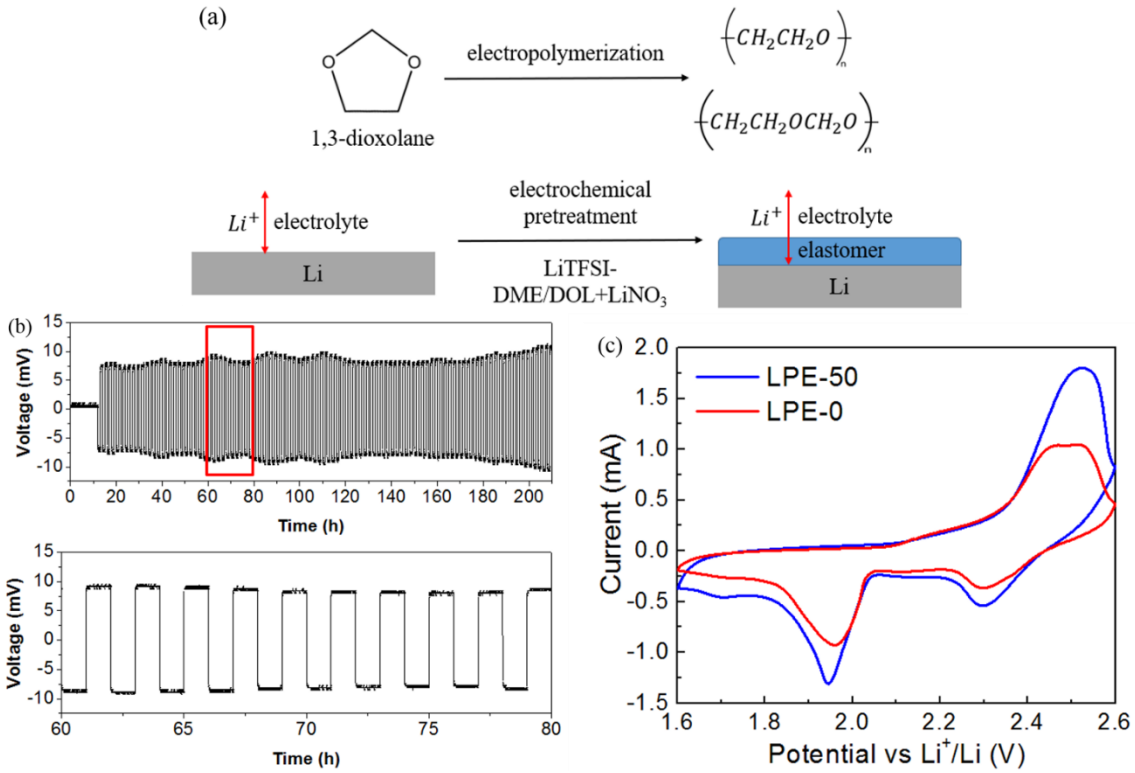

Figure 2-3 **(a)** Brief demonstration of electropolymerization and elastomer formation process. **(b)** Pretreatment cycling profiles of Li-Li symmetric cell. **(c)** Cyclic voltammetry profile of Li-S full cell.

The polymeric elastomer formation process is briefly described in Figure 2-3.[1, 130] DOL undergoes electropolymerization to form a polymeric and continuous layer on the surface of Li anodes which covers and protects the anodes from further parasitic chemical

reactions.[1, 119] Figure 2-3 (b) shows the Li/Li symmetric cell cycling curves which demonstrate the pretreatment process. At a constant small current condition (0.03 mA cm^{-2}), the pretreatment cycling process displays a small overpotential (<0.015 V) and stable cycling patterns. It indicates that the stripping and plating of Li is happening easily on the surface while the electrochemical polymerization of DOL taking place. The rather flat symmetric cell cycling curve proves there is no dendrites growing or "dead Li" forming on the surface.[131] This 0.03 mA cm^{-2} current density is smaller than the threshold current density that can trigger the growth of Li dendrites.[132, 133] Therefore, it is proper to be used for the pretreatment of Li metal to electrochemically grow the elastomeric ASEI layer.

In Figure 2-3 (c), the 50-cycle pretreated Li anode (LPE-50) shows the same characteristic CV curve as a conventional (LPE-0) Li-S battery with pristine Li metal. During discharging process, Li-S generally displays two peaks at 2.3 V and 1.9 V correspond to elemental S being reduced to long-chain polysulfides and long-chain polysulfides further become short-chain polysulfides. This resemblance indicates that the pretreated anode samples did not alter the electrochemistry of the Li-S battery.

2.3.2 Study of ASEI by Varying Cycle Numbers of Pretreatment

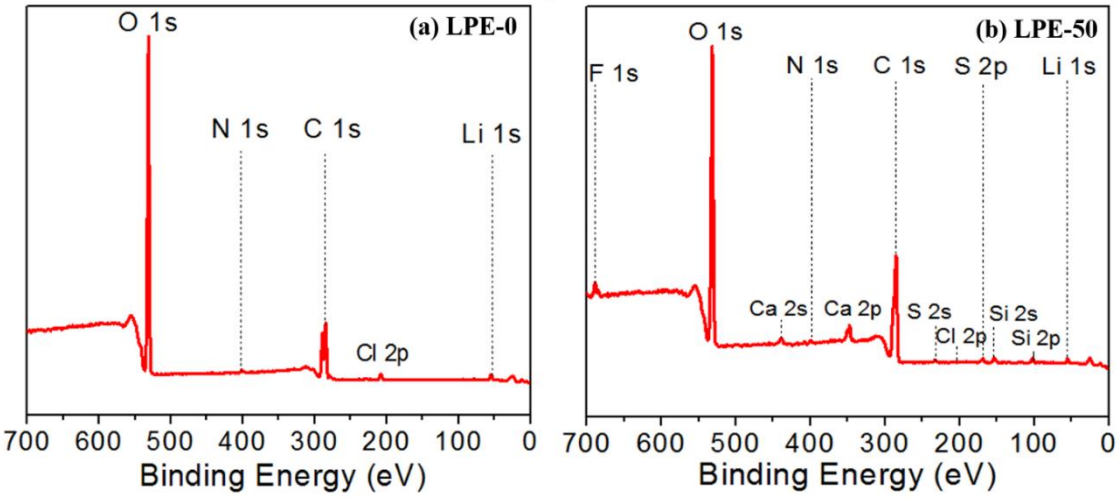

Figure 2-4 Partial XPS survey spectra of **(a)** LPE-0 and **(b)** LPE-50.

LPE-0		LPE-50	
Name	At%	Name	At%
C 1s	34.5%	C 1s	51.0%
O 1s	40.2%	O 1s	30.6%
Li 1s	24.7%	Li 1s	15.4%
N 1s	0.6%	N 1s	0.8%
S 2p	-	S 2p	0.6%
F 1s	-	F 1s	1.6%

Table 1 Atomic percent of each element in LPE-0 and LPE-50 samples.

The first control study that was done is to study the surface chemistry and electrochemical performance of the electrochemically protected Li metal anodes by varying the cycle number of the pretreatment. Each charge/discharge is an hour and the cycle number of pretreatment controls the total amount of charge passed through and the duration of the reaction time. A small cycle number may not result in an ASEI thick enough to fully cover the surface to protect Li metal anode while a large cycle number may lead to an ASEI too thick to allow the transport of Li^+ ions. Thus, understanding the surface chemistry and

chemical composition at the cycle number that results in the best battery performance is extremely crucial for the development of this electrochemically formed ASEI.

To investigate the surface chemistry of the pretreated Li anodes and the composition of the surface SEI layer, high-resolution XPS scan and analysis were performed on untreated and various pretreated Li anodes. Figure 2-4 shows partial XPS survey spectra of LPE-0 and LPE-50 samples. Target elements and contaminants are both labeled. As shown in Figure 2-4 (b), the F 1s peaks around 690 eV and S 2p peaks spanning from 162 eV to 172 eV are attributed to the pretreatment, during which an SEI layer formed on the surface and the decomposition and deposition of LiTFSI salt also occurred. In Figure 2-4 (a), the XPS peak for C 1s in LPE-0 spectrum comes mostly from adventitious hydrocarbon and lithium carbonate, and the O 1s peak is due to native carbonate layer on Li. Based on Table 1, which compares the atomic percent of each element in the two samples, it should be noted that the amount of carbon on the surface of the anode significantly grew, which can be attributed to the electropolymerization of DOL.[1, 130, 134, 135] The decrease in the relative amount of Li in the XPS spectrum of LPE-50 also indicates the Li surface was covered by the polymeric layer. The low intensities of N, S and F peaks suggest residual LiTFSI and inorganic salts which could be embedded in the layer.[1, 15]

High-resolution XPS spectra were obtained to investigate the detailed surface chemistry and chemical composition before and after the electrochemical pretreatment. Figure 2-5 shows the high-resolution C 1s and N 1s XPS spectra of pristine LPE-0 as baseline. The peaks in high-resolution C 1s and N 1s XPS spectra are due to the highly reactive surface of Li and the solvent vapors in the glove box.

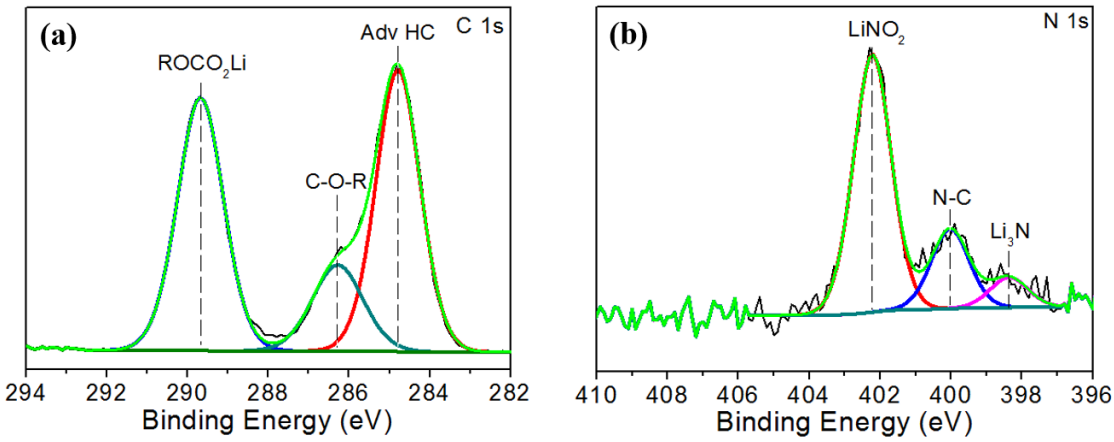

Figure 2-5 High-resolution **(a)** C 1s and **(b)** N 1s XPS spectra of LPE-0.

High-resolution XPS spectra confirmed the formation of the controlled SEI on Li anodes through pretreatment processes. Figure 2-6 shows the high-resolution C 1s, N 1s, F 1s and S 2p XPS spectra of the LPE-50 sample. In Figure 2-6 (a), the high-resolution C 1s XPS spectrum displays several characteristic peaks of the components of the polymeric surface layer. Figure 2-6 (e) shows the unit structure of the major component of the polymeric elastomer layer.[1, 130] There are two types of carbon in this unit, which were labeled as C1 and C2 respectively. C1 corresponds to the C-O-R peak at 286.5 eV in Figure 2-6 (a), and C2 corresponds to the O-C-O peak at 287.6 eV in Figure 2-6 (a). As can be seen in Figure 2-6 (a), the ratio of peak area of C1/peak area of C2 is around 2:1. This result confirms the successful formation of controlled, polymeric layer under constant small current density conditions. In Figure 2-6 (c), the $LiNO_3$ peak at 407.6 eV in the spectrum of LPE-50 is from the additive $LiNO_3$ in the electrolyte. The LiN_xO_y peak at 403.8 eV is the characteristic peak of SEI layer formed on Li anode due to the reaction between the Li anodes and $LiNO_3$.[74, 130] For peaks shown in S 2p spectrum in Figure 2-6 (d), the peak at 169.3 eV corresponds to the formation of sulfone structure from the LiTFSI salt. The peaks

ranging from 168.4 eV to 164.4 eV are sulfur compounds generated during pretreatment via complex electrochemical reactions.

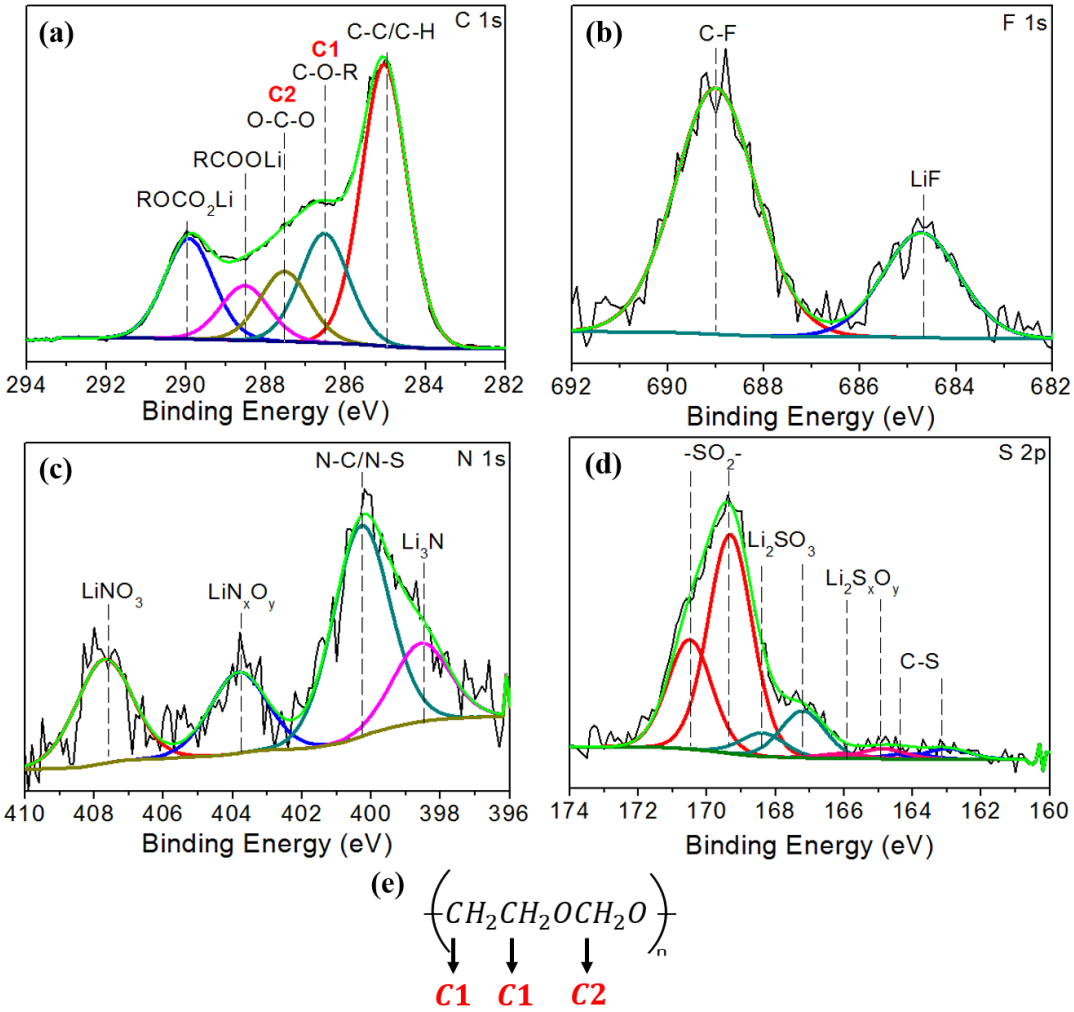

Figure 2-6 High resolution **(a)** C 1s, **(b)** F 1s, **(c)** N 1s and **(d)** S 2p XPS spectra of LPE-50. And **(e)** unit structure of the major component of the polymeric layer.

We further studied the surface morphology changes and the thickness of the polymeric SEI layer formed by pretreatment on Li anodes with scanning electron microscopy (SEM) and focused ion beam (FIB). The surface SEM image of pristine, untreated LPE-0, and smooth and uniform surface morphology of the LPE-50, Li anode pretreated for 50 cycles, can be seen in Figure 2-7. It shows the surface of Li metal anode has been well covered by the

ASEI after being pretreated for 50 cycles. The smoothness of the surface also decreases the chance of nucleation of dendrites and their drastic growth.[136, 137]

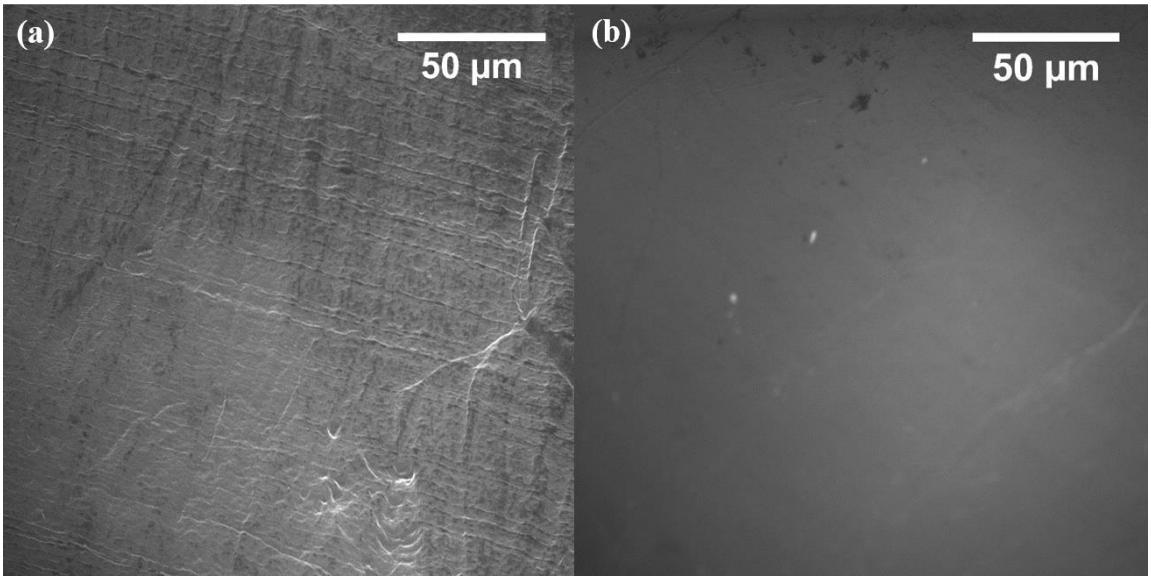

Figure 2-7 SEM surface images of **(a)** LPE-0 and **(b)** LPE-50.

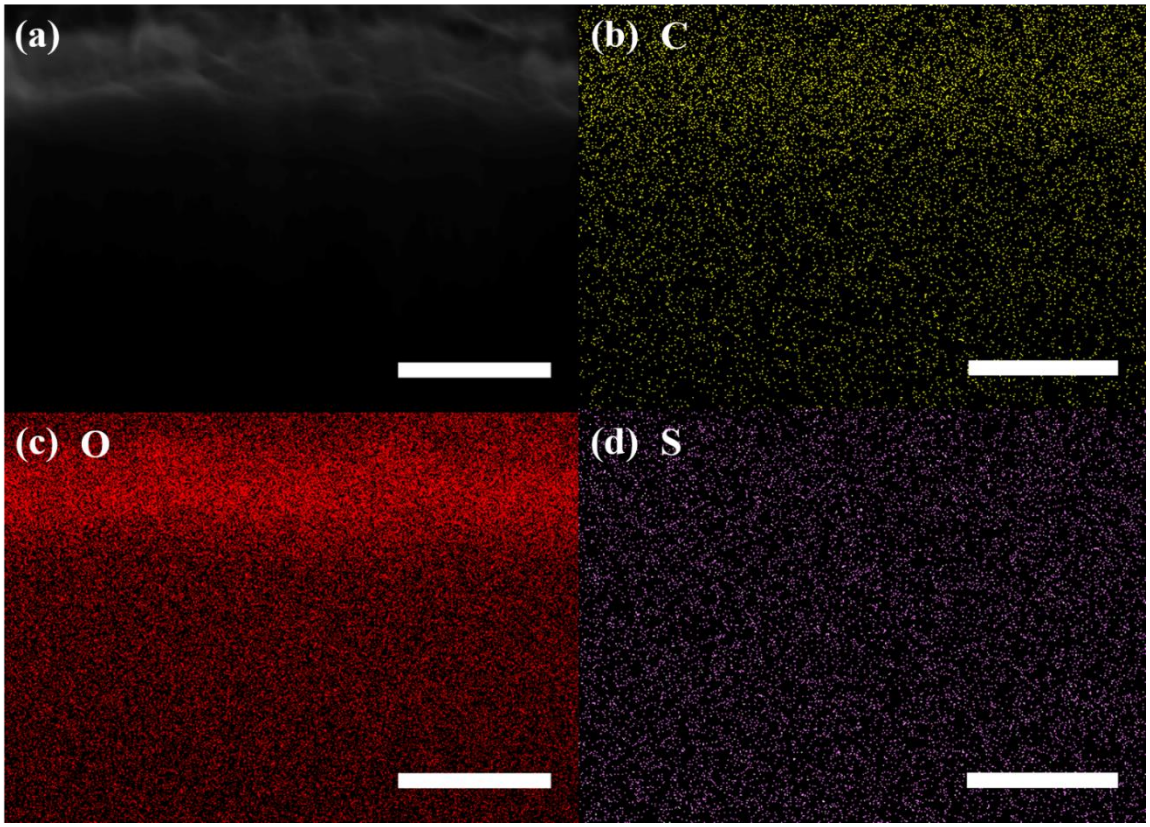

Figure 2-8 EDS mapping of **(a)** field of view, **(b)** C, **(c)** O and **(d)** S of LPE-100 sample. Scale bar of all the images is 1.0 µm.

To further verify the chemical components of the artificial SEI layer, we performed FIB cross-sectioning and used EDS mapping to examine the cross-section of LPE-100 sample. Figure 2-8 (a) is the field of view of the EDS mapping and the artificial layer is on the top. Figure 2-8 (b) and Figure 2-8 (c) show the clear existence of C and O in the area where the artificial SEI layer resides. On the other hand, Figure 2-8 (d) shows S signal is very weak in the mapping area which indicates S-containing components only exist on the very surface of the anode.

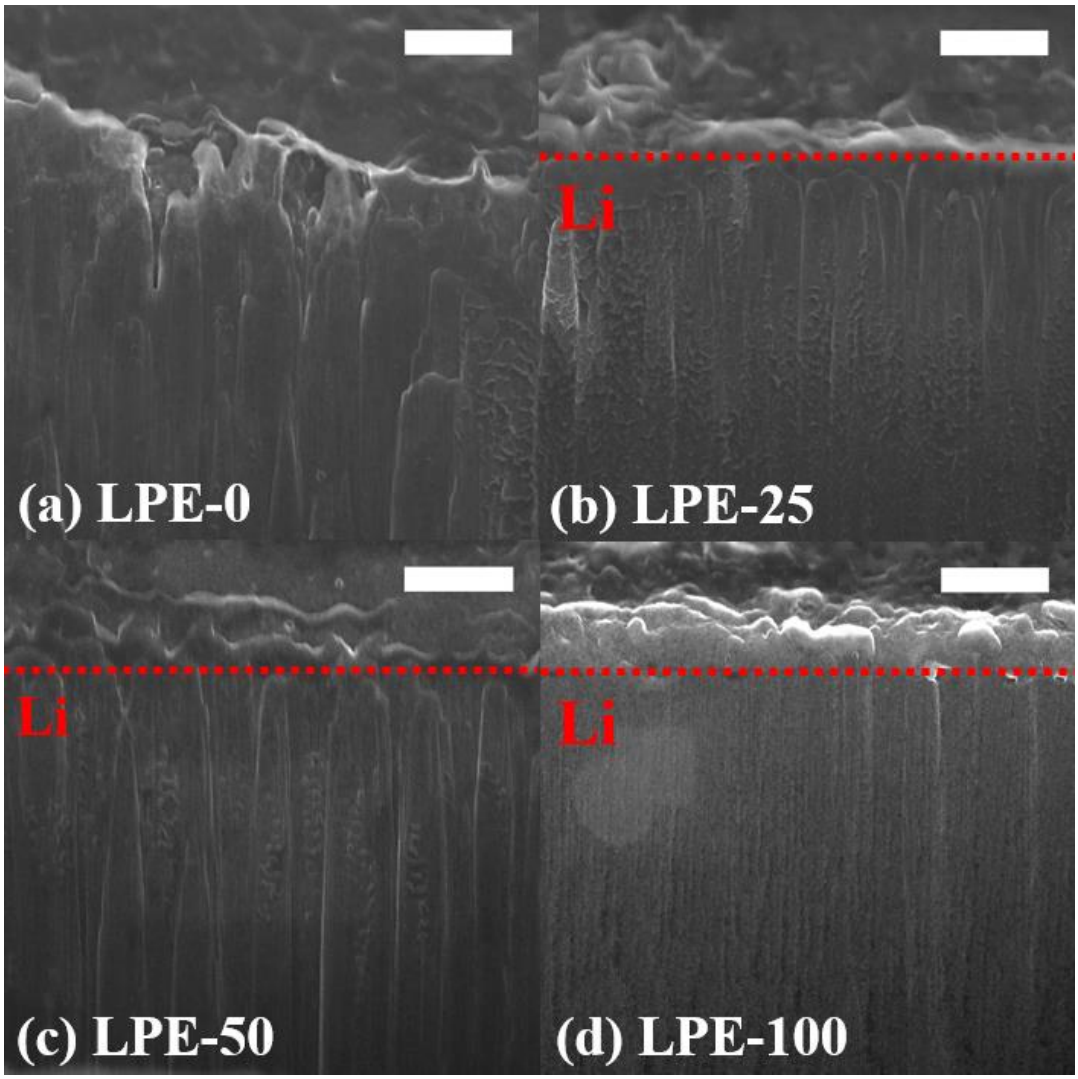

Figure 2-9 SEM cross-section images of **(a)** LPE-0, **(b)** LPE-25, **(c)** LPE-50 and **(d)** LPE-100. Scale bar of all the images is 1.0 μm.

The SEM cross-sectional images of Li anodes with various pretreatments are shown in Figure 2-9 (b) to Figure 2-9 (d) show the SEM cross section images of pretreated samples. There is a distinct difference between the surface layer and the bulk Li metal, where the bulk Li shows a columnar structure, as a result of FIB milling. There is a possibility that the increasing of pretreatment cycle number might promote cross-linking of the polymer chains formed by electropolymerization of DOL monomers.[1, 127, 130, 134, 135] Such cross-linking of the surface polymer could have multiple effects. On one hand, the mechanical properties of the polymeric layer could be improved, and the layer becomes more resilient, which means the layer could more effectively accommodate volume change and suppress dendrite growth during cycling. Conversely, if the degree of cross-linking is too high, it would pose a tremendous obstacle for the diffusion of Li^+ from bulk to the surface, thus affecting the rate capability and overall specific capacity. Therefore, an optimized procedure of pretreatment conditions is needed.

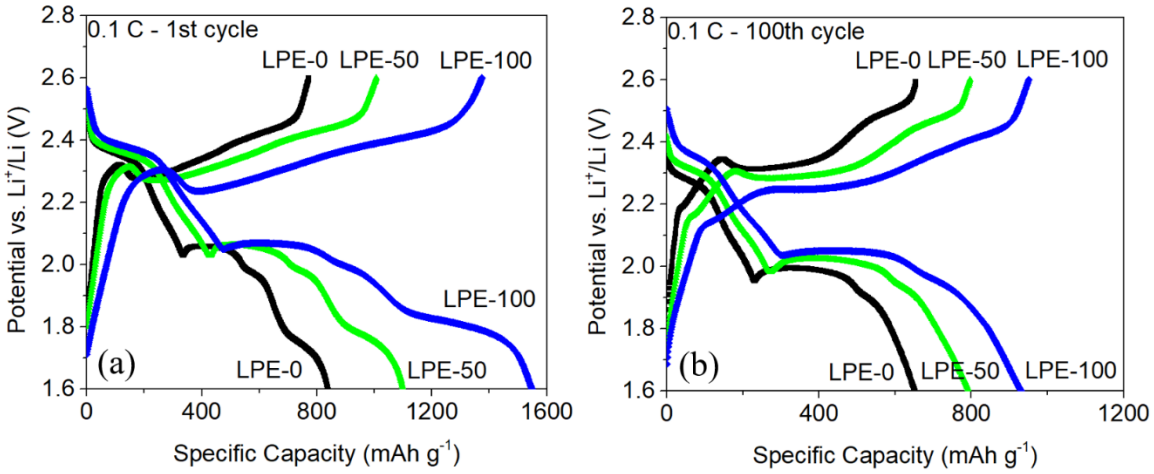

Figure 2-10 Charge and discharge profiles of LPE-0, LPE-50 and LPE-100 at **(a)** 1st cycle and **(b)** 100th cycle being cycled at 0.1 C.

We evaluated the battery performance of Li-S full-cells with both untreated and pretreated Li anodes under different conditions paired with ACC/S composite cathodes. The cells

were galvanostatically charged and discharged at different C-rates to evaluate their cycling performance and power capability. The charge and discharge profiles of samples LPE-0, LPE-50 and LPE-100 are shown in Figure 2-10, Figure 2-11 and Figure 2-12.

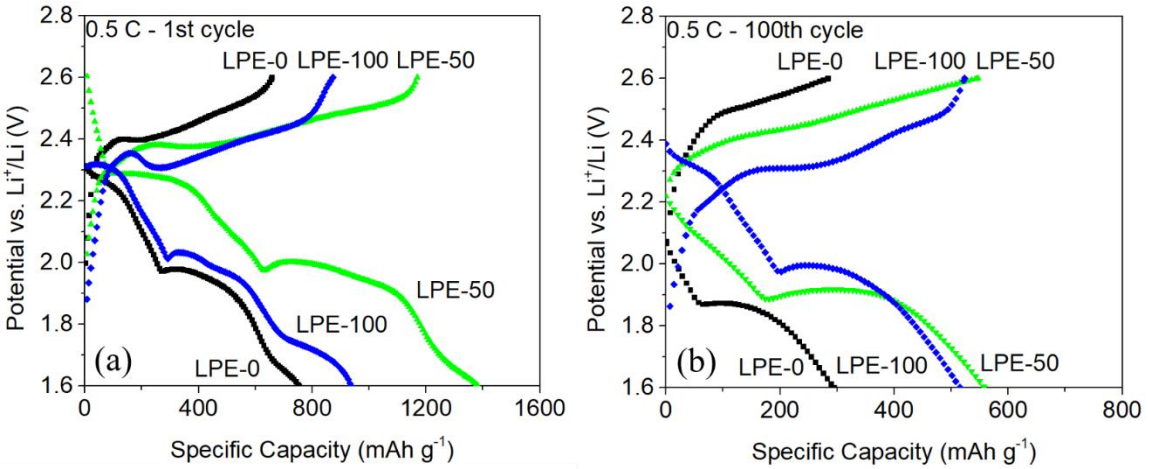

Figure 2-11 Charge and discharge profiles of LPE-0, LPE-50 and LPE-100 at **(a)** 1st cycle and **(b)** 100th cycle being cycled at 0.5 C.

Figure 2-10, Figure 2-11 and Figure 2-12 show the charge and discharge profiles of LPE-0, LPE-50 and LPE-100 at 1st cycle and 100th cycle being cycled at 0.1 C, 0.5 C and 1.0 C. C-rate is defined as how fast the theoretical capacity of the battery can be fully discharged. At 1.0 C-rate, the battery would be fully discharged in one hour. Using C-rate instead of current density in battery studies is a great way to normalize the different masses of the electrodes. At all C-rates, the charge and discharge profiles of all samples at 1st cycle show distinct plateaus which indicate the phase changes due to the electrochemical reactions. The potentials of those plateaus are very close which again confirm that the artificial SEI layers on the anodes did not alter the electrochemical behaviors of the cells at the beginning of cycling. However, when comparing to charge and discharge profiles at 100th cycle cycled at different C-rates, it shows at 100th cycle, LPE-50 and LPE-100 samples still retain relatively stable plateaus between 1.9 V and 2.0 V vs. Li^+/Li, but

untreated LPE-0 sample loses such plateau especially at high C-rate 1.0 C at 100th cycle. This demonstrates that with the polymeric SEI layer on samples LPE-50 and LPE-100, it successfully mitigated the shuttle reactions while unprotected LPE-0 could not endure the polarization at high current densities. This serves as another evidence that the artificial SEI layer greatly improved the battery performance of Li-S full-cells.

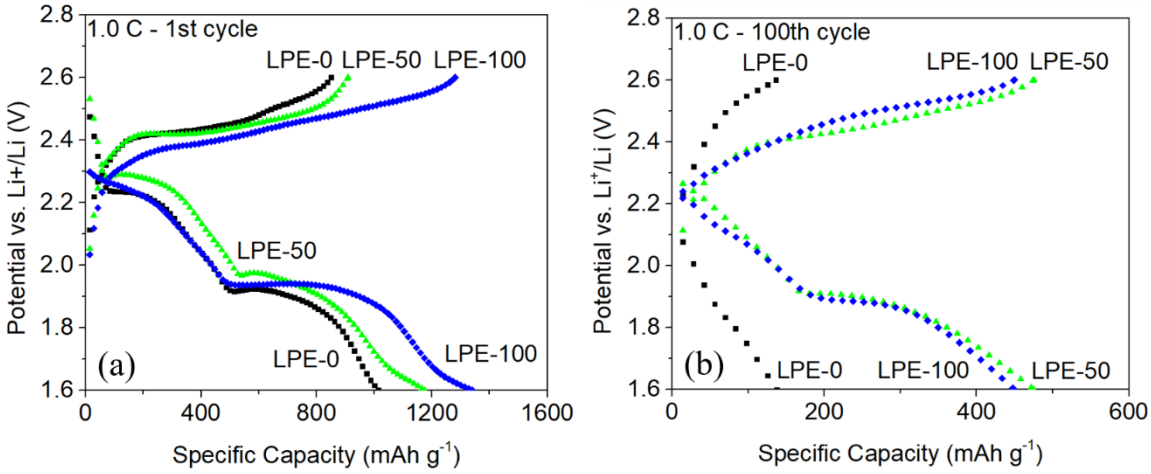

Figure 2-12 Charge and discharge profiles of LPE-0, LPE-50 and LPE-100 at **(a)** 1st cycle and **(b)** 100th cycle being cycled at 1.0 C.

Figure 2-13 shows the Li-S full-cell galvanostatic cycling profiles at 0.1 C 0.5 C and 1.0 C. At all three C-rates (0.1 C, ~0.3 mA cm^{-2}; 0.5 C, ~1.5 mA cm^{-2}; and 1 C, 3.0 mA cm^{-2}), cells with LPE-50 and LPE-100 anodes exhibit improved specific capacity compared to cells with LPE-0 (untreated) anodes. The specific capacities of the cells were calculated based on the weight of the sulfur. As summarized in Figure 2-13 (d), at 0.1 C, LPE-100 has the largest specific capacity of 919 mAh g^{-1} after 100 cycles compared to 651 mAh g^{-1} of LPE-0. At 0.5 C, LPE-50 has a specific capacity of 557 mAh g^{-1} compared to 301 mAh g^{-1} of LPE-0. At 1.0 C, LPE-50 has a specific capacity of 475 mAh g^{-1} compared to 138 mAh g^{-1} of LPE-0. All samples demonstrate that the controlled pretreatment of anodes effectively enhances the specific capacity of long-term cycling of Li-S full cells,

particularly demonstrating the superior performance at the high power (current) cycling conditions. This indicates the controlled formation of the polymeric layer successfully alleviates shuttle reactions at the anode side while maintaining excellent Li ion conductivity. Therefore, the loss of S active material from cathode side is reduced, and the further erosion of the Li anode and the deposition of ionically insulating reduction products Li_2S_2/Li_2S is mitigated.

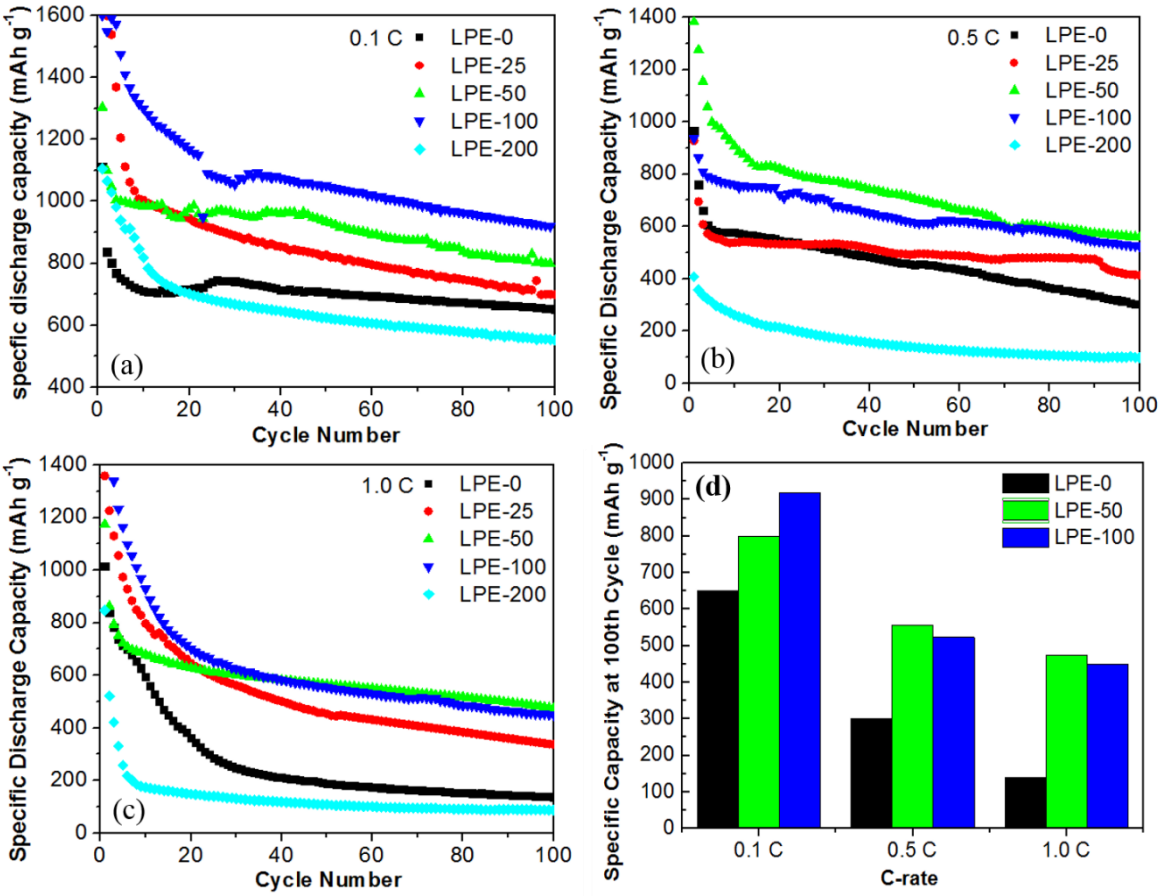

Figure 2-13 Li-S full-cell galvanostatic cycling profiles at **(a)** 0.1 C **(b)** 0.5 C and **(c)** 1.0 C. And **(d)** specific capacity comparison of LPE-0, LPE-50 and LPE-100 at the 100th cycle at different C-rates.

Additionally, at all three C-rates there is a relatively consistent trend that LPE-50 and LPE-100 have the best battery performance. With an increase in C-rate, LPE-50 eventually is better than LPE-100. Further, LPE-200 has an even lower specific capacity compared to

the untreated LPE-0 especially at higher C-rates. This result indicates that there is an optimal range of pretreatment cycle numbers. For LPE-200, the degree of cross-linking of polymeric SEI layer generated from pretreatment may be too high for Li^+ to diffuse through, which essentially curtails the electrochemical reactions. On the other hand, LPE-50 and LPE-100 prove to have a reasonable thickness and degree of cross-linking of the SEI layer which guarantees a successful diffusion of Li^+ while still being able to maintain its structure stability and surface uniformity to suppress dendrite growth and accommodate volume change. The fact that performance of LPE-50 gradually surpasses LPE-100 at higher C-rates can be explained by the fact that mass transfer is a more limiting factor when current density increases. To facilitate the diffusion of Li^+, the SEI layer needs to be thinner and less compact to provide more efficient ion transport, while not compromising too much on its ability to suppress dendrites and alleviate shuttle reactions. This finding can serve as an important guideline when pretreating anodes for full-cells cycled at even higher current density.

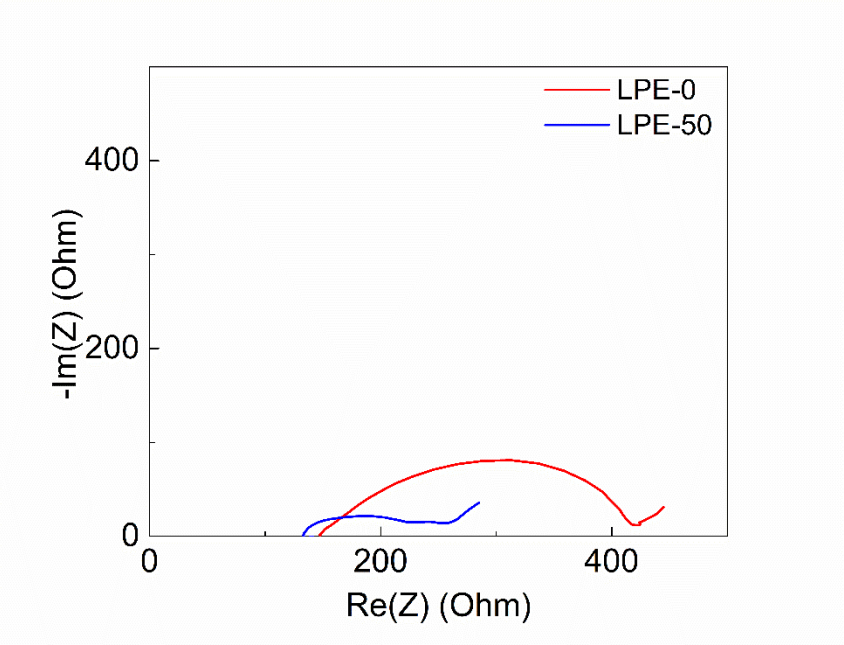

Figure 2-14 EIS spectra of Li-S full-cell at 50th cycle.

The assembled Li-S full-cells were also tested for electrochemical impedance spectroscopy (EIS) to study charge transfer and diffusion impedance at the interface after a protective ASEI layer was formed on the surface of Li metal anode. Figure 2-14 shows the EIS of Li-S full-cells with LPE-0 and LPE-50 anodes at 50th cycle after they were electrochemically cycled at 0.5 C. First of all, the double semicircles in LPE-50 curve presents a multi-interphase structure, which again confirms the successful formation of the polymeric elastomer, which has Li surface/elastomer and elastomer/electrolyte multi-interphases. The results also show after the pretreatment, LPE-50 has a much smaller charge transfer resistance (semi-circle) compared to the untreated LPE-0. This is largely due to the improvement of surface conditions between anode and electrolyte. Such reduction of charge transfer resistance also explains the greatly enhanced rate capability of the pretreated anodes. With charge transfer resistance decreases, it is easier for the transfer of Li^+ ion throughout the pretreated surface even at high C-rate.

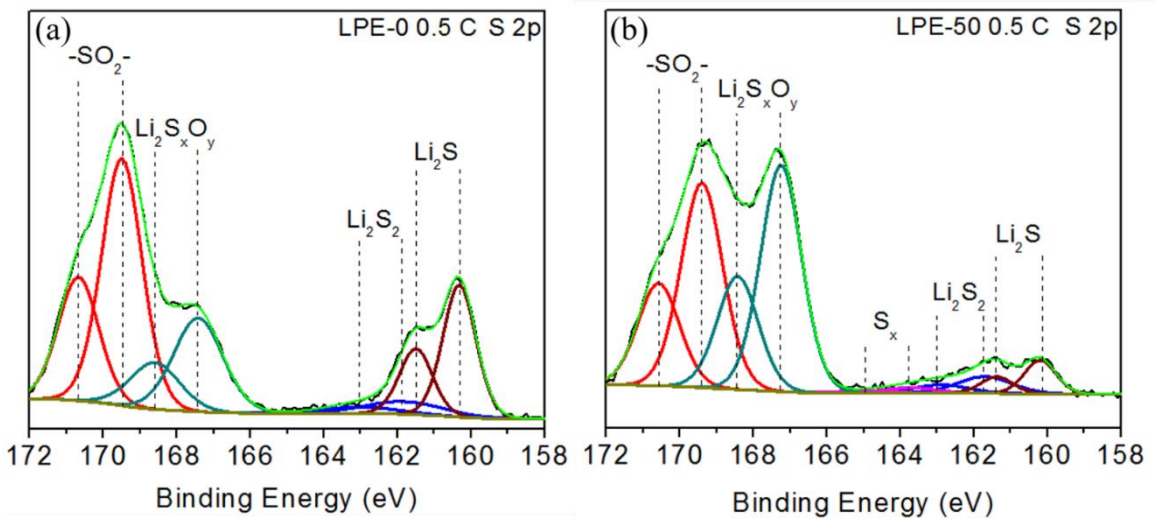

Figure 2-15 High-resolution S 2p XPS spectra of **(a)** LPE-0 and **(b)** LPE-50 after being cycled in Li-S full-cells at 0.5 C for 100 cycles.

To study the surface chemistry of the Li anodes and how the polymeric layer mitigated shuttle reactions, we conducted XPS analysis on LPE-0 and LPE-50 samples after they were cycled in Li-S full-cells at 0.5 C for 100 cycles. Figure 2-15 shows the high-resolution S 2p XPS spectra of LPE-0 and LPE-50. The results show that LPE-50 sample, which has the polymeric layer to protect the anode, has a much lower amount of Li_2S_2 and Li_2S components at only 11.2% based on the relative peak areas. In comparison, the unprotected LPE-0 has a much higher amount of Li_2S_2 and Li_2S at 26.9%. Overall, S counts 6.1% of surface components of LPE-0 sample while it only counts 4.4% in LPE-50 sample. These results demonstrate that with the polymeric layer, LPE-50 is much more successful at mitigating shuttle reactions compared to the unprotected LPE-0. The better battery performance of LPE-50 can be attributed to the smaller amount of insulating and insoluble

Li_2S_2 and Li_2S generated, which not only hinder the transport of Li ions but also lead to capacity loss.

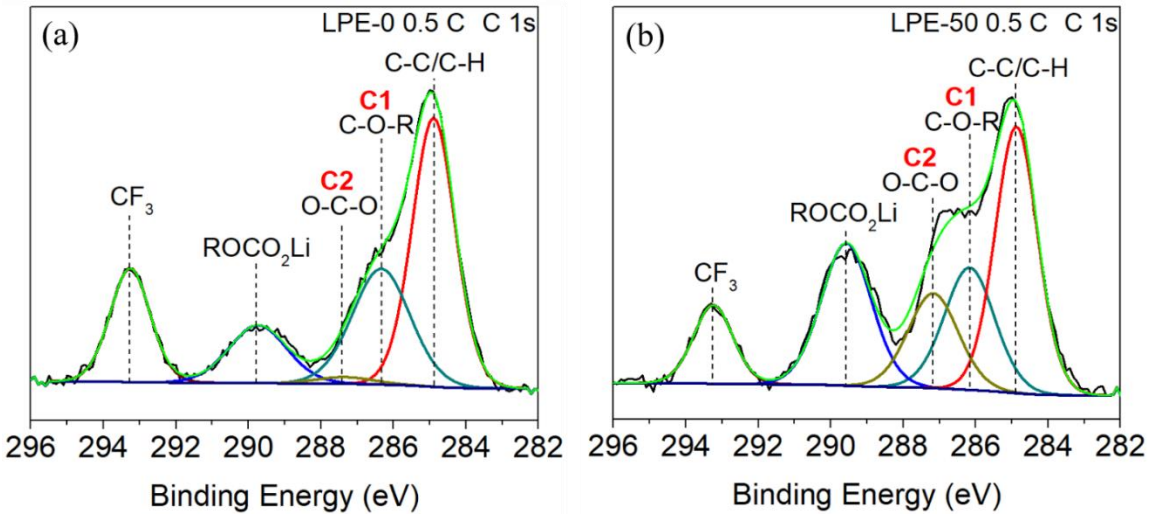

Figure 2-16 High-resolution C 1s XPS spectra of **(a)** LPE-0 and **(b)** LPE-50 after being cycled in Li-S full-cells at 0.5 C for 100 cycles.

Figure 2-16 shows the high-resolution C 1s XPS spectra of LPE-0 and LPE-50 after full-cell cycling. The CF_3 peak comes from the salt of the electrolyte LiTFSI. LPE-50 has a much higher O-C-O (C2) peak compared to LPE-0, which indicates even after cycling in full-cell at high current density, the LPE-50 sample still relatively maintained its polymeric elastomer layer, while there is little poly-DOL formed at 0.5 C current density for full-cell cycling, or the poly-DOL component is more imbedded beneath the surface. This is another important evidence that the ASEI can preserve its structure and chemical composition to serve its protective function.

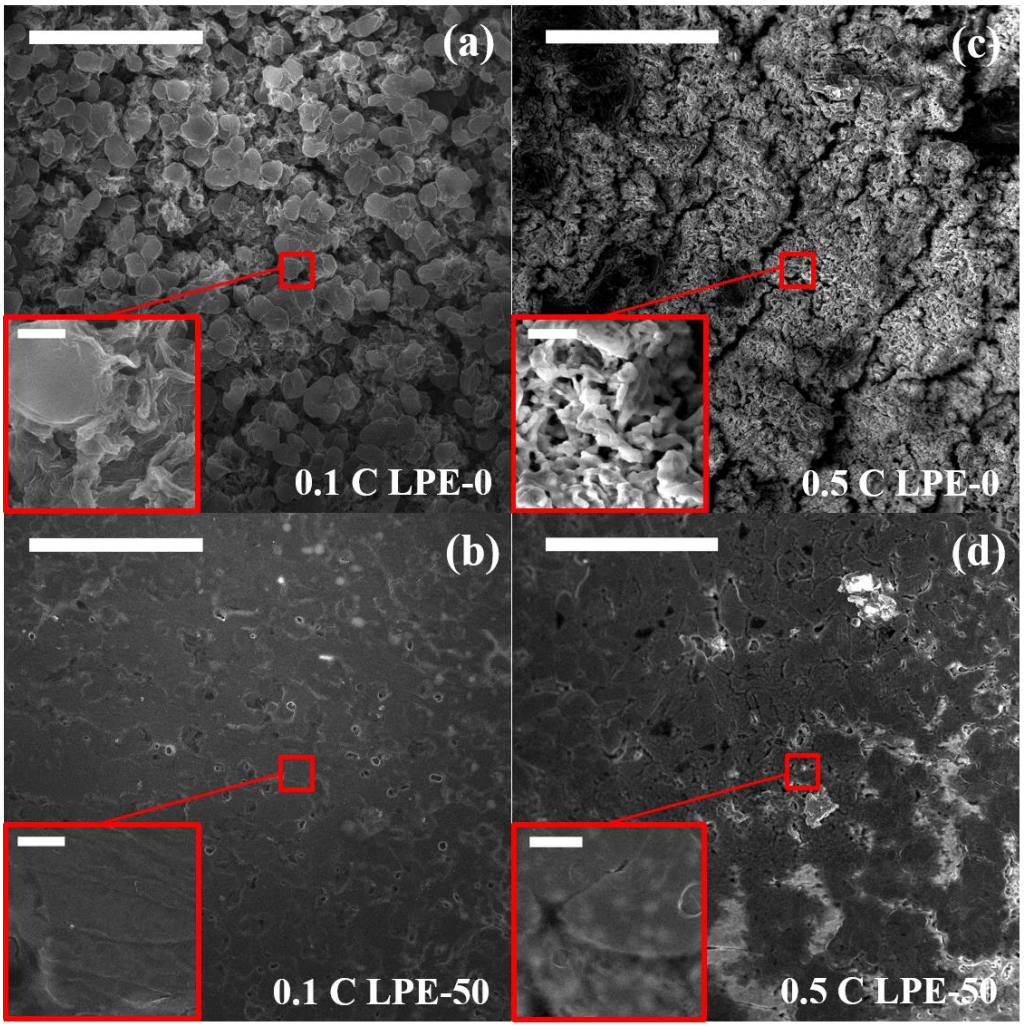

Figure 2-17 Surface SEM images of **(a)** LPE-0 and **(b)** LPE-50 after being cycled in Li-S full-cells at 0.1 C for 100 cycles. And **(c)** LPE-0 and **(d)** LPE-50 after being cycled in Li-S full-cells at 0.5 C for 100 cycles. The insets show higher resolution SEM micrographs. Major scale bar of all the images is 50-µm long. Inset scale bar of all the images is 2-µm long.

To study how the optimized formation of the polymeric layer suppressed the dendrite growth, stabilized the Li metal surface, and contributed to the improvement of the battery performance, we performed SEM imaging on Li anodes, which were cycled after 100 cycles at various C-rates in Li-S full-cells. At 0.1 C, shown in Figure 2-17 (a), for the Li anodes without optimized pretreatment, the surface consists of 5 µm large-sized pieces of Li grains agglomerated together with small high surface area features surrounded. At 0.5 C shown in Figure 2-17 (c), the entire surface of untreated LPE-0 samples formed three-

dimensional Li dendrites after high current cycling. In contract, the Li metal with optimized pretreatment exhibits smooth surface morphology after cycling, shown in both Figure 2-17 (b) and (d). This indicates that the layer can withstand high C-rates, and simultaneously suppresses dendrite growth and curbs shuttle reactions. This observation provides insights of why LPE-0 (untreated) anode demonstrates an acceptable capacity after 100 cycles at 0.1 C-rate – the interfaces allow more uniform Li nucleation and deposition under smaller current density. Nevertheless, at higher C-rates, the severe Li dendrite formation results in fast anode degradation and battery decay. Under high current density passage, the SEI layer was not able to maintain a stable structure and a smooth surface but leads to continual erosion of the anode by electrolyte and rampant dendrite growth, as apparent in Figure 2-17 (c).

The Coulombic efficiency of the Li-S full-cell was also calculated to understand how much does the ASEI protective layer help to mitigate the shuttle reactions. The Coulombic efficiency of Li-S full-cell is calculated by the following equation,

$$CE\ (Coulombic\ Efficiency) = \frac{discharge\ specific\ capacity\ at\ (n+1)th\ cycle}{charge\ specific\ capacity\ at\ nth\ cycle}$$

Equation 2.1

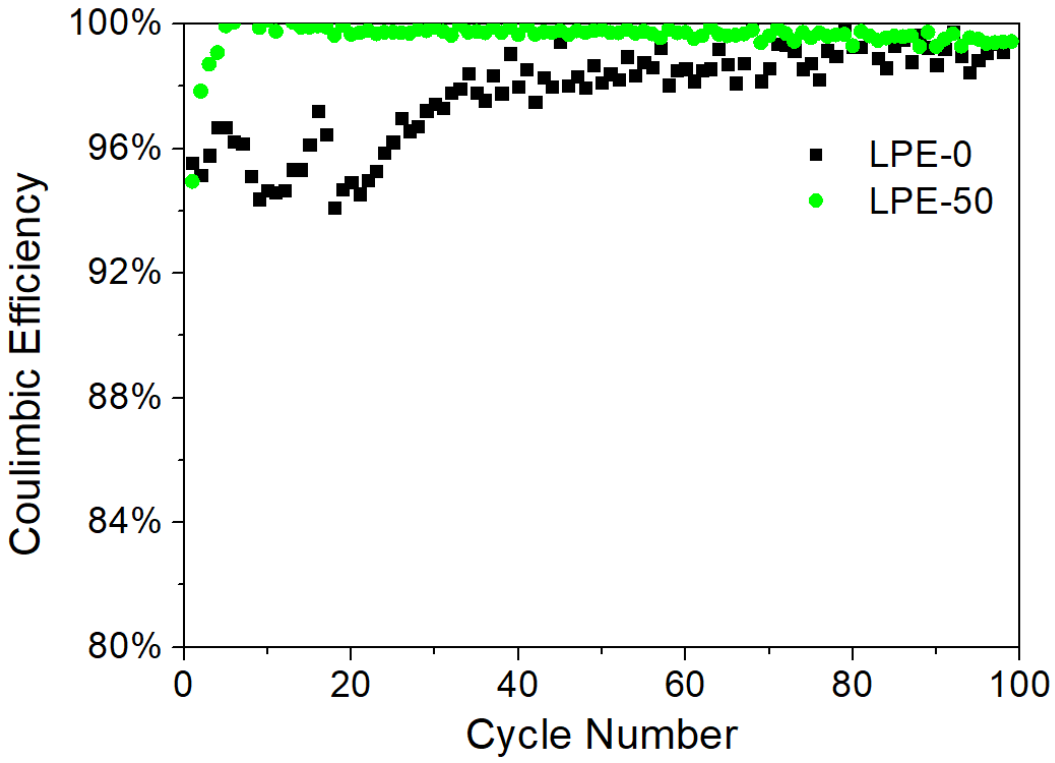

Figure 2-18 Li-S full-cell Coulombic efficiency profile of LPE-0 and LPE-50 at 0.5 C

Both LPE-0 and LPE-50 cells were discharged at 0.5 C first. At early stage of cycling, the pristine LPE-0 sample only has a very poor Coulombic efficiency as low as ~94% and it takes over 40 cycles to finally stabilize to a still low Coulombic efficiency of ~98%. Nonetheless, the protected LPE-50 sample has a Coulombic efficiency over 99% and it stabilized to this value after first 5 cycles. This is another evidence of the superior performance of the polymeric SEI layer which significantly prevents the reaction between polysulfides and the anodes, thus successfully protecting it.

2.3.3 Study of ASEI by Varying Current Density of Pretreatment

The second control study that was done is to study the surface chemistry and electrochemical performance of the electrochemically protected Li metal anodes by varying the current density used for the pretreatment. Increasing the current density can

change the total amount of charge going through the cell, but most importantly it has the probability of altering the electrochemical reactions happening on the surface of Li metal and change the chemical composition or structure which would certainly affect its function as a protective layer. In addition, high current density, generally about 1 mA cm^{-2}, can trigger the growth of Li dendrites and the degradation of the anodes. On the other hand, a current density too low may not be enough to initiate the electrochemical reactions on the surface thus resulting in a failed layer.

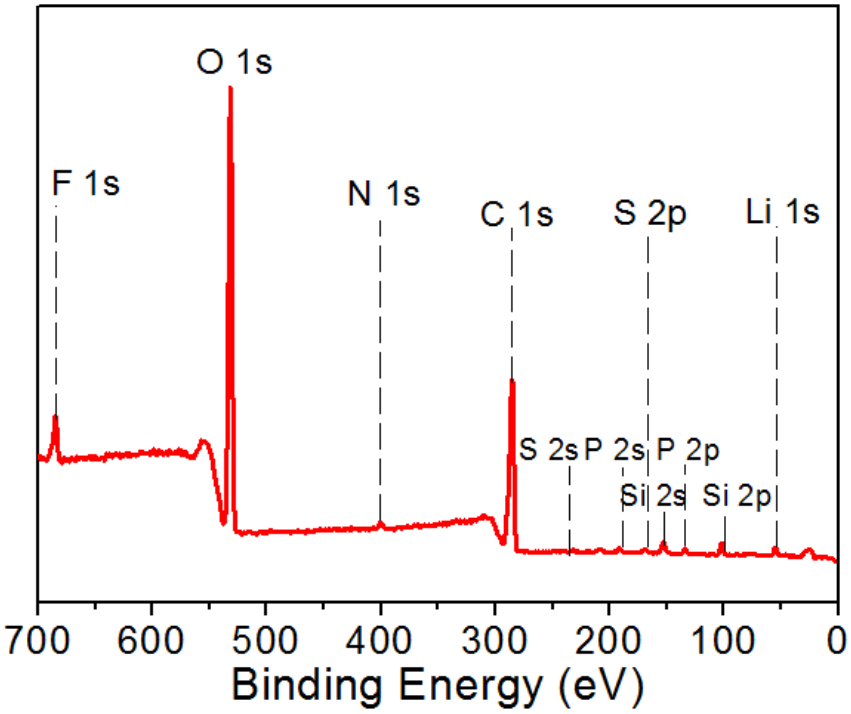

Figure 2-19 Partial XPS survey spectrum of LPE-50-x10.

To reveal the effect of pretreatment current density, we pretreated the Li anodes for 50 cycles at 0.30 mA cm^{-2}, a current density ten times larger than the one for other LPE samples. The new sample is annotated as LPE-50-x10. The partial XPS survey spectrum is shown in Figure 2-19. Table 2, which shows the atomic percent of each element in LPE-50-x10. Comparing to Table 1, the amount of carbon on the surface dropped while the

amount of oxygen increased. This indicates the change of chemical composition and surface chemistry at high current density of pretreatment.

LPE-50-x10	
Name	At%
C 1s	44.7%
O 1s	33.4%
Li 1s	16.9%
N 1s	1.3%
S 2p	0.5%
F 1s	3.1%

Table 2 Atomic percent of each element in LPE-50-x10 sample.

Figure 2-20 shows the high-resolution C 1s, N 1s, F 1s and S 2p XPS spectra of LPE-50-x10. The most distinct change in XPS spectra of LPE-50-x10 is shown in Figure 2-20 (a) that in the high-resolution C 1s spectrum, the O-C-O (C2) peak at 287.6 eV almost disappeared compared to that of the LPE-50 shown in Figure 2-6 (a). The ratio of peak area of C1/peak area of C2 equals 2 is regarded as evidence of formation of polymeric layer and electropolymerization of DOL monomers in Figure 2-6 (a). Therefore, the nearly disappeared O-C-O peak in Figure 2-20 (a) indicates more drastic reactions with the LiTFSI salt and the additive $LiNO_3$ to form a complex inorganic/organic mixture with little electropolymerization of DOL. As Table 2 shows, the relative amount of F on the surface of LPE-50-x10 sample is 3.1%, which is almost twice of that on the surface of LPE-50 sample, which is 1.6%. Based on Figure 2-20 (b), the peak area ratio of LiF to C-F is 2:1 in LPE-50-x10 compared to that of LPE-50 which is 1:2 in Figure 2-6 (b). Such a huge

increase of LiF peak intensity in the F 1s spectrum of LPE-50-x10 confirms the fast breakdown of LiTFSI salt at high current density. These all indicate very different surface reactions and surface layers are formed on Li anode at high current density with less desired property, which largely affects their protective functionality in Li-S chemistry that will be shown in the next section.

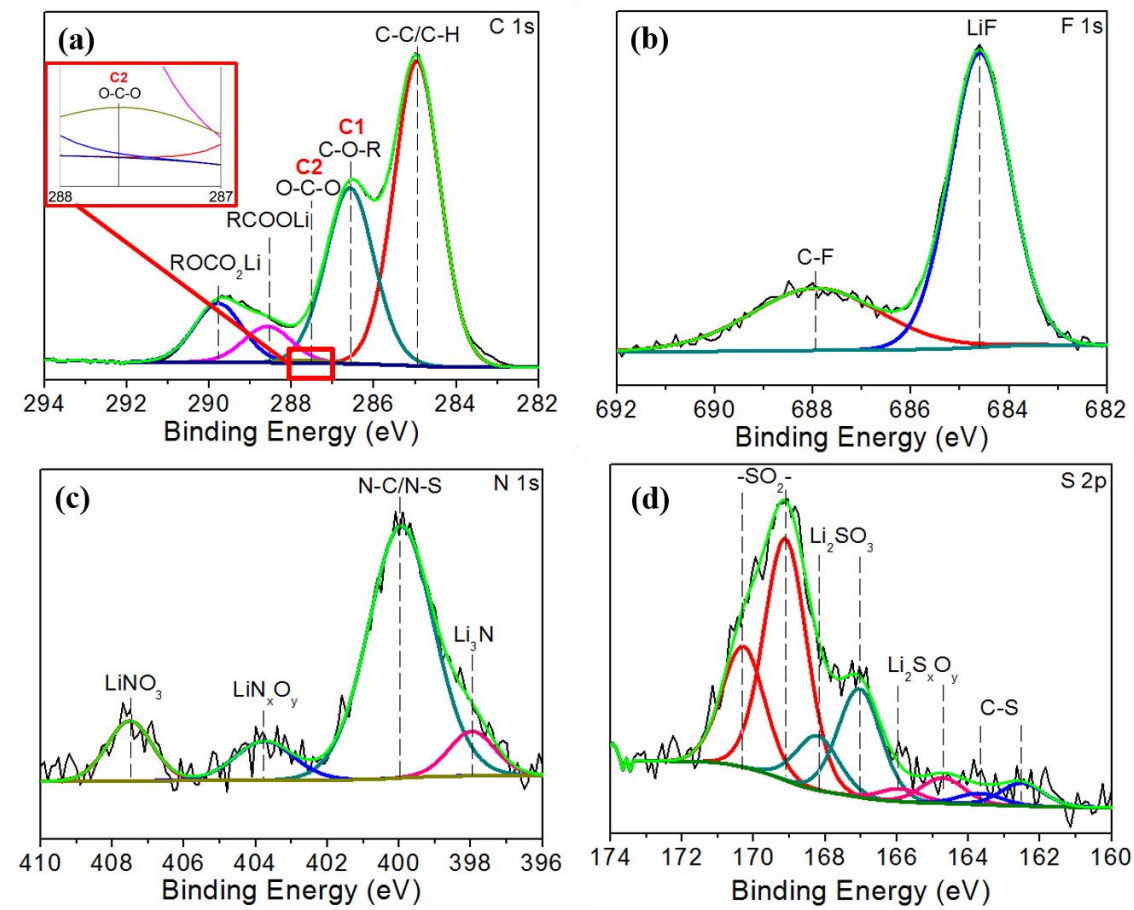

Figure 2-20 High resolution **(a)** C 1s, **(b)** F 1s, **(c)** N 1s and **(d)** S 2p XPS spectra of LPE-50-x10.

The SEM image of cross-section of LPE-50-x10 is shown in Figure 2-22 and the layer corresponds to the ASEI layer formed on the surface is much thicker than what was shown in Figure 2-9 and hard to see the boundary between Li and the ASEI layer.

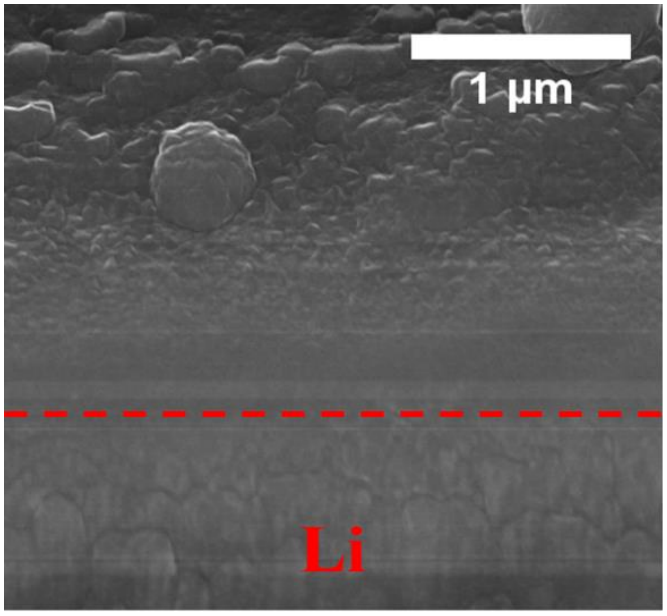

Figure 2-22 SEM cross section image of LPE-50-x10.

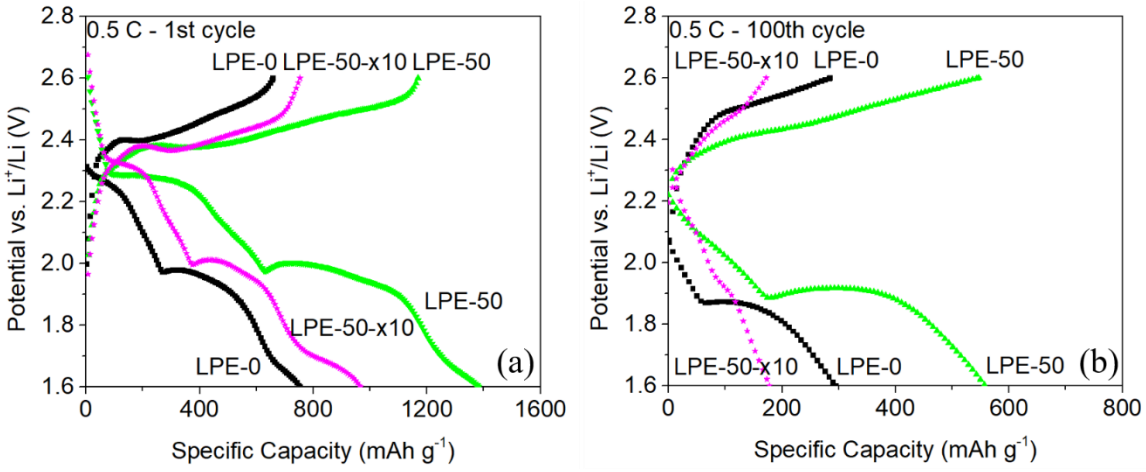

Figure 2-21 Charge and discharge profiles of LPE-0, LPE-50 and LPE-50-x10 at **(a)** 1st cycle and **(b)** 100th cycle being cycled at 0.5 C.

Li-S batteries were tested to demonstrate the cell performance with various pretreatment conditions of Li anodes. The charge and discharge profiles of LPE-0, LPE-50 and LPE-50-x10 are shown in Figure 2-21. Similarly, all three samples display distinct plateaus at same potential at 1st cycle. However, at 100th cycle, LPE-50-x10 has nearly lost its plateaus and

shown very low discharge specific capacity. This again confirmed with large pretreatment current density, the formed ASEI layer is unable to protect the anode surface.

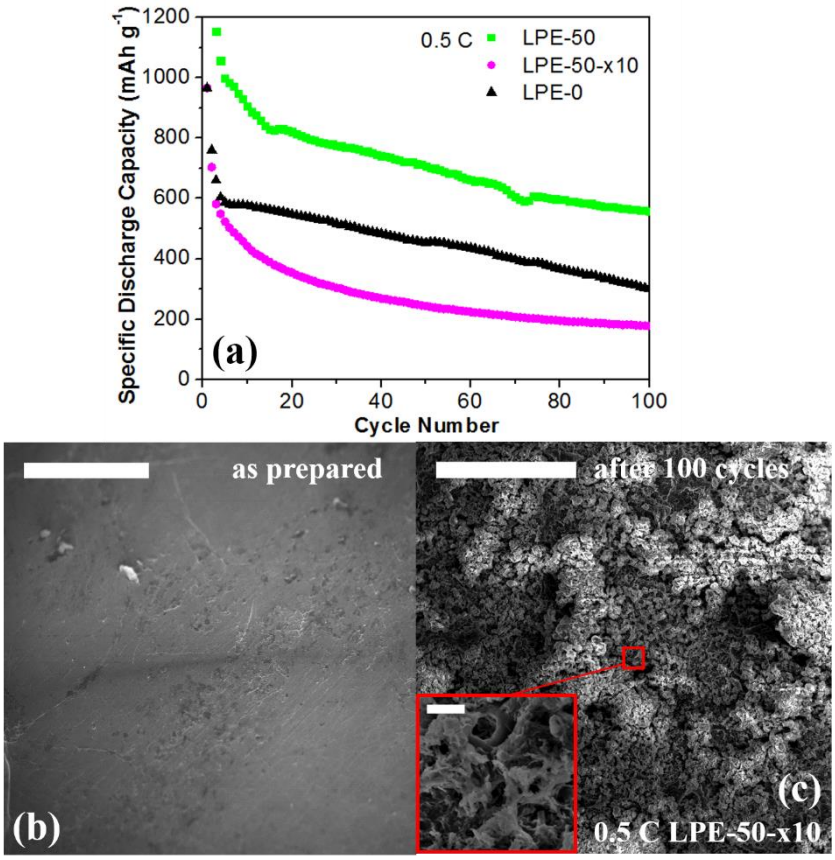

Figure 2-23 **(a)** Li-S full-cell galvanostatic charge and discharge profile at 0.5 C. **(b)** SEM surface image of LPE-50-x10 after pretreatment and **(c)** post-cycling surface SEM images of LPE-50-x10 after being cycled in Li-S full-cells at 0.5 C for 100 cycles. The insets show higher resolution SEM micrograph. Major scale bar of both images is 50-µm long. Inset scale bar is 2-µm long.

The Li-S full-cell performance was also studied. Figure 2-23 (a) shows the galvanostatic cycling profile of LPE-0, LPE-50 and LPE-50-x10. For LPE-50-x10, the cells decay fast and have a specific capacity of 177 mAh g^{-1} at 100 cycles, which is an even lower specific capacity compared to the one of LPE-0 (no pretreatment). Figure 2-23 (b) show the surface SEM images of LPE-50-x10 after pretreatment. Compared to the surface SEM image of LPE-50 after pretreatment shown in Figure 2-7 (b), the surface of LPE-50-x10 is much

rougher and a porous SEI layer may be formed. And it locally increased current density through pores which caused more severe dendrite growth during charge-discharge cycling, as shown in Figure 2-23 (c), the post-cycling surface image of LPE-50-x10 after being cycled in Li-S full-cells at 0.5 C for 100 cycles. Moreover, as Figure 2-20 shows, the surface layer has a very different chemical composition at high pretreatment current density. Obviously, the changed chemical composition and the poor conformality of the surface layer formed by high current density pretreatment cannot serve as an effective protection layer to suppress the dendrite formation (Figure 2-23 (c)), to improve the electrode stability, and Li-S cell performance. Instead, it exhibited negative effect to the Li-S full cell cycling performance.

This result demonstrates the importance of using small current density, which is equivalent to 0.01 C cycling, for pretreatment to form an ideal SEI layer. Such small current density guarantees the formation of a conformal, polymeric SEI layer that can accommodate volume change and stay conformal during electrochemical cycling, especially at high C-rates. Nevertheless, at large pretreatment current density, the DOL decomposes and undergoes more complex electrochemical reactions instead of simply electropolymerizing, along with the fast breakdown of Li salts. Moreover, the large current density 0.3 mA h cm^{-2} used for pretreatment is similar to 0.1 C for cycling with our mass loading. The poor battery performance at large pretreatment current density also serves as evidence that the naturally formed *in situ* SEI layer on the surface of unprotected anodes is not enough to protect the anodes from forming dendrites or parasitic reactions. These outcomes plausibly contribute to the damaged, unstable, and non-conformal surface layer that is unable to

protect Li anode from the undesired parasitic chemical and electrochemical reactions, and therefore leads to a fast capacity decay.

2.4 Conclusion and Future Work

2.4.1 Conclusion

The pretreatment of the Li anode at constant small current successfully formed a controlled, conformal and polymeric SEI layer which demonstrated exceptional battery performance in terms of specific capacity and power capability. An optimal pretreatment cycling number, LPE-50 was determined. Such improvement of performance largely came from the optimized surface conditions which effectively suppressed dendrite growth, accommodated volume changes during cycling, and prevented further erosion of Li anode. In addition, it retained excellent Li ion conductivity at optimal thickness. There may be a growing degree of cross-linking within the polymeric structure with the increase of pretreatment cycling number. The degree of cross-linking has both pros and cons in terms of polymeric properties and battery performance. Further investigation and manipulation of the cross-linking is crucial to the success of this anode protection method and it will be a continuing focus of our research.

2.4.2 Future Work and Prospect

Previous study has shown that "solvent-in-salt" electrolytes, which have ultrahigh concentration of LiTFSI salts can greatly improve the cyclability of the Li-S batteries by reducing the solubility of polysulfides and greatly increasing the Li-ion transference number.[138] However, using electrolytes of very high concentration can lower the energy

density of the battery system overall and may be too costly for industrial manufacturing. It could instead be a smart strategy for pretreatment of Li metal anodes which requires less electrolytes. However, there is a boundary to draw because high concentration of salt would also increase the viscosity of the electrolyte and lower the ionic conductivity of the electrolyte.[138] Therefore, the next step for the electrochemical pretreatment of Li metal anodes is to control the concentration of the Li salt in order to establish a correlation between it and the surface chemistry and chemical composition of the ASEI. In addition, because DOL is the main component in the ASEI and poly-DOL plays the major role in providing the flexible yet sturdy structure, it is worth studying the effect of using an electrolyte with higher DOL ratio or even pure DOL for the pretreatment of Li metal anodes. Pure DOL electrolyte is not feasible due to the less than half utilization rate of sulfur active material but it could be a great choice for pretreatment because no elemental sulfur is involved.[23, 139]

Another effort that can be pursued is to increase the amount of LiF in the ASEI which has proved to be able to fine tune the surface morphology and have large electrochemical stability window. This can be done by using lithium bis(fluorosulfonyl)imide (LiFSI) salt to replace LiTFSI salt due to the smaller anion size, higher ionic conductivity and easier to decompose on the surface of Li metal to donate F.[140, 141] Ether solvents used in the electrolytes can also be fluorinated to generate more LiF in the ASEI, which has seen some success in previous study in the cycling of Li-S full-cells.[142-144] At last, substituting the additive with fluorine containing compounds other than conventional $LiNO_3$ is another direction.[145]

The electrochemically pretreated Li metal is not restricted to liquid electrolyte Li-S batteries system, but could also be applied to other Li metal batteries system, including high voltage cathode (HVC) Li-ion batteries by pairing with $LiCoO_2$, $LiMn_2O_4$ and $LiNiMnCoO_2$ cathodes, which are important for the fulfillment of electric vehicles and grids. The pretreated Li metal can also be used with solid-state electrolytes, many of which have narrow electrochemical stability window and are prone to react with Li metal.[146] They also suffer from poor solid-solid contact as well. The malleable poly-DOL can be a natural wetting agent that could greatly diminish the interfacial impedance and the ASEI can serve as a barrier to block the degradation reactions between direct contact of Li and solid-state electrolyte.[147] Essentially, this ASEI can act as a pseudo-SSE to improve the anode/SSE interface and achieve great electrochemical performance. All in all, the electrochemical protection of Li metal is simple, feasible and can be finely tuned by varying the conditions of formations to meet diverse demands in different systems. Its application may not be restricted to liquid electrolyte Li-S batteries but can be deployed in many Li metal batteries system, and the electrochemical pretreatment strategy using poly-DOL might be potentially used in other metal anode systems.

3. Towards Solid-State Li-S Batteries and the Development of $Li_{10}GeP_2S_{12}$ (LGPS) Solid-State Electrolyte

The project described in this chapter was done in collaboration with Dr. Alexander Kozen and John Hoerauf of University of Maryland, Dr. Chuan-Fu Lin and Binh Hoang of the Catholic University of America. Dr. Kozen ran all the ALD coating processes, all the XPS characterizations and their data analysis. Binh Hoang and John Hoerauf participated in the fabrication of LGPS pellets after the method was developed by the author of the dissertation, Yang Wang. All the electrochemical testing and data analysis were done by the author of the dissertation, Yang Wang.

3.1 Introduction

3.1.1 Pros vs. Cons of Solid-State Electrolytes for Li-S Batteries

The inflammability of organic liquid electrolytes widely used in Li batteries, including Li-S batteries, has always been an issue due to the profound safety hazard. Therefore, using a nonflammable solid-state electrolyte (SSE) to replace the inflammable electrolyte is an ideal way to mitigate the safety concerns long associated with Li-ion and Li metal batteries, which has the potential to finally realize the goal of safely using Li metal in batteries to achieve much higher specific capacity and energy density.[81, 147] In addition to the intrinsic nonflammable nature of solid-state electrolytes, they also hold the following advantages over conventional liquid electrolyte, especially for Li-S batteries system. First, it can stop the diffusion of polysulfides and solve the low Coulombic efficiency problems from the

root by preventing the shuttle reactions from happening. Second, the stiffness of the SSE may be able to suppress the growth of dendrites on the surface Li metal based on some studies, which is another grave concern of safety. Moreover, SSEs generally have good mechanical strength, wide temperature ranges and high Li-ion transference number. The fact that they can be manufactured in large scale and tightly pressed with electrodes makes them more favorable for practical applications.[81, 148, 149]

However, solid-state electrolytes still face daunting challenges for wide commercialization due to series of intrinsic and practical reasons. First, SSEs generally have lower ionic conductivity of Li^+, many are several orders of magnitude lower than conventional liquid electrolytes. Second, the contact between SSEs and electrodes is bad due to the non-conformal morphologies of solids. The interfacial resistance that arises from the often point-to-face or point-to-point contacts worsens the capacity and energy density of the batteries. This issue is particularly severe in Li-S batteries on the interface between SSE and sulfur cathode. Sulfur is already being plagued by the intrinsic electronic insulating nature and requires conductive carbon substrates to improve it. The lack of contact would make it even harder to exploit sulfur encapsulated in carbon networks.[149] Third, SSEs, depending on the specific material, have different electrochemical windows. Therefore, it may be electrochemically unstable against either or both electrodes which can lead to rapid degradation and cell failure. Another very troubling fact discovered in recent years is Li dendrites can still grow in SSEs, often through the grain boundaries inside the solid state electrolyte pellets, due to the often-neglected electronic conductivity of SSEs, which is higher than liquid electrolytes.[150] Due to the high electronic conductivity, dendrites not only can grow from anodes to cathodes, but can grow in the middle of SSEs, especially

along the grain boundary, which is defined as the interface between LGPS particles, and inside voids and cracks. All those urgent issues demand attention in order to push the solid-state technologies forward.[81, 147]

3.1.2 $Li_{10}GeP_2S_{12}$ (LGPS), the Promising Candidate

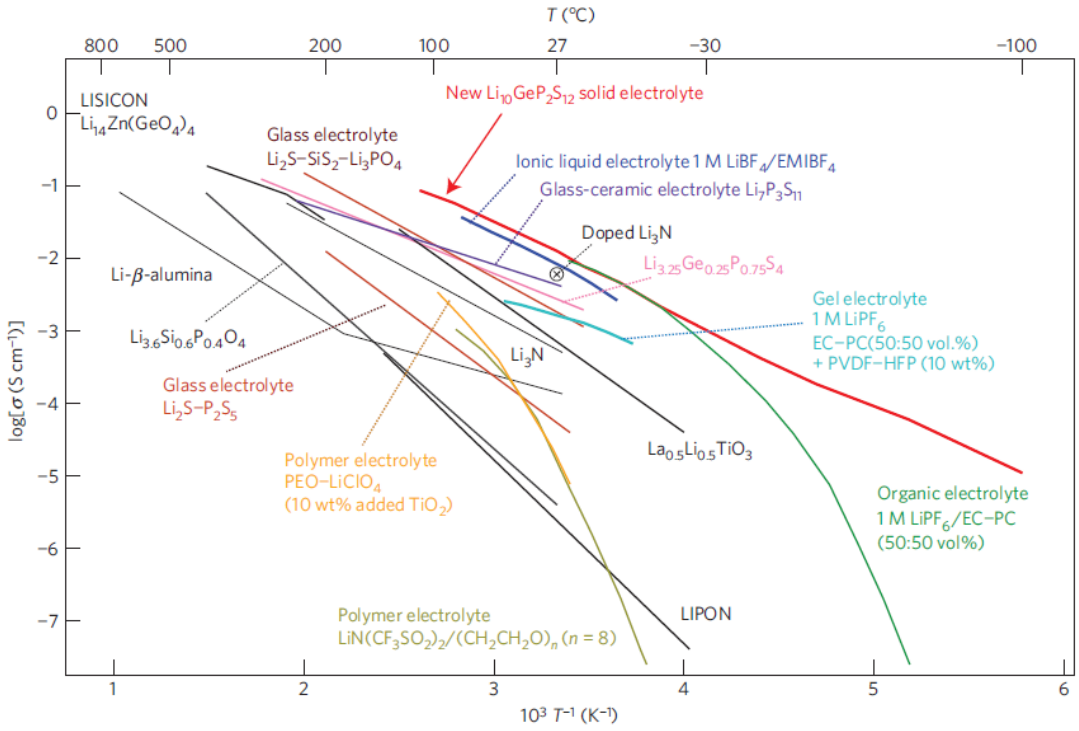

Figure 3-1 Thermal evolution of ionic conductivity of the new $Li_{10}GeP_2S_{12}$ phase, together with those of other lithium solid electrolytes, organic liquid electrolytes, polymer electrolytes, ionic liquids and gel electrolytes. Reproduced with permission.[3]

In 2011, Kamaya et al. first discovered a sulfide superionic conductor $Li_{10}GeP_2S_{12}$ (LGPS) and it has since changed the landscape of solid-state electrolytes. LGPS has a theoretical ionic conductivity of 1.2 x 10^{-2} S cm^{-1}, which is comparable or even higher than commonly used liquid electrolytes and far higher than many other solid-state electrolytes, as shown in Figure 3-1. $Li_{10}GeP_2S_{12}$ has a three dimensional framework structure consisting of $(Ge_{0.5}P_{0.5})S_4$ tetrahedra, PS_4 tetrahedra, LiS_4 tetrahedra and LiS_6 octahedra, as shown in

Figure 3-2. In crystalline solid materials, the transport of ions depends on the concentration and distribution of defects. In order to have high ionic conductivity in solids, an open crystal structural framework, a high concentration of mobile ion carriers and highly polarizable ions to lower the migration energy barriers are all essential.[81] The structure has a one-dimensional (1D) lithium conduction pathway along the c axis. Mo et al. also studied it has weak conduction pathways formed by corner sharing LiS_4 tetrahedra in the ab plane. The fast 1D diffusion along the c direction and slower Li^+ diffusion in the ab plane

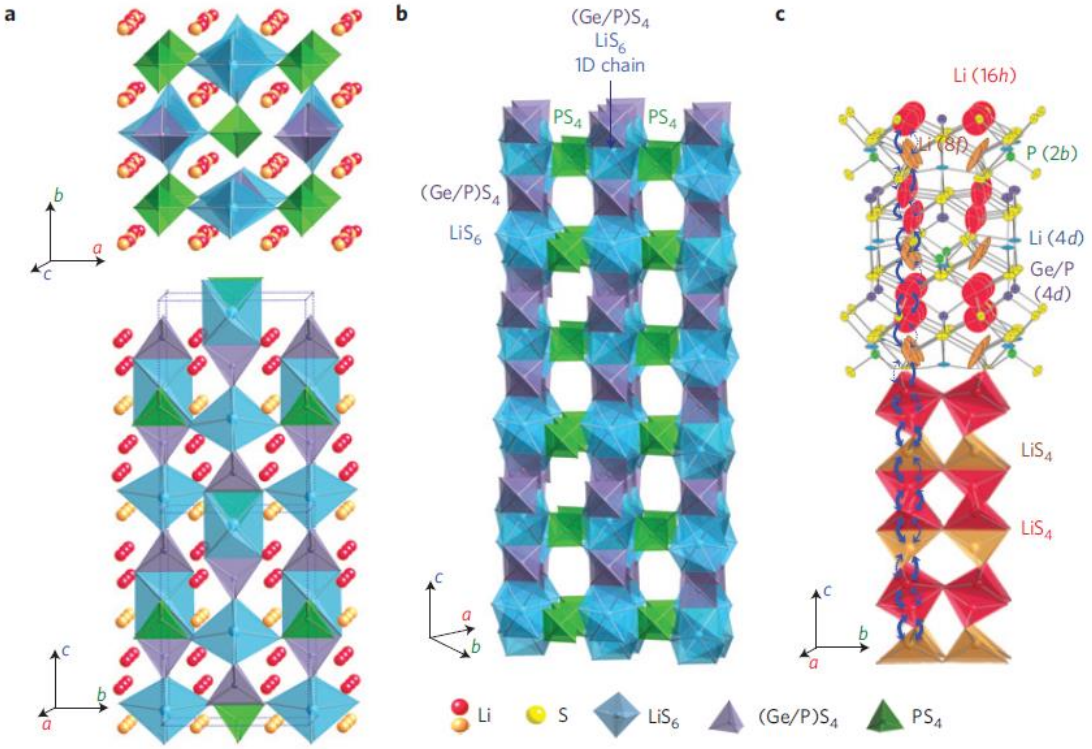

Figure 3-2 Crystal structure of $Li_{10}GeP_2S_{12}$. **(a)** The framework structure and lithium ions that participate in ionic conduction. **(b)** Framework structure of $Li_{10}GeP_2S_{12}$. One-dimensional (1D) chains formed by LiS_6 octahedra and $(Ge_{0.5}P_{0.5})S_4$ tetrahedra, which are connected by a common edge. These chains are connected by a common corner with PS_4 tetrahedra. **(c)** Conduction pathways of lithium ions. Zigzag conduction pathways along the c axis are indicated. Lithium ions in the LiS_4 tetrahedra (16h site) and LiS_4 tetrahedra (8f site) participate in ionic conduction. The anisotropic character of the thermal vibration of lithium ions in three tetrahedral sites gives rise to 1D conduction pathways. Reproduced with permission.[3]

contributed to the exceptional ionic conductivity that LGPS has.[3, 151, 152]

Currently, LGPS powder of ionic conductivities ranging from half of the theoretical value, to near the theoretical value with a grain size as small as 3 microns is commercially available and well-defined. The most common way of using it is by cold pressing the powder into disk pellets,[153-155] thanks to the fact that LGPS has a Young's modulus in between oxide SSEs and polymer SSEs which makes it softer.[152, 156, 157] However, it has been observed that the cold pressed LGPS pellets have a very porous structure and porous structures are not beneficial for accomplishing its high ionic conductivity, as the pores act as barriers to Li^+ migration in the SSE.[158] Moreover, pellets pressed at low temperature often have particles poorly agglomerated together and lack good contact. Additionally, it is reported that cold pressing of sulfides can result in the formation of an intermediate layer and may induce irreversible side reactions during electrochemical testing which would decrease the cell performance.[157, 159, 160] In order to fully realize its potential of high ionic conductivity, hot press to fabricate the pellets is necessary. Hot press is one of the most common ways for materials fabrication since it may yield favorable crystalline structures that have higher ionic conductivities.[161-164] Hot press under high pressure to make pellets can greatly densify the pellets and decrease the porosity to increase the mechanical strength of the pellets which is extremely important to withstand the drastic volume change of electrodes during cycling, while the annealing can also largely reduce the grain boundary impedance to have more robust electrochemical properties.[163-166] However, it is not always good to press the pellets at a temperature too high because it may exacerbate the microcracks within the SSE due to the growth of grain size at higher temperature.[160, 164] It is important to note that hot pressing of an already made powder into pellet does not change the ionic conductivity of the bulk material, but by densifying it to improve the contact

within SSEs and decrease grain boundary resistance. To our knowledge, the fabrication of LGPS by hot press has not been reported before and it will be discussed in the following section.

3.1.3 Issues on the Interface and the Strategies of Surface Protection

Although LGPS has high ionic conductivity and several advantages over other common SSEs, it suffers from its incompatibility with both Li metal anodes and conventional Li-ion cathodes. The thermodynamic electrochemical stability window of LGPS is only from 1.7 V to 2.5 V (vs. Li^+/Li), which makes it a lot narrower than common SSEs and oxide SSEs.[151, 152, 167] On the anode side, at below 0.6 V (vs. Li^+/Li), the Ge in LGPS would form alloy with Li and the product is electronic conductive which makes it prone of continuous degradation and facilitates the growth of Li dendrites.[168-170] On the cathode side, due to the high voltages of conventional Li-ion cathodes, the oxide cathodes with transition metal would spontaneously react with sulfide to form metal sulfides and such side reaction products build a non-passivating mixed ionic and electronic conducting interface, which allows the degradation to go on and generate an incompatible interface that would lower the ionic conductivity.[152, 157, 171, 172] Nonetheless, the low operation voltage of S cathodes, which is generally a disadvantage due to the lowered energy density of the battery, turns out to be a good thing since it falls within the electrochemical window of LGPS and make them compatible.[156, 157]

Quite a lot of work has been done to address the interfacial incompatibility issue to improve the electrochemical stability.[173-177] One of the most feasible and effective method is surface protection using artificial SEI (ASEI) layer, either on the electrodes or on the surface of LGPS pellets. By using the ASEI, it can block the direct contact electrodes and LGPS solid-

state electrolyte thus preventing the spontaneous interfacial reactions from happening upon assembly of the cells. By applying the appropriate ASEI that has an electrochemical stability window that matches the cathodes and the anodes, it can effectively bridge the gap of electrochemical window between the electrodes and LGPS, therefore protecting LGPS from unwanted side reactions.[159, 178]

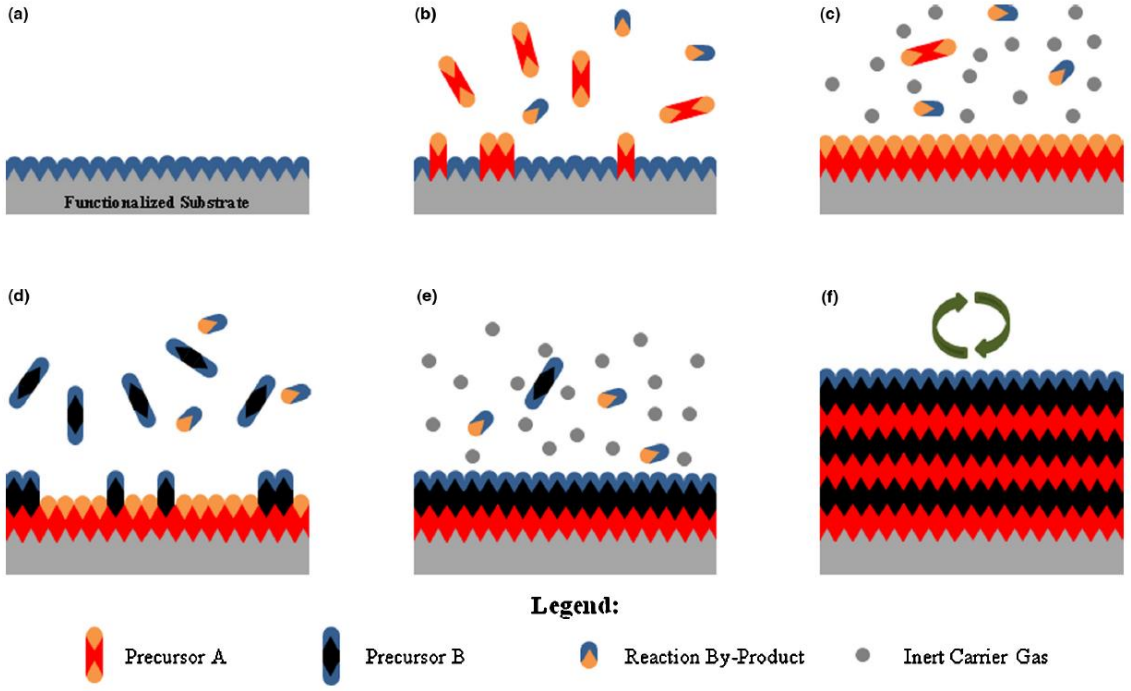

Figure 3-3 Schematic of ALD process. (**a**) Substrate surface has natural functionalization or is treated to functionalize the surface. (**b**) Precursor A is pulsed and reacts with surface. (**c**) Excess precursor and reaction by-products are purged with inert carrier gas. (**d**) Precursor B is pulsed and reacts with surface. (**e**) Excess precursor and reaction by-products are purged with inert carrier gas. (**f**) Steps 2–5 are repeated until the desired material thickness is achieved. Reproduced with permission.[2]

To be a good ASEI candidate, the material itself must be chemically and electrochemically stable against both the SSE and electrodes within the operation voltage window. It needs to have reasonable mechanical strength that can suppress the dendrites but also malleable enough to accommodate the volume change. It must have ionic conductivity high enough to retain the energy density of the cell. The ASEI should be electronically as insulating as

possible to prevent the growth of dendrites and plating of Li on top of the ASEI which would make every effort moot.[159]

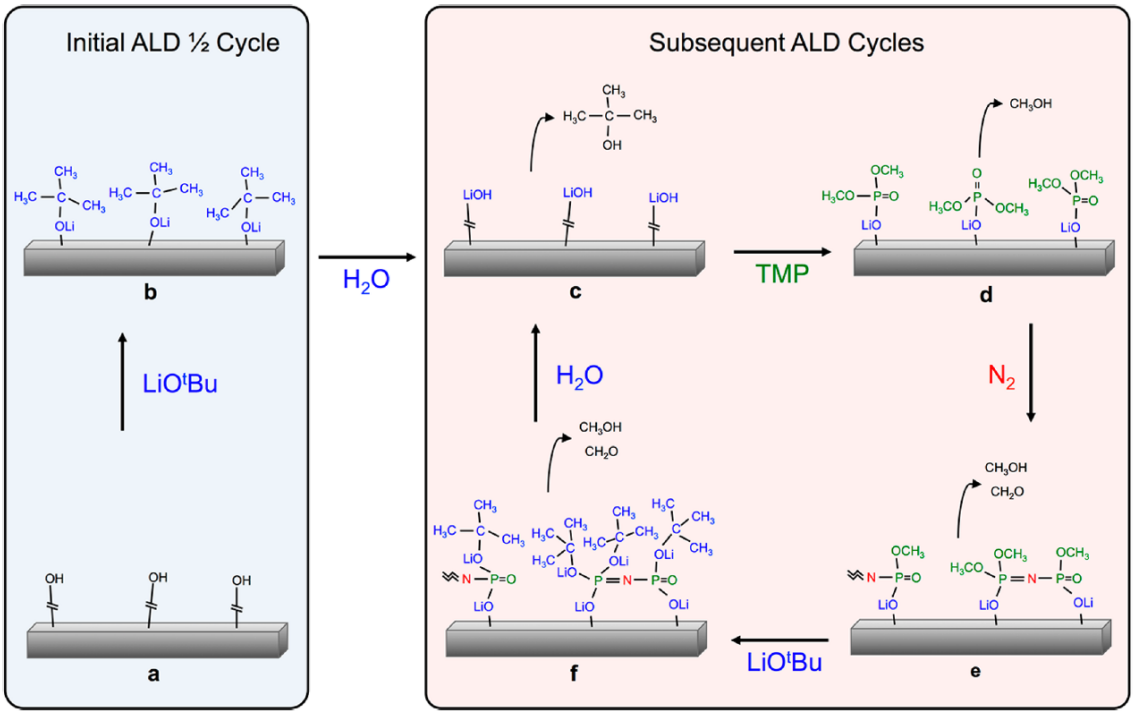

Figure 3-4 Cartoon of the Proposed ALD LiPON Process Chemistry. (**a**) Hydroxyl terminated substrate; (**b**) metastable surface after the LiOtBu pulse; (**c**) H_2O pulse removes the tert-butanol ligands and forms LiOH on the surface; (**d**) TMP reacts with surface LiOH through ligand exchange reaction, evolving CH_3OH; (**e**) N_2 plasma cross-links phosphorous atoms and evolve CH_3OH and CH_2O; (**f**) LiOtBu reacts with $-OCH_3$ ligands and evolves both CH_2OH and CH_2O. The initial LiOtBu and H_2O pulses shown in (**a**) and (**b**) are required "activate" the substrate prior to deposition. For all subsequent ALD cycles, the process chemistry in (**c**) through (**f**) is repeated as one ALD cycle. Reproduced with permission.[5]

Atomic Layer Deposition (ALD) is an effective method to create such an ideal ASEI layer. It is a thin film deposition technique employs self-limiting gas-solid reactions. As shown in Figure 3-3, a functionalized substrate first reacts with pulsed in precursor A. By controlling the reaction time, the surface of the substrate can be completely saturated while no more than one monolayer of reaction product can grow on the substrate. Subsequently, carrier gas purges out all unreacted remaining precursor A and reaction by-products. A second precursor B is then pulsed in and reacts with the just formed monolayer to build up another monolayer. Then the remaining precursor B and by-products are purged out. By

repeating such steps, with finely tuned pulsing time and the total number of steps and choosing the right precursors, a thin film with desired thickness, composition and a conformal morphology can be developed.[2] ALD has found broad success in depositing metal oxide thin films and has been small-scale commercialized.[2, 179, 180] Among all the viable deposited products, lithium phosphorus oxynitride (LiPON) is a promising candidate due to its large electrochemical stability window against both high voltage cathodes and Li metal anodes, and an acceptable ionic conductivity of ~10^{-6} S cm^{-1}. It has found success in microscale all-solid-state batteries but is generally too thin to serve as solid-state electrolyte. However, that makes it a perfect candidate to be the ASEI for LGPS.[181, 182] In this Chapter, the LiPON ALD-coating process was developed by Kozen et al. and operated by Dr. Alexander Kozen. The illustration of the protocol is shown in Figure 3-4.[5] It uses lithium tert-butoxide (LiOtBu), H_2O, trimethylphosphate (TMP), and plasma N_2 as precursors. The layer is thin, conformal and has demonstrated good electrochemical stability up to 5.5 V vs Li^+/Li and ionic conductivity up to $2x10^{-6}$ S cm^{-1}. Therefore, it is being used to coat the surface of LGPS to serve as a protective ASEI.[5]

Another surface protection strategy is to use the Li protected by elastomer, which is formed by electrochemical polymerization of DOL, as anodes which has been extensively discussed in Chapter 2. This elastomeric ASEI consists of both inorganic components and organic poly-DOL has demonstrated excellent properties to suppress dendrites, accommodate volume change and prevent side reactions from electrolytes and polysulfides.[29] Naturally, this ASEI layer on the surface of Li metal anodes may also serve as a barrier to block the detrimental reactions between Li metal anodes and LGPS SSE. The sulfide SSEs including LGPS are especially vulnerable to large cycling current

densities due to the Li metal/SSE interface can experience large strains from volume expansion and nonuniform Li stripping and plating during cycling, which easily leads to cell failure.[159]

3.1.4 Objectives

In this chapter, our research focused on the control study of hot press of LGPS using a commercial powder purchased from MTI, Inc. We characterized and electrochemically tested the LGPS pellets pressed at different temperatures. An optimal pressing temperature was narrowed down and was used to press pellets for further ASEI surface protection. We studied using ALD-coated LiPON as an ASEI for LGPS to serve its protective purpose. The surface chemistry of LGPS with or without ASEI were also studied to understand how LGPS degrades upon atmospheric exposure, upon reaction with H_2O and O_2 in controlled conditions, and upon exposure to liquid carbonate electrolytes, and ultimately how LiPON ASEI layers can mitigate these degradation reactions.

3.2 Experimental

3.2.1 The Fabrication of LGPS Pellets

Commercially available $Li_{10}GeP_2S_{12}$ (LGPS) powder was purchased from MTI Corp. The stand-alone SSE pellets were prepared by pressing 0.120 g of LGPS powder at ~300 MPa using a hydraulic press and a heatable die set (temperature control range 25 ºC - 250 ºC) with a diameter of 12.7 mm (0.5”) in an Ar-filled glove box. The pressure was added, and the pressing started when the die set was heated to the desired temperature. After 5 minutes, the heating program was turned off to let the die set cool down naturally. For different

pressing temperatures, the allowed cooling down time was different to ensure safe operation but the total pressing time under ~300 MPa pressure was kept at 45 minutes. To acquire dense pellets with optimal mechanical and electrochemical characteristics, different pressing temperatures were used including 100 ºC, 150 ºC, 175 ºC and 200 ºC. As control, pellets were also pressed at room temperature (20 ºC) which are described as cold pressed pellets.

Three different masses of LGPS powder, 0.12 g, 0.24 g and 0.40 g respectively were used for pellet pressing at 150 °C and ~300 MPa to obtain hot pressed LGPS of different thicknesses to deconvolute the EIS spectra.

3.2.2 Electrochemical Testing and Characterizations

Electrochemical impedance spectroscopy (EIS) was used as the main tool to study the interfacial evolution under different conditions and investigate the changes of ionic conductivity of different interfacial and bulk components. 0.75 mm thick Li ribbon (Alfa Aesar) was cut into 12.7 mm in diameter disks with a 1/2-inch punch. Li/LGPS/Li symmetric cells were assembled in an Ar-filled glove box for testing. The frequency range was set between 1 MHz and 10 mHz, and the AC amplitude of the measurement is 10 mV. The EIS measurements results were processed by EC-lab software using Z-fitting. Equivalent circuits were also simulated. The equation used for calculating the ionic conductivity of the bulk LGPS pellet with the simulated impedance is shown in Equation 3.1,

$$\sigma = \frac{1}{R} \text{ x } \frac{l}{A}$$

Equation 3.1

where σ is the ionic conductivity, R is the impedance, l is the length of the cross-section of the conducting medium and A is the area of the conducting medium.

Cyclic voltammetry (CV) was used to study the electrochemical evolution of the LGPS pellets with or without the ALD-coated LiPON ASEI layer over a wide voltage window. Li/LGPS/Li symmetric cells were assembled for testing. The voltage window is from +5.0 V to -0.5 V (vs. Li^+/Li) with a scan rate of 0.1 mV s^{-1}. The cells were run by testing EIS+CV alternately over time and a total of four cycles of EIS and three cycles of CV were run. Galvanostatic charging and discharging was used to study the battery performance of the LGPS pellets and to examine the effect of ASEI with ALD-coated LiPON. Li/LGPS/Li symmetric cells were assembled for testing. Cells were tested at 1 mA cm^{-2} current density with a compliance voltage window of -5 V to +5 V (vs. Li^+/Li) then run at 3 mA cm^{-2} current density with the same voltage window. For both current densities, each charging or discharging cycle is 5 minutes, for a total of 30 full cycles. As a baseline, the 3 mA cm^{-2} current density is close to 1 C current as in C-rate for the cycling of liquid electrolyte Li-S batteries, and 10 C current for liquid electrolyte Li-ion batteries. Generally, 0.05 C current density is used for solid-state Li-S batteries cycling.

3.2.3 The Designs of Cells for the Electrochemical Testing of LGPS Pellets

To find the most reliable way to electrochemically test LGPS pellets, different configurations of electrochemical cells were designed and tested over time. Conventional CR 2032 coin cells with two 0.2 mm thick, 15 mm in diameter 304 stainless steel spacers plus one 1.2 mm high 304 stainless steel spring washer were used each cell. The spring washer was later replaced by one 1.6 mm thick, 12.7 mm in diameter nickel foam disk to provide better contact and accommodation of cell compactness. I-cells were later designed by drilling through a union, 12.7 mm in diameter perfluoroalkoxy alkane (PFA) Swagelok

tube fitting, with 304 stainless steel rod as current collector from both ends. At last, split cells purchased from MTI Corp with an inner diameter of 15 mm were used. All the electrochemical testing results presented in the following sections were using the split cells, unless otherwise specified.

3.2.4 ALD LiPON Coating Process

LGPS pellets were transferred to an Ultratech Fiji F200, where the LiPON ALD films were deposited at 150 °C using the precursors lithium tert-butoxide (LiOtBu) (Aldrich, 99.7%), deionized H_2O, trimethylphosphate (TMP) (Aldrich, 99.9%), and N gas (Praxair, grade 5.0). Argon (Airgas, grade 5.0) was used as a carrier gas. The base pressure of the ALD reactor was $< 2 \times 10^{-6}$ Torr, and a process pressure of 200 mTorr was maintained via Ar gas flow. The solid LiOtBu precursor was kept at 165 °C and was delivered to the ALD chamber using a bubbler with 40 standard cubic centimeters per minute (sccm) argon carrier gas flow. ALD films were deposited using precursor saturation doses of 20 s for the LiOtBu, 0.06 s for the H_2O, and 0.4 s for the TMP with 30 s purges after each precursor dose. The $^{P}N_2$ exposure was fixed at 10s at a 40 sccm flow rate and a plasma power of 300 W, and a 5 s purge step was included after the $^{P}N_2$. The growth rate of ALD LiPON was 0.55 Å/cycle as determined by spectroscopic ellipsometry (J.A. Woollam M-2000D, λ = 193−1000 nm) using a B- spline optical model on silicon substrates included with each deposition.[5] 10 nm-thick LiPON was coated onto LGPS pellets for XPS analysis because the detection limit in thickness of material of XPS analysis is around 10 nm and any thicker LiPON could completely block the detection of LGPS underneath it. 20-nm-thick LiPON was coated onto LGPS pellets for electrochemical testing.

After LiPON deposition, samples were transferred directly into an Ar-filled glovebox, where they were flipped upside down to expose the other side of the pellets, loaded back into the vacuum system, and the LiPON deposition was repeated on the uncoated side of the pellets.

3.2.5 Characterizations

Post-deposition, samples were transferred under UHV from the ALD system to a Kratos Ultra DLD XPS system. Survey spectra were collected without charge neutralization using a 12 kV monochromatic Al Kα X-ray source in hybrid lens mode with a step size of 1 eV and pass energy of 160 eV. High-resolution spectra were collected using a 12 kV monochromatic Al Kα X-ray source in hybrid lens mode with a step size of 0.1 eV and pass energy of 20 eV. XPS data were analyzed using CasaXPS with peak area quantification normalized by standard photoionization cross sections corrected for our instrument geometry23 and a Shirley background algorithm.[5]

To understand if the hot pressing of LGPS at higher temperature could have altered the surface chemistry of the LGPS pellets, both LGPS pellet cold pressed at 20 °C and hot pressed at 150 °C were analyzed using XPS with same experimental conditions described above.

SEM cross-section imaging was done with a Tescan XEIA Plasma FIB/SEM.

3.3 Results and Discussion

3.3.1 The Roadmap of Cell Design for the Electrochemical Testing of LGPS Pellets

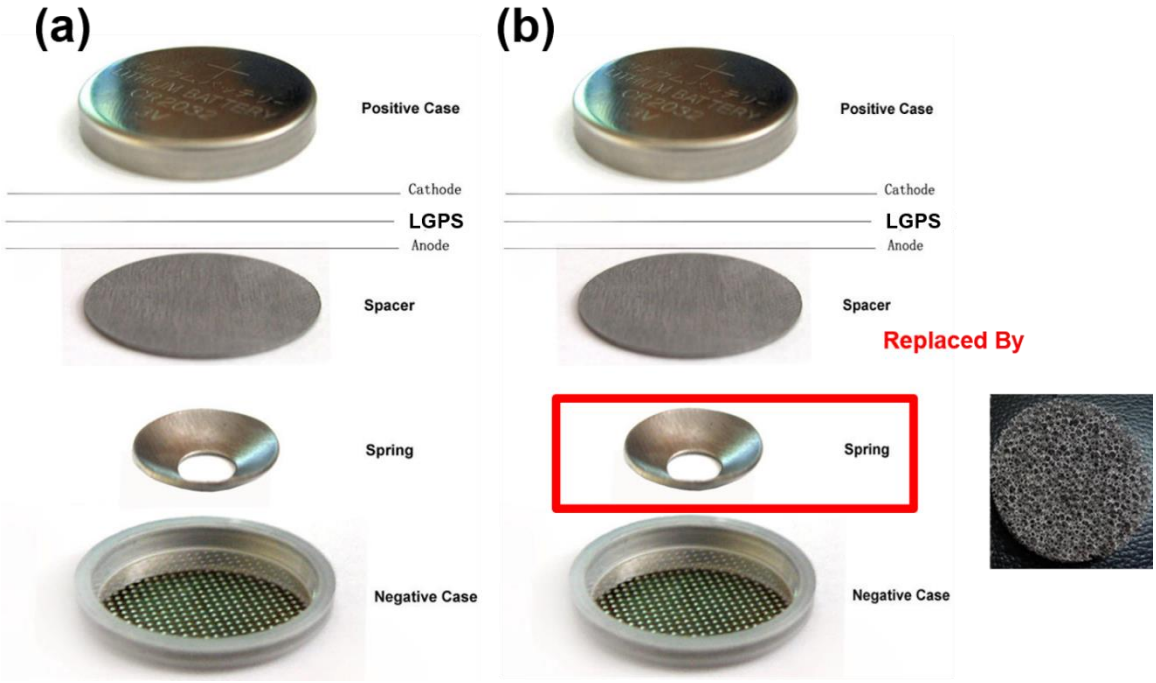

Figure 3-5 Coin cell configuration for Li/LGPS/Li symmetric cell testing. (**a**) with stainless steel spring washer and (**b**) the spring washer is replaced by a more squeezable and accommodating Ni foam disk.

An electrochemical cell with proper configuration is crucial for the reliable measurements of LGPS pellets. We started with the most basic and conventional method, by putting the Li/LGPS/Li sandwich in CR 2032 coin cells with two thin stainless steel spacers plus one stainless steel spring washer in each cell, as shown in Figure 3-5 (a). However, we quickly discovered that this option is not viable. The LGPS pellet was crushed into tiny pieces when the coin cells were assembled using a crimping machine. LGPS pellet is quite brittle and the stainless-steel spring washer is not accommodating enough. Even though the pressure of the crimping machine can be adjusted, the presser inside the cell is impossible

to measure and control. Therefore, the actual measured EIS spectra do not represent the bulk LGPS but the tiny pieces. Due to this concern, we replaced the stainless-steel spring washer with nickel foam, which can be greatly squeezed and provides better accommodation when the cells are crimped. Nonetheless, the replacement did not change the irreproducibility of the measurements using coin cells and we faced a new issue which is bad contact due to the insufficient compactness inside the cell caused by Ni foam not being supportive of the cell structure enough.

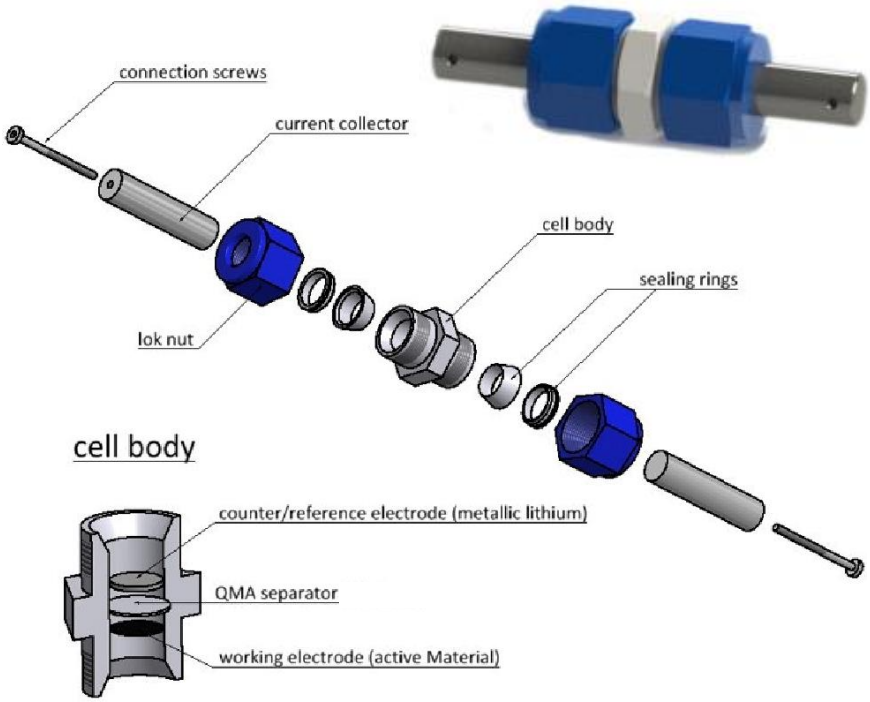

Figure 3-6 I-cell configuration for Li/LGPS/Li symmetric cell testing. It is based on a drilled-through PFA Swagelok tube fitting with union opening 12.7 mm in diameter. The figure is created by Dr. Alexander Kozen.

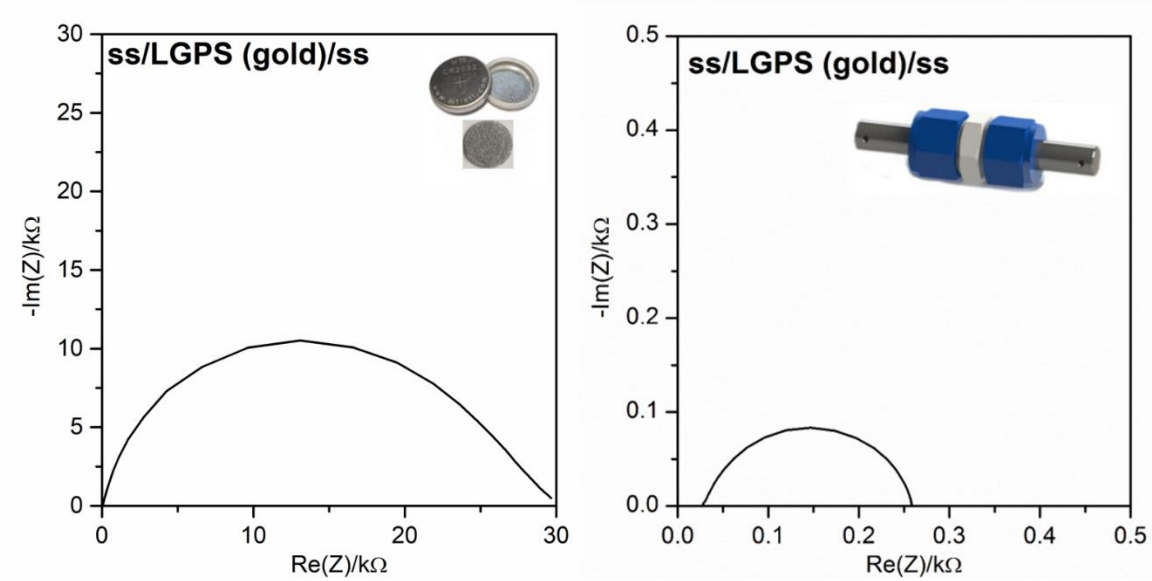

Figure 3-7 EIS measurement comparison between two cells. The left is the EIS spectrum with coin cell. The right is the EIS spectrum of I-cell.

The failure with coin cells led us to explore other alternatives and the first candidate is an I-cell as shown in Figure 3-6. We summarized that the issues we encountered with using coin cells is a) impossible to control the compactness of the cell to not crush the pellet while b) maintaining a good contact between each part of cell to get reliable measurements. The drilled-through I-cells allow us to fully press the two stainless steel rods together, which serve as current collectors and connection to the external circuit, to get good contact while we can still control the tightness and the force applied to not crush the pellets. We did see great improvement in terms of reproducibility of the measurements but also the reliability of the measurement, as shown in Figure 3-7. The EIS was done by measuring a stainless-steel disk/LGPS/stainless steel disk sandwich. Gold was sputtered on both sides of LGPS to improve contact due to the rough surfaces of both LGPS pellet and stainless-steel disk rendered extremely large interfacial impedance. It is clearly shown on the right that by using the I-cell, lower cell impedance results in an ionic conductivity closer to the theoretical value of LGPS. The ionic conductivity calculated from the measured impedance

is a lot closer to theoretical ionic conductivity of LGPS, though it's still 20 times larger than the values we measured from split cells, which will be shown later. However, we did not stick with I-cells for a long time because we soon found that the assembly of I-cells are hard to be consistent. Because it is open on both ends, fixing one stainless steel rod on one side while gently but tightly enough to close from the other side is clumsy and difficult to achieve reproducibly in a glovebox. In addition, due to the inner diameters of the I-cell, the LGPS and the Li disks were all the same size in diameter, putting them together with good contact proved to be challenging.

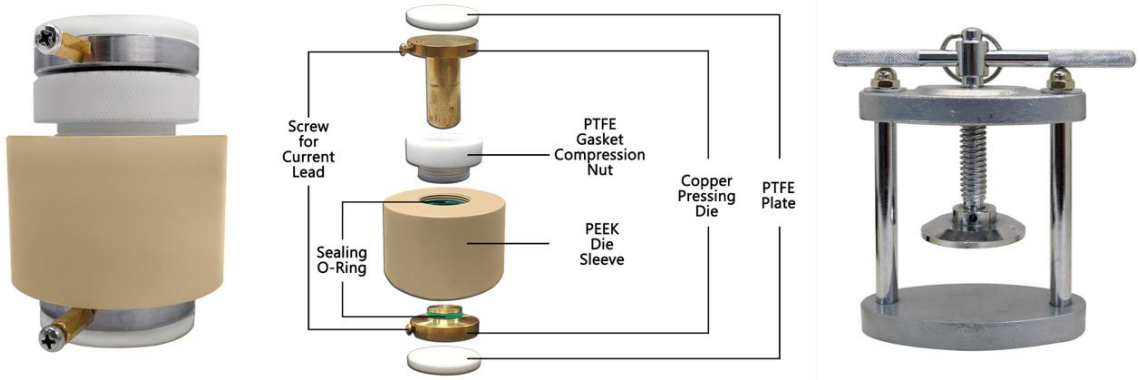

Figure 3-8 Split compression cell and the manual press used to hold it under constant pressure.

Therefore, we came to our last candidate which is the split cell we bought from MTI Corp and it proved to be a success, as show in Figure 3-8. The split cell offered total reliability and reproducibility of the results and maintained good contact of each component without crushing the LGPS pellets. We also summarized the error of measurement and the measured ionic conductivity comparing all four cell designs which is shown in Figure 3-10. It also shows that the split cells have the smallest error in measurements and result in the largest measured ionic conductivity. Based on the results, all the following tests were all done with split cells, unless specifically stated.

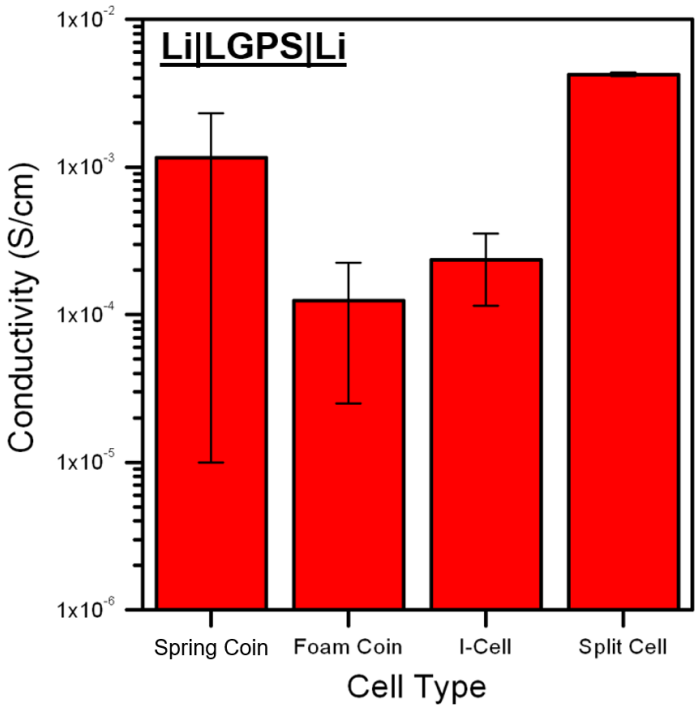

Figure 3-10 Comparison of different cell designs and the errors in measurement. Figure was made by Dr. Alex Kozen.

3.3.2 The Optimization of Hot Pressing of LGPS Pellets

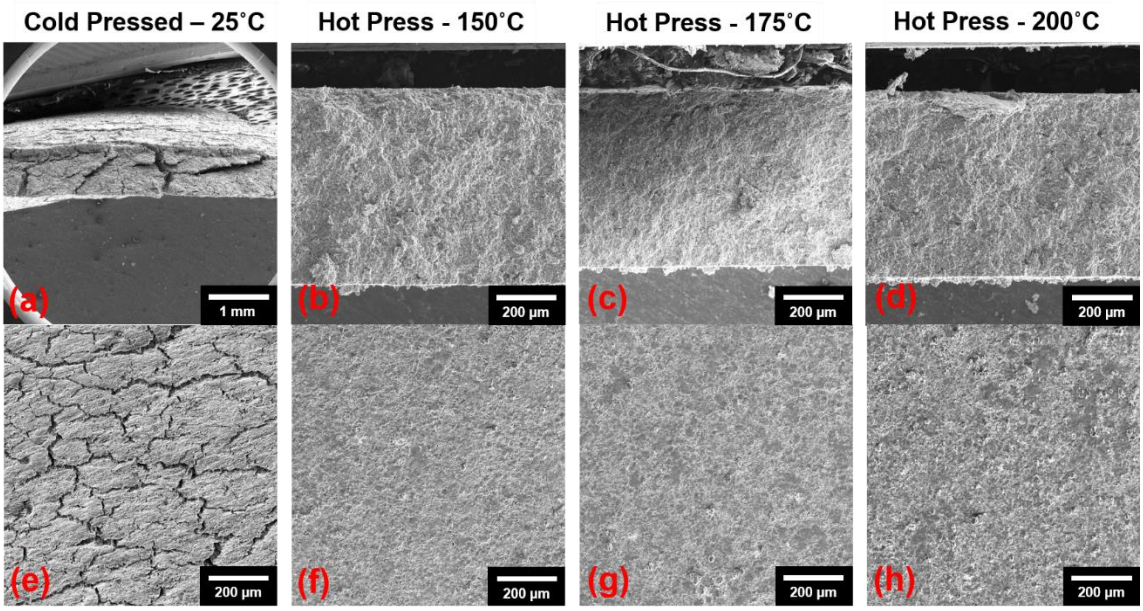

Figure 3-9 SEM cross-section images of LGPS **(a)** cold pressed at 20 ºC and hot pressed at **(b)** 150 ºC, **(c)** 175 ºC and **(d)** 200 ºC, and SEM surface images of LGPS **(e)** cold pressed at 20 ºC and hot pressed at **(f)** 150 ºC, **(g)** 175 ºC and **(h)** 200 ºC. The SEM images were captured, and the figure was made by Dr. Alexander Kozen.

In order to determine the optimal temperature for fabrication of LGPS pellets, we studied the effect of pressing temperature on the ionic conductivity and pellet density and proved the necessity of hot pressing. The SEM cross-section images of four different LGPS pellets cold pressed at 20 ºC, hot pressed at 150 ºC, 175 ºC and 200 ºC respectively are shown in Figure 3-9. It is clearly shown that the cold pressed pellets have large micron-level cracks both on the surface, as shown in the inset, and throughout the entire pellet. Such large cracks have multiple detrimental effects. First, it decreases the overall ionic conductivity due to the bad contact. The cold pressed pellet appears to consist of bulk materials barely agglomerate and hold together by force, without a robust, cohesive structure. The lack of good contact as a whole increases the grain boundary resistance and lowers the ionic conductivity of the pellet. Second, such large cracks indicate a lack of mechanical strength which would cause the SSE to easily fail under drastic volume change of electrodes during electrochemical cycling, and potentially due to the volume change of LGPS during electrochemical reactions as well. Third, it provides an easy pathway for the growth of dendrites through the open cracks. Even though LGPS is not flammable, which reduces the safety hazard, it still results in the failure of the batteries by short-circuiting. Last but not least, LGPS requires surface protection to extend its electrochemical stability window and to work with Li metal. However, with micron-sized cracks, ALD-coated LiPON would not be able to fully cover the surface of LGPS pellets nor the voids and cracks inside, which makes the ASEI protection moot. As a comparison, the SEM images of three hot pressed pellets show a dense and compact cross-section with no visible cracks or voids. It shows that the hot pressing of LGPS pellets successfully densified the structure and improved the

contact which can greatly reduce the grain boundary resistance to yield enhanced electrochemical performance.

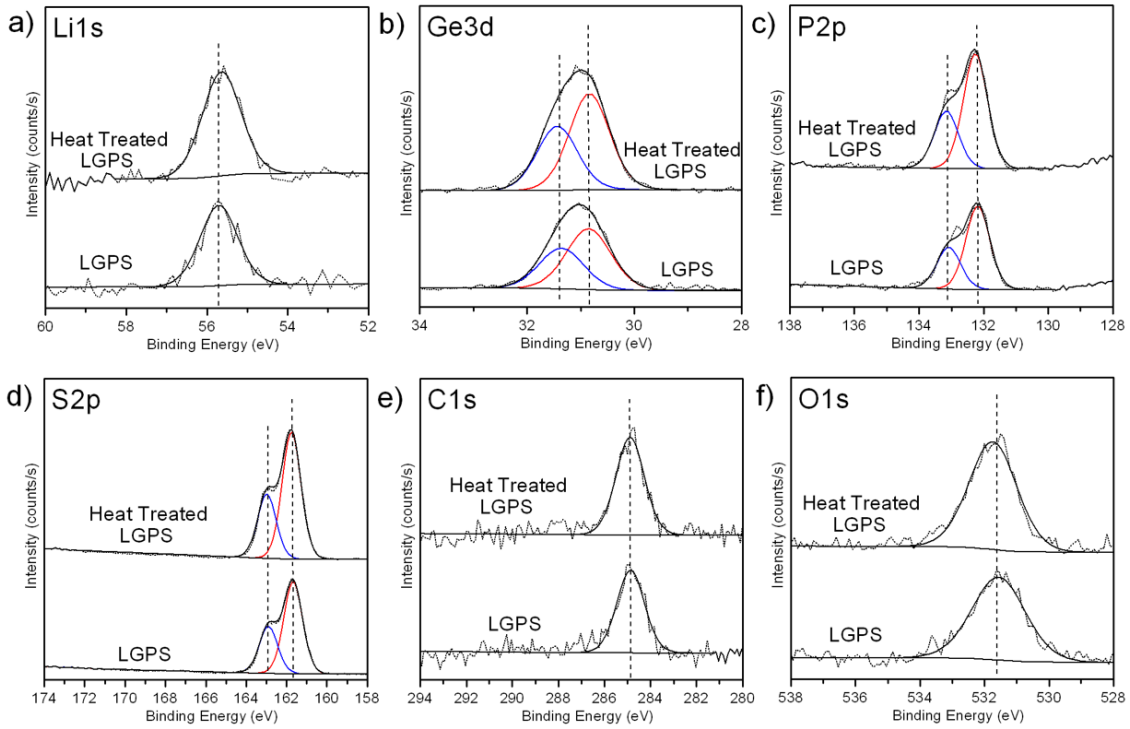

Figure 3-11 High resolution **(a)** Li 1s, **(b)** Ge 3d, **(c)** P 2p, **(d)** S 2p, **(e)** C 1s and **(f)** O 1s XPS spectra of LGPS pellets cold pressed at 20 °C and hot pressed at 150 °C. Figures created by Dr. Kozen.

To understand if hot pressing of LGPS pellets at higher temperature could alter the surface chemistry and chemical composition of the pellet, XPS analysis were conducted on both LGPS pellets cold pressed at 20 °C and hot pressed at 150 °C and the high resolution spectra are shown in Figure 3-11. There essentially are no changes in any of the spectra and the peaks of hot pressing and cold pressing fully align with each other. It can be concluded that hot pressing at 150 °C does not change the surface chemistry or chemical composition of LGPS pellets.

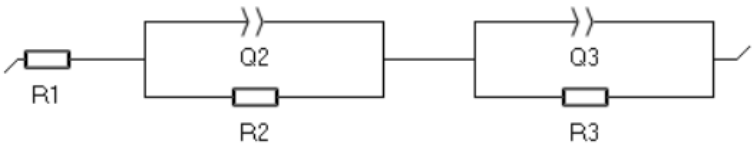

Figure 3-12 Equivalent circuit of Li/LGPS/Li configuration with no ASEI. R1 correspond to contact resistance. R2 and Q2 correspond to bulk LGPS pellet. R3 and Q3 correspond to the interfacial degradation layer formed between Li and LGPS.

In order to narrow down the optimal pressing temperature, we used electrochemical impedance spectroscopy (EIS) to measure and simulate the ionic conductivity. For a Li/LGPS/Li symmetric cell configuration without ALD-LiPON coating, we expect it to consist of the following components. First, a contact resistance including the resistance of the wires, the Li metal and stainless-steel rods used in the connection of the circuit. Second, the bulk LGPS pellet which functions as a resistor and the ionic conduction within the SSE can be represented with a capacitor. The capacitor can be replaced with a constant phase element (CPE) which describes a circuit component that models the behavior of an electrical double layer which is an imperfect capacitor. Therefore, the bulk LGPS can be represented with a parallel R/C or R/Q (Q represents CPE) circuit unit. Similarly, the interfacial layer made of degradation products of reactions between Li metal and LGPS can also be represented by an R/C or R/Q circuit unit.[183] The equivalent circuit for the simulation of EIS spectra is shown in Figure 3-12.

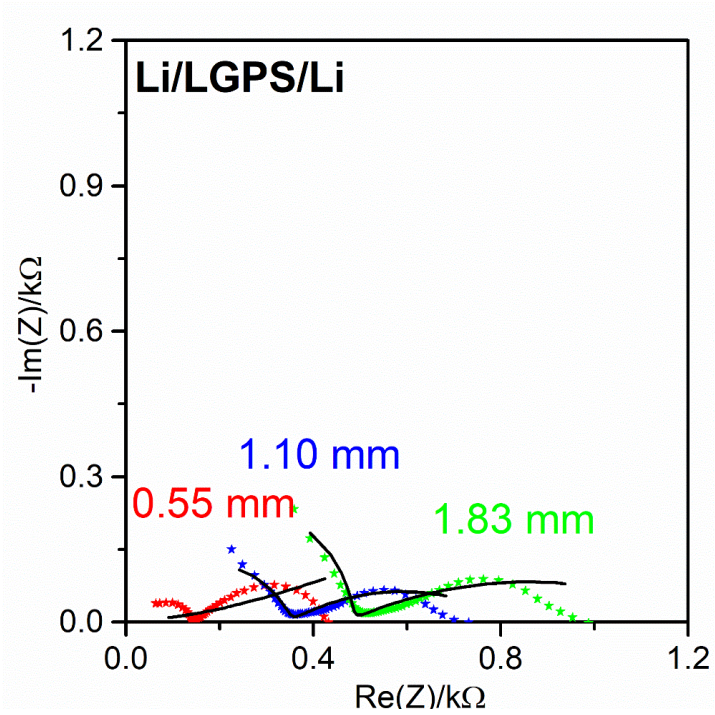

Figure 3-13 EIS spectra of hot-pressed LGPS pellets of different thicknesses in a Li/LGPS/Li configuration. The pellets were tested in I-cells.

In order to deconvolute the EIS spectra of Li/LGPS/Li symmetric cells, we first manipulated the thickness of the hot pressed LGPS pellets in order to correlate the circuit unit in EIS with the component in a symmetric cell. This is based on the assumption that the resistance of the bulk LGPS is proportional to the thickness of the pellet, while the charge transfer impedance resulted from the degradation reactions between Li metal and LGPS would be independent of the thickness of the pellet at the first cycle of EIS measurement. Therefore, we pressed three sets of LGPS pellets at 150 °C with 0.55 mm, 1.10 mm and 1.83 mm in thickness respectively. We were able to adjust the thickness by changing the mass of LGPS powder used for pellet pressing since we assume that at same pressing temperature and pressure, the density of the hot-pressed pellet would be constant thus thickness is proportional to mass. Figure 3-13 shows the EIS spectra of hot-pressed

LGPS pellets of different thicknesses in a Li/LGPS/Li configuration which were tested in I-cells. Due to limitation of the instrument, the first semi-circles at the high frequency region which is the start of a spectrum was not able to be shown in spectra of 1.10 mm-thick and 1.83-mm thick pellets and were instead presented as straight lines. However, it did not prevent us from fitting the curve and extrapolating to the high frequency region by using the equivalent circuit model shown in Figure 3-12 to calculate the ionic conductivity of bulk LGPS pellet. It was calculated that the impedance corresponds to the first semi-circle is proportional to the thickness of the pellet and the ionic conductivity of the bulk LGPS is calculated to be 2.35×10^{-4} S cm^{-1}. It is important to note that this value is more than an order of magnitude lower than the theoretical value and the one we will present later which was measured using the split cell. It is largely due to I-cell could not provide the best contact as split cell, so that the measured impedance is larger. On the other hand, the second semi-circle on the right remains the same in shape and size as the thickness of the pellet change. Therefore, we were able to attribute the first semicircle on the left in high frequency region to the impedance of bulk LGPS pellet and the second semicircle on the right in low frequency region to the interface formed by degradation reactions between Li metal and LGPS pellet.

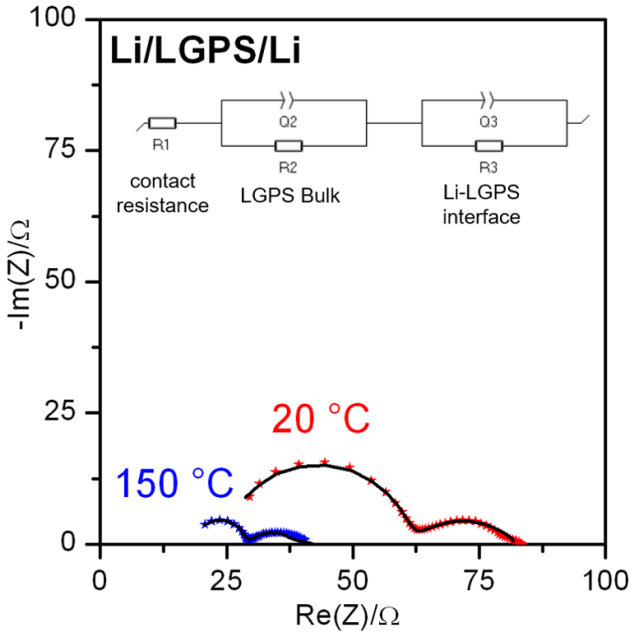

Figure 3-14 EIS spectra of LGPS pressed at 20 °C and 150 °C in a Li/LGPS/Li configuration.

To study the effect of hot pressing vs. cold pressing, we used split cells to measure the EIS spectra of pellet cold pressed at 20 °C and hot pressed at 150 °C, and the EIS spectra of them are shown in Figure 3-14. It shows that the 20 °C pellet has a much larger resistance than the 150 °C pellet in terms of size of semi-circle. Based on the equivalent circuit model, the calculated ionic conductivity of 20 °C pellet is 1.16 x 10^{-3} S cm^{-1} while the 150 °C pellet is 4.25 x 10^{-3} S cm^{-1}, which is closed to the 1.0 x 10^{-2} S cm^{-1} theoretical value. It again proves that hot press is essential for the enhancement of LGPS pellets. Such enhancement can be attributed to the densification of the structure which leads to better contact within the pellet among LGPS particles, which is shown in Figure 3-9. At the same time, the grain boundary impedance is also significantly reduced due to the densification.

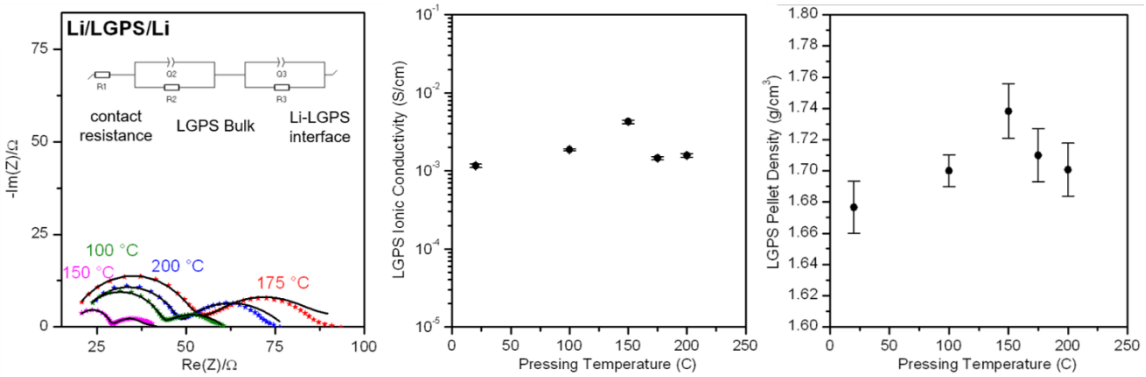

Figure 3-15 (**Left**) EIS spectra of LGPS pellets pressed at 100 °C, 150 °C, 175 °C and 200 °C in a Li/LGPS/Li configuration, (**middle**) calculated ionic conductivities of LGPS pellets pressed at various temperatures, and (**right**) calculated densities of LGPS pellets pressed at various temperatures.

To find the optimal temperature for fabrication of LGPS pellet, we measured the EIS spectra of pellets hot pressed at different temperatures. Figure 3-15 shows the EIS spectra of LGPS pellets pressed at 100 °C, 150 °C, 175 °C and 200 °C, and the calculated densities of LGPS pellets pressed at various temperatures. The 150 °C pellet still has the smallest semi-circle while 100 °C and higher temperature have larger ones. It is calculated that the ionic conductivity of 100 °C pellet is 1.87 x 10^{-3} S cm^{-1}, the 175 °C pellet is 1.45 x 10^{-3} S cm^{-1}, the 200 C pellet is 1.58 x 10^{-3} cm^{-1}. With the ionic conductivity of cold pressed pellet in consideration as well, the trend of ionic conductivity as of the pressing temperature shows that the ionic conductivity first increases with the increase in pressing temperature, which can attribute to the densification of the structure and mitigation of grain boundary impedance, then the ionic conductivity drops with the pressing temperature further going up. This is also in line with the trend of densities of LGPS pellets pressed at various temperatures shown in Figure 3-15 in which pellet pressed at 150 °C has the highest density. The reason for the reverse effect of ionic conductivity vs. temperature is not exactly clear, but not uncommon based on previous studies on hot pressing of other

materials.[160, 164] First, the increase in temperature may change the crystalline structure of the material and result in an unfavorable structure for the conduction of Li^+ ions. This is less likely the case for LGPS since the powder is commonly synthesized over 550 °C, though it is not entirely ruled out that under high pressure such as the 300 MPa used for pressing, the structure may be more sensitive to the change of temperature. Another explanation is that though high temperature can make the structure denser and decease the grain boundary impedance, it can also exacerbate the cracks, defects and voids on the surface and within the bulk LGPS pellet since high temperature and high pressure sintering often leads to stiffer structure. Such change of mechanical property can make it more susceptible to breakdown of structure due to the drastic volume change of electrodes during cycling, and the less malleable surface of the pellet may cause worse contact with Li metal. This is also partially supported by the trend of pellet density vs. pressing temperature in which the density dropped when pressing temperature further increased. All in all, 150 °C was determined to be the optimal pressing temperature for both the enhanced ionic conductivity and densified structure. Although impedance-wise the difference between 150 °C pellet and the pellets pressed at higher temperatures is small and the pellets pressed at higher temperatures may be more mechanically robust, the time and cost come with the increasing temperature do not justify the temperature going further higher.

3.3.4 LiPON Coated LGPS Pellets

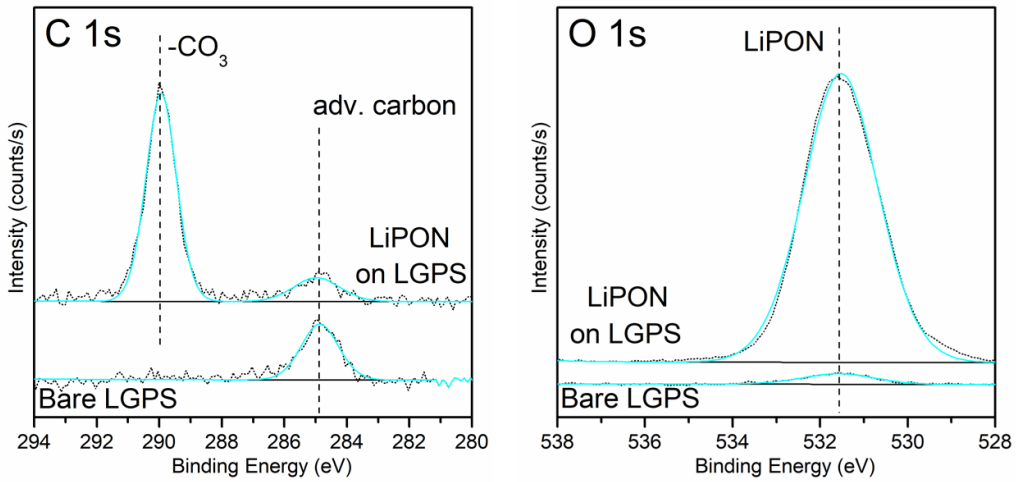

Figure 3-16 High resolution C 1s, N 1s and O 1s XPS spectra of LGPS pellets before and after LiPON coating. XPS analysis was run and the data was plotted by Dr. Kozen.

To understand the surface chemistry before and after ALD LiPON-coating processes on both sides of LGPS, XPS analysis was run and the results of high resolution C 1s and O 1s XPS spectra are shown in Figure 3-16. It can be seen that the surface of bare LGPS is very clean except the common adventitious carbon peak. After ALD LiPON coating, carbonate CO_3 peak is shown due to the ALD LiPON process which causes some chemical decomposition of the precursors at higher temperature.

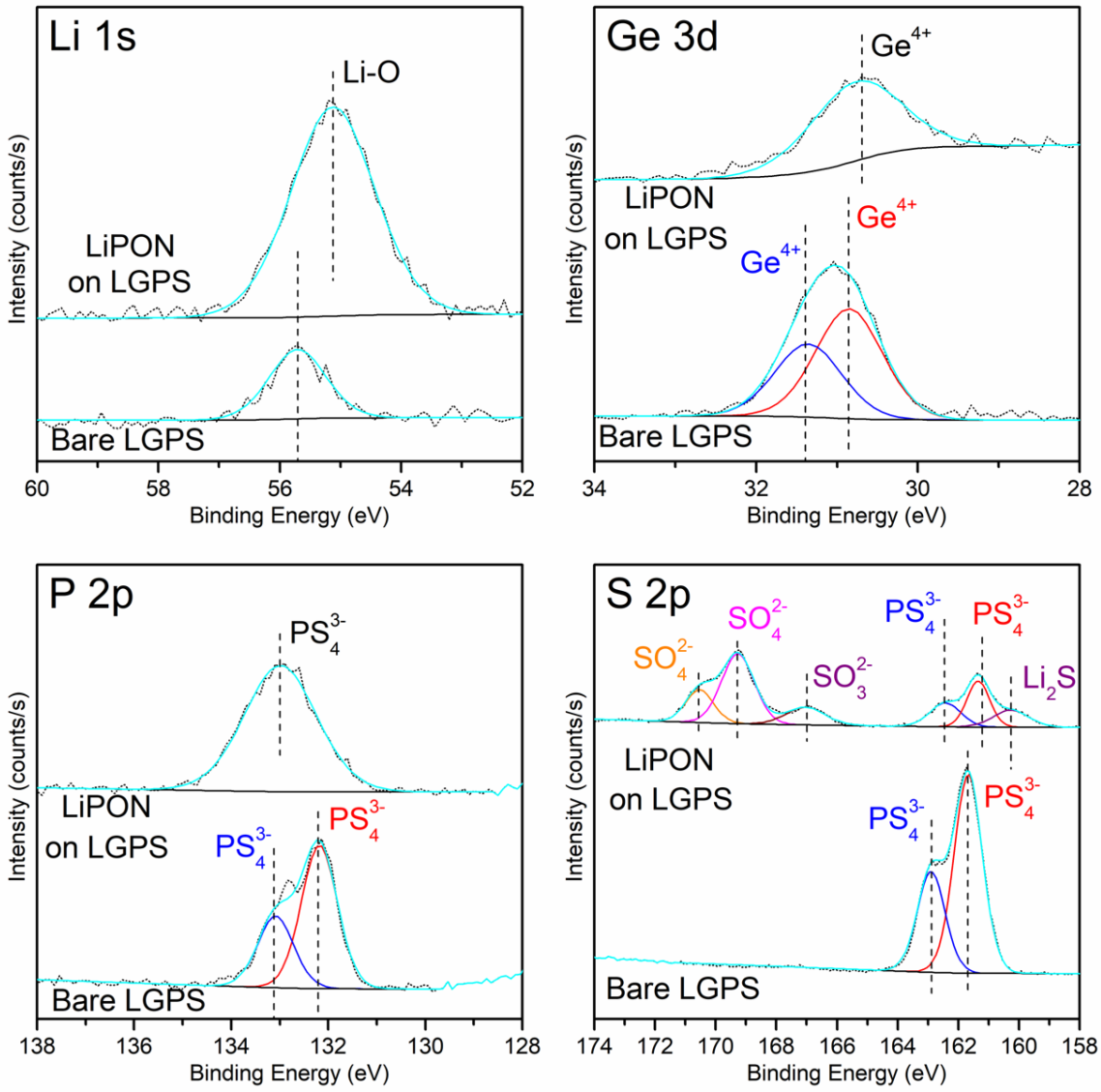

Figure 3-17 High resolution Li 1s, Ge 3d, P 2p and S 2p XPS spectra of LGPS pellets before and after LiPON coating. XPS analysis was run and the data was plotted by Dr. Kozen.

Figure 3-17 shows the high-resolution Li 1s, Ge 3d, P 2p and S 2p XPS spectra. The post-ALD LiPON coating results clearly show peaks more corresponding to the composition of LiPON as a result of LGPS being covered 10 nm beneath it which weakened the signals, [152]as in the cases of Li 1s, Ge 3d and P 2p, where there is little changes except it features more of composition of LiPON. The most important discovery is in S 2p spectra that after

LiPON coating, there are significantly more S-O peaks in addition to the P-S peaks. LiPON itself does not contain sulfur so it could only come from the reactions between LiPON and LGPS, or due to the evaporation of sulfur during the deposition heating process, which may coat chamber walls and react with the residual on it, then the products re-deposit onto the sample during the ALD process. The exact effect of this new S-O requires more study but overall, 20-nm ALD LiPON coating did not significantly alter the surface chemistry.

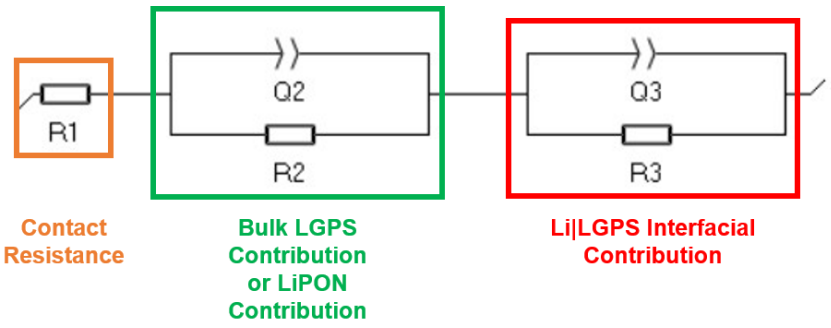

Figure 3-18 Equivalent circuit for EIS+CV series study. Contribution from bulk LGPS was not counted due to the extremely small value in impedance compared to other components.

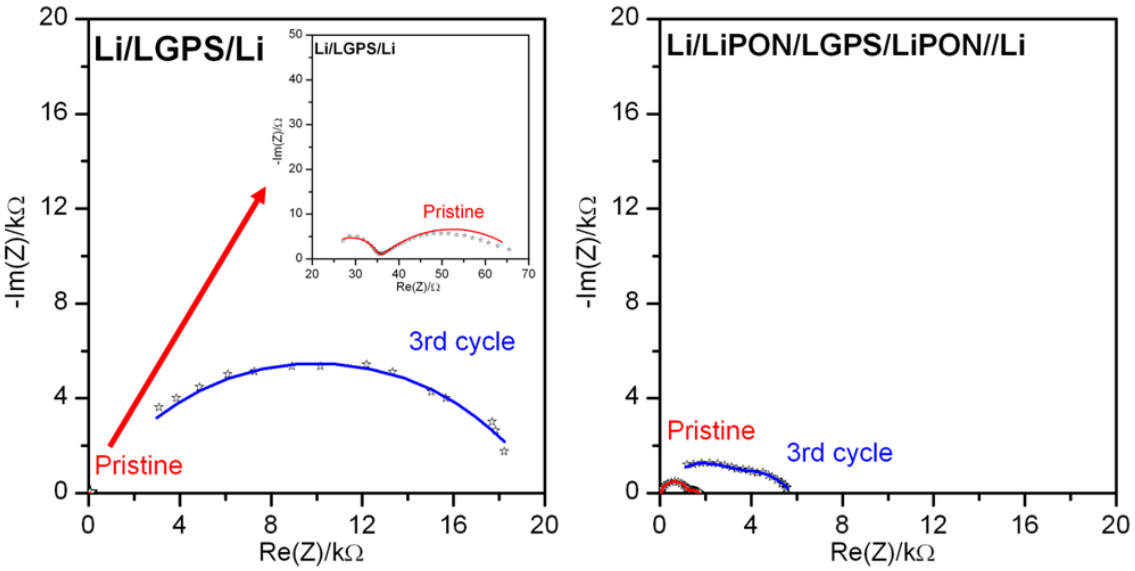

Figure 3-19 The first and third cycles of EIS spectra of Li|LGPS|Li cells with (left) bare and (right) 20-nm LiPON coated LGPS pellets respectively. EIS was measured from 1 MHz to 10 mHz with a perturbation voltage of 10 mV. EIS was measured before and after each CV run.

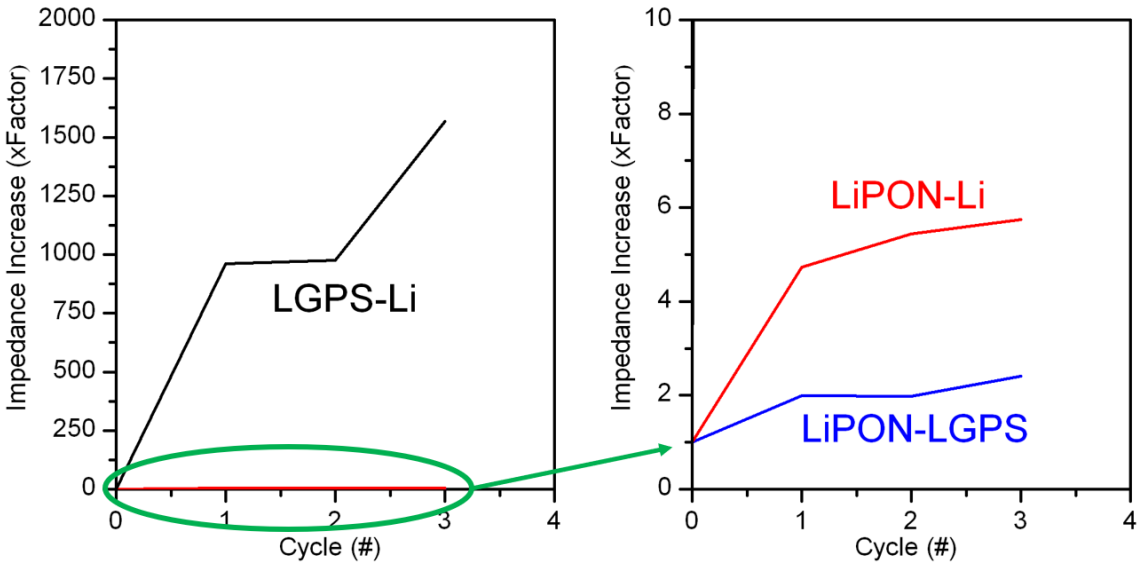

Figure 3-20 Increase in calculated charge transfer impedance at three interfaces over cycles of CV run. Cycle 0 corresponds to the initial EIS before the first cycle of CV was run.

To understand the degradation reactions between Li metal and LGPS pellet, and if LiPON coating mitigates such effect, Li|LGPS|Li symmetric cells were tested in series of EIS + CV measurements to monitor the degradation reactions and change in impedance. The equivalent circuit used to simulate this process is shown in Figure 3-18. The contribution of bulk LGPS in impedance was not counted in bare LGPS sample after first CV run and not counted in LiPON coated sample entirely due to bulk LGPS contribution is at least 50 times smaller than all other components in the solid-state cells. The first and third cycles of EIS spectra of Li|LGPS|Li cells with bare and 20-nm LiPON coated LGPS pellets are displayed in Figure 3-19. EIS was measured before and after each of the three CV runs. The charge transfer impedances at all three interfaces Li|LGPS, Li|LiPON and LiPON/LGPS were calculated using the equivalent circuit, and the increase in charge transfer impedance were plotted over cycles of CV run, which is shown in Figure 3-20. It is clearly shown that the bare LiPON cell has very low impedance initially before CV run

started, which is consistent with result shown in Figure 3-14. However, starting from the second cycle of EIS after the first cycle run of CV, the charge transfer impedance caused by interfacial degradation reactions between Li and LGPS increased by almost 1000 times and only became worse over more cycles of CV runs. In contrast, the cell with 20-nm LiPON coated LGPS has higher initial impedance due to the ionic conductivity of LiPON is four orders of magnitude lower than LGPS, but it only has its impedance increased slightly after each of three cycles of CV. The impedance at LiPON|LGPS interface also shows very small increase over CV cycles. This is strong evidence that LiPON coating successfully mitigated the degradation reactions at the interface. This result is directly confirmed by the images of post-cycling Li metal in two cells. Both cells were disassembled after entire testing and the images of Li metal post-cycling are shown in Figure 3-21. Both Li metal anodes have small amount of residual LGPS attached but it is clearly distinguishable that the Li metal cycled with bare LGPS has turned completely black, depicting the severity of the degradation reactions. On the other hand, the Li metal cycled with 20-nm LiPON coated LGPS still retained its metallic appearance and color.

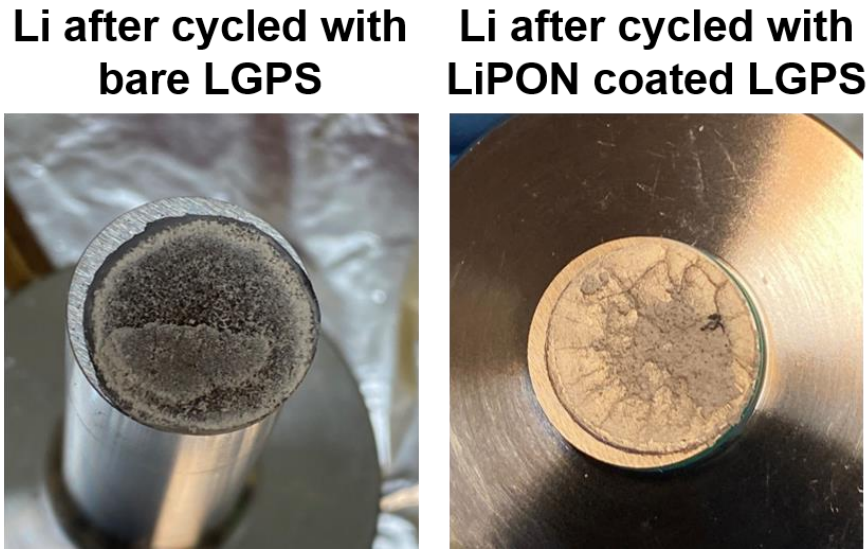

Figure 3-21 Images of Li metal of disassembled Li|LGPS|Li cells after being cycled with bare or 20-nm LiPON coated LGPS after series of EIS+CV cycling. Residual on the surface is LGPS.

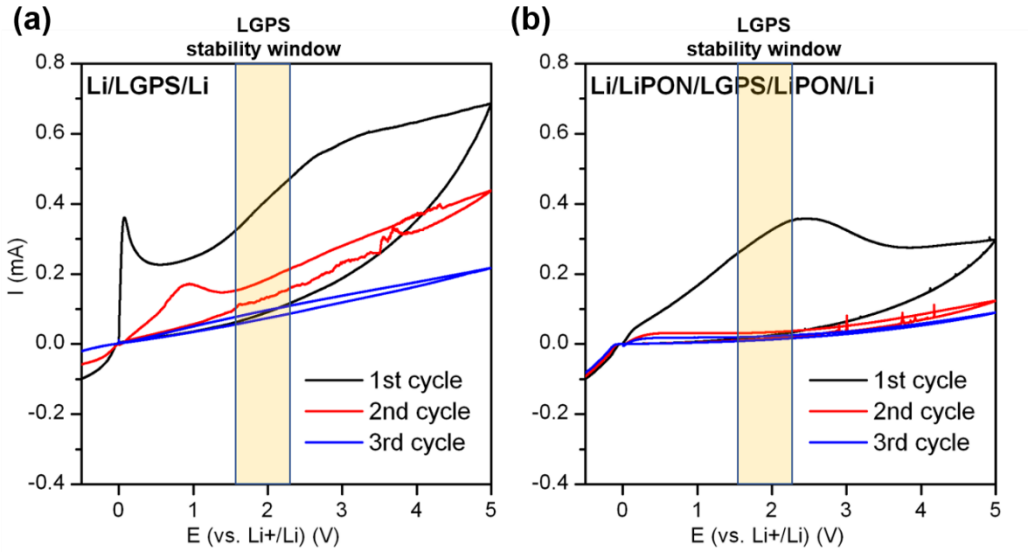

Figure 3-22 Cyclic voltammetry diagrams of (**a**) Li|LGPS|Li cells with bare and (**b**) 20-nm LiPON coated LGPS pellets. Scan rate is 0.1 mV s^{-1} and the voltage window is from -0.5 V to 5 V. CV was run in between each EIS measurement. Highlighted region is the electrochemical stability window of LGPS.

The diagrams of multiple CV run in between EIS measurements are shown in Figure 3-22. In the first cycle of CV diagram of bare LGPS sample, the sharp oxidation peak from 0 to 1 V vs. Li^+/Li which corresponds to the alloying reactions of Li-Ge and Li-P between Li metal and LGPS. The broad region for the rest of the first cycle of CV depicts the capacitive behavior. The large and steeper slope of the CV profile indicates the formation of thicker degradation layer at the Li/LGPS interface by alloying reactions and the formation of Li_2S composition. There still is an oxidation peak, though a lot broader in the second cycle of CV, which indicates the degradation reactions were continuing to happen. As for the CV diagram of 20-nm LiPON coated LGPS sample, it has a very broad oxidation peak centered around 2.5 V which could be a result of the Li-S component of LGPS[152] or due to the coating of LiPON in which the interface between LiPON and LGPS was being stabilized. The smaller slope of CV profile also indicates the interfacial layers formed on LiPON coated LGPS sample during CV run are less resistive than the ones formed on bare LGPS.

Most importantly, starting from second cycle of CV, there is no peaks visible anymore. CV diagrams also show that the interfacial degradation reactions are irreversible too. The smaller current and lack of redox peaks again confirmed the findings in EIS spectra and increase in impedance at three interfaces over cycles of CV run that LiPON coating is effective in mitigating the degradation reactions.

3.4 Conclusion and Future Work

3.4.1 Conclusion

$Li_{10}GeP_2S_{12}$ is a promising sulfide solid-state electrolyte that has high ionic conductivity that is comparable to conventional liquid electrolytes. However, cold pressed LGPS pellets have porous structure which makes it prone to cracking thus sacrificing its high ionic conductivity. Additionally, it has narrow electrochemical stability window which renders it reactive with Li metal anodes and many potential high voltage cathodes and easily form degradation layers on the interfaces that further jeopardizes its exceptional battery performance. In this study, first we used a hot pressing method to fabricate the LGPS pellets using commercialized powder under high pressure and high temperature at the same time, which has not been reported before. Our results show that hot pressing significantly densified the pellet and eliminated all micron-sized cracks shown in cold pressed pellets under SEM. Such densification of the material can greatly improve the intrinsic contact and minimize grain boundary, which would transfer to the enhancement of ionic conductivity and electrochemical robustness. During our study of the hot press method, we explored different configurations of testing cells and the pros vs. cons of each type. We also narrowed down the range of optimal pressing temperature which is determined to be

150 °C. Higher temperature may result in a denser structure that lowers grain boundary but it could also exacerbate the cracks, voids and defects inside the pellets that worsens the contact inside the pellet and at the interface which results in lowered density and ionic conductivity.

Second, we explored using ASEI to protect LGPS to mitigate the interfacial degradation reactions and extend the electrochemical stability window, which has never been reported before as well. We found that though the ionic conductivity of LiPON is three orders of magnitude lower than LGPS which results in larger overpotential and initial impedance. By applying a 20-nm thin layer of ALD-coated LiPON, it can effectively mitigate the interfacial degradation reactions after one CV cycle.

3.4.2 Future Work

Unfortunately, due to the outbreak of COVID-19 that put UMD campus under lockdown and severe restrictions to research, we were not able to retest electrochemically pretreated Li metal anodes, which have an elastomeric ASEI, in split cells. Preliminary data of symmetric cells in I-cell configuration with elastomer protected Li metal cycled at 3 mA cm^{-2} show promising results that it can fully function. This will be one of the top priorities in the future work. We believe that the elastomer protected Li metal anodes would have good compatibility with LGPS pellets and provide great contact at the interface due to the malleable feature of the elastomer which can essentially serve as a Li-ion conducting wetting agent. This property would be especially valuable at ultrahigh current density cycling, which triggers drastic volume change of Li metal and potentially the solid-state electrolyte, and irreversible damages to the interface that lead to abysmal interfacial contact and poor battery performance. We also believe that in order to work in a solid-state system,

the protocol of the electrochemical pretreatment needs to be adjusted to meet the needs of LGPS. Thinner layer, higher ionic conductivity and rich poly-DOL component would be the keys to accomplish this goal because this ASEI has stronger capability to accommodate the larger volume change in solid-state batteries and necessity of low resistance of the ASEI. These could be potentially achieved by increasing the concentration of the salt and ratio of DOL solvent in the electrolyte for pretreatment, and a smaller cycle number of electrochemical pretreatment that would result in a thinner layer. We will also use LiPON coated LGPS and elastomer protected Li together to test if double protection can offer greater stability and battery performance.

Another plan for future work is to study the chemical stability of LGPS pellets against moisture and organic solvents with or without ASEI protection. The oxophilicity of germanium and phosphorous atoms make them unstable against oxygen.[157, 184] LGPS is also very sensitive to moisture which would quickly react and generate harmful H_2S which can not only cause acute poisoning, but also is irreversibly toxic to many catalysts, including those needed to control the oxygen and water levels of working glove boxes. If the concentration of H_2S generated reaches the threshold, it is also very explosive.[157, 185] To put LGPS into industrial application, it is inevitable to expose it to air during manufacturing, transport and storage, even if in a dry room condition that has relative humidity (RH%) only around 1%. LGPS is also proposed to be used in hybrid system, which has liquid electrolyte or catholyte on the cathode side, having LGPS in direct contact with Li metal can serve as a mechanical separator and anode interlayer. It is especially used with S cathodes that have poor electronic conductivity and requires wetting from electrolyte to fully utilize the sulfur impregnated inside the carbon substrate. Therefore,

understanding the quantitative stability of LGPS against moisture, oxygen and organic electrolytes are important for practical applications. In addition, we seek to understand the role LiPON plays in mitigating these degradation phenomena.

The last and most challenging plan would be configuring a full solid-state cell with sulfur or Li-ion high voltage cathodes as cathode and Li metal as anode. It requires the extension of the electrochemical stability window of LGPS to meet both anode and cathode materials. A LiPON coated LGPS with liquid electrolyte on the cathode side would enable such a configuration by fully utilizing the S active material with wetting from liquid electrolyte and mitigating interfacial degradation reactions with Li with LiPON protection, to eventually achieve a hybrid full-cell system that can provide high energy density and function at high power demand. In addition, further decreasing the thickness of LGPS pellet to lower its resistance and/or creating LGPS with polymer or binder to enhance internal contact to increase ionic conductivity are also worth future exploration.

4. Exploration of Electrochemical Protection of Mg Metal Anode

The project described in this chapter was done in collaboration with Dr. Emily Sahadeo of University of Maryland. Some work discussed in this chapter has been published on Chemical Communications. All the matrix-assisted laser desorption/ionization analysis (MALDI) – time of flight (TOF) mass spectroscopy analysis was done and processed by the author of the dissertation, Yang Wang. Sample preparations and electrochemical testing were shared between Dr. Sahadeo and Yang Wang. The data processing and analysis of XPS results were done by Dr. Sahadeo.

4.1 Introduction

Magnesium metal, the 8th most abundant element in the earth's crust, has drawn a lot of attention as the next step beyond lithium-ion battery technology due to its low reduction potential (-2.37 V vs. SHE) and high volumetric capacity (3,832 mAh cm^{-3}) as anodes in Mg rechargeable batteries. Most importantly, Mg metal anodes strip and plate without the formation of dendrites which makes them much safer than Li metal. The abundance of Mg metal and its low cost make it even more appealing to the industry. By assembling with another cost-effective and high-energy density sulfur cathode, together the Mg-S batteries can have a high theoretical energy density (3200 Wh L^{-1} and 1700 Wh kg^{-1}).[89, 91, 186]

However, the numerous advantages did not come without a cost that severely hinders its broader application and fulfillment. Electrolytes of Mg rechargeable batteries decompose on the surface of Mg similar to the behavior of those in Li-ion or Li metal batteries. However, unlike the solid electrolyte interphase layers formed on Li metal or graphite, the

SEIs on Mg metal are completely passivating to the transport of Mg^{2+} which terminate further electrochemical reactions.[187] Being larger in size and divalent compared to Li^{+}, it makes the transport of Mg^{2+} through any layer more difficult as well due to the increased electrostatic repellent force.[89, 91, 93]

A conventional way in the Mg batteries community to mitigate this passivation issue is by using more complex salts and solvents that do not passivate the Mg metal surface or to a much lesser extent.[188-191] However, many of those electrolytes are nucleophilic and would react with the electrophilic sulfur in a Mg-S batteries system.[90-92] In a battery system with complex shuttle effect plus the passivation of Mg metal, an Mg^{2+} ion conducting ASEI on the surface of Mg metal anodes may just be the key to solve the double jeopardy. Most importantly, by having such an ASEI, the system may be able to use conventional electrolytes for Mg-ion or Mg-S batteries, and free from synthesis of complex electrolytes and meet the electrochemical and chemical stability requirements of both the cathodes and the Mg metal anodes.[186, 191-195]

So far, most of the work is at the proof-of-concept stage and it remains very challenging.[196-198] In order to have an ASEI that can match the performance of ASEIs in Li batteries system, it should be able to conduct Mg^{2+} ions, allow reversible Mg stripping and plating, enable high Coulombic efficiency of the anode and protect the Mg metal from reactions with the electrolyte or polysulfides in the case of Mg-S batteries.[186] Only a few works have been presented in the field of Mg metal anode protection. It has been reported that by adding iodine as an additive in an $Mg(TFSI)_2$/DME electrolyte, MgI_2 is formed in the SEI and can conduct Mg^{2+} ions.[199] Further, protection using a cyclized polyacrylonitrile polymer with magnesium triflate ($Mg(CF_3SO_3)_2$) enabled use of $Mg(TFSI)_2$/propylene

carbonate (PC) electrolyte containing water in a full cell with a V_2O_5 cathode.[200] Both works show significant decrease in overpotential for Mg deposition and dissolution in Mg-Mg symmetric cells and are an important step forward.

In this dissertation, we explored the possibility of using electrochemical pretreatment which has been successfully demonstrated in Li-S batteries system to protect the Mg metal anodes. We intend to similarly grow a composite layer mainly consists of poly-DOL that is capable of protecting Mg from passivation and corrosive side reactions while conducting Mg^{2+} ions. Because of the uniqueness of Mg metal and Mg^{2+}, such a layer requires much finer tuning to optimize. It is also crucial to understand the change of surface chemistry and morphology in correlation with the conditions of pretreatment. As it is shown in this dissertation, our work is still on relatively early stage and ongoing as of today. However, it has also demonstrated that Mg anode protection by electrochemical protection is viable. Similar work has not been reported in this field and it can be groundbreaking in both methodology and the enhancement of Mg batteries performance.

4.2 Experimental

4.2.1 Electrochemical Pretreatment

0.1 mm thick Mg foil (Sigma-Aldrich) stored inside an Ar filled glovebox (LC-100) was first polished with 600, 1200, 200 grits sandpapers then wiped with Kimwipes wetted with DME, and then dried before any use. The 9.5 mm in diameter Mg metal anodes were punched from the polished Mg foiled and placed onto 304 stainless steel spacers (15.5 mm diameter x 0.5 mm). Those Mg metal anodes were assembled into symmetric coin cells (CR2025, MTI Corp) with Celgard separators and 80 μL of electrolytes. Three different

types of electrolytes were made, including 0.35 M $Mg(TFSI)_2$ (Sigma) in DME:DOL (1:1, v/v), 0.35 M LiTFSI in DME:DOL (1:1, v/v) and 0.35 M LiTFSI in TEGDME (Tetraethylene glycol dimethyl ether, Sigma):DOL (1:1, v/v). During pretreatment, these symmetric coin cells were cycled for different discharge/charge cycles (i.e. 15 and 30) of different hold times (1 h, 1.5 h and 2 h) per discharge or charge process at a low current density of 0.03 mA cm^{-2} using a Bio-Logic potentiostat.

4.2.2 Electrochemical Testing

To study the effectiveness of ASEI layer, the cells of pretreatment were disassembled in the glove box and the pretreated Mg metal anodes were vigorously rinsed with DME and fully dried under vacuum. They were then placed onto 304 stainless-steel spacers and assembled into symmetric coin cells (CR2025) with Celgard separators and 80 μL of 0.25 M $Mg(TFSI)_2$ in DME electrolyte. The cells were cycled for 100 cycles, 30 minutes hold per discharge or charge process at 0.03 mA cm^{-2}. Untreated pristine Mg metal anodes are used as control.

4.2.3 Characterizations

The pretreated Li anode samples and untreated control samples were transferred via an air-tight glove bag with dry nitrogen atmosphere to an XPS system for surface chemical analysis. The samples were exposed to the dry nitrogen atmosphere for less than 1 minute. XPS data were collected on a Kratos axis 165 X-ray photoelectron spectrometer operating in hybrid mode, using monochromatic Al Ka x-rays (240 W). Charge neutralization was required to minimize sample charging, the working pressure of the instrument was 5 x 10^{-8} Torr or better throughout data collection. Survey spectra and high-resolution spectra were collected with pass energies of 160 eV and 40 eV respectively. Peak fitting was done using Casa XPS software after application of a Shirley background, using peaks with a 30 % Lorentzian, 70% Gaussian product function. All peaks within a region were fixed to have peaks of equal FWHM (full width at half maximum), the spin-orbit split components of the S 2p were fixed to have spin-orbit splitting of 1.18 eV and area ratios of 2:1 for the 3/2, 1/2 components respectively. All spectra were calibrated to the C-C/C-H peak at 285.0 eV.

The matrix-assisted laser desorption/ionization (MALDI) – time of flight (TOF) mass spectroscopy measurements were performed on a Bruker Autoflex MALDI-TOF mass spectrometer. The mass spectra were obtained in the linear positive mode with 2,5-dihyroxybenzoic acid as the matrix. The mass range was from 500 to 5000 Daltons.

4.3 Results and Discussions

4.3.1 Using $Mg(TFSI)_2$-DOL Electrolyte and the Unexpected Discovery

We first wanted to replicate the strategy used in the electrochemical protection of Li metal anodes by making 0.35 M $Mg(TFSI)_2$ in DME/DOL electrolyte and assembling Mg-Mg symmetric cells to cycle them at low current density. $Mg(NO_3)_2$ was not similarly added due to any dense passivation layer would not be desirable. However, we quickly discovered one phenomenon that has never been reported before, that the electrolyte we made gellified to become extremely viscous gel within hours and eventually became white solid. As a new project derived from the electrochemical protection of Mg metal anodes in collaboration with Dr. Emily Sahadeo, we found that Mg^{2+} ions as Lewis acid can chemically catalyze the polymerization of DOL to form poly-DOL. Such results are shown in Figure 4-1. Figure 4-1(a) shows the MALDI-TOF MS spectrum of the polymerized DOL sample. This soft ionization method generated molecular ion peaks up to the scanning limit 5000 Da and the inset of the zoomed in the region shows a clear patten of ~74 Da in difference between two adjacent main peaks is the molecular weight of a DOL monomer.

This pattern is consistent through the entire spectrum. Figure 4-1(b) shows the completely polymerized, solid sample and still being polymerized and gellified sample.[201]

We did assemble a few coin cells immediately after the electrolyte was made while it was still in clear liquid form. The galvanostatic charging and discharging profile is shown in

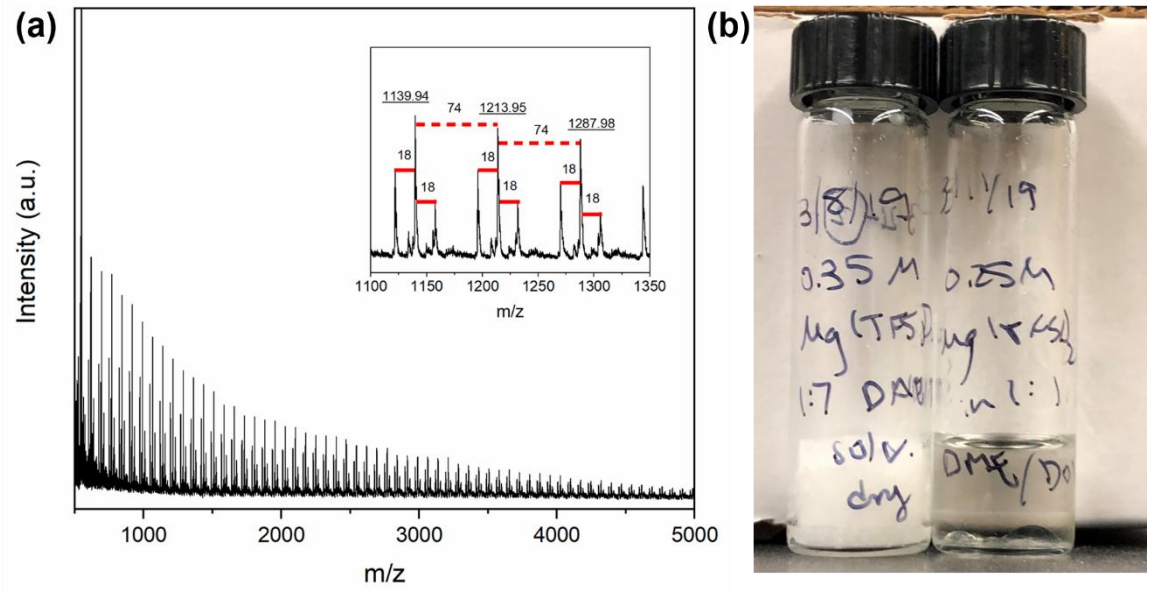

Figure 4-1 (**a**) MALDI-TOF MS spectrum of the polymerized sample. The ~74 Da in difference between two adjacent main molecular ion peaks is the molecular weight (MW) of one DOL monomer. The ~18 Da in difference between satellite peak and main peak indicating there is water molecule adduct in the polymer chain. (**b**) The photo of polymerized samples. The one on the left is the fully polymerized, solid sample and the one on the right is the still being polymerized and gellified sample. Photo is taken by Dr. Sahadeo.

Figure 4-2. The overpotential spiked at the first several cycles as the surface MgO layer was breaking down. Even though it was stable in the next two dozen cycles, the overpotential is above 2 V vs Mg^{2+}/Mg which is a lot larger than untreated pristine Mg-Mg symmetric cells. This could result from the polymerization of DOL and the solidification of the electrolyte which greatly decreased the ionic conductivity and increased the overpotential. Due to the catalytic reactions, we concluded that using $Mg(TFSI)_2$ with DOL solvent is not a viable option. As an alternative, we explored to use LiTFSI in DME/DOL or TEGDME.DOL electrolytes instead for the Mg-Mg symmetric cells. There have been

reports of Mg/Li dual-ion systems and we hypothesized that by having a small amount of Li^+ in the electrolyte, we could "activate" Mg to participate in the electrochemical stripping and plating processes which would engage with DOL to form the poly-DOL ASEI layer.

4.3.2 Using LiTFSI-DOL Electrolyte and the Comparison of Cosolvents

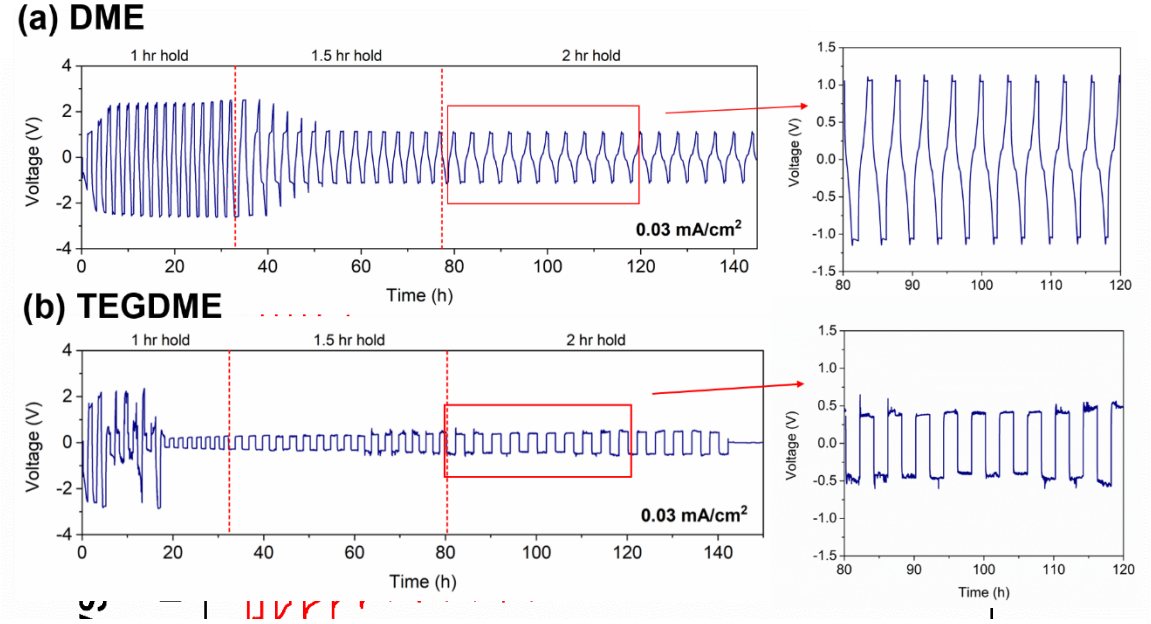

Figure 4-3 Galvanostatic charging and discharging profiles of Mg-Mg symmetric cells cycled in LiTFSI-DOL electrolytes with (**a**) DME and (**b**) TEGDME as cosolvent. Figure created by Dr. Emily Sahadeo.

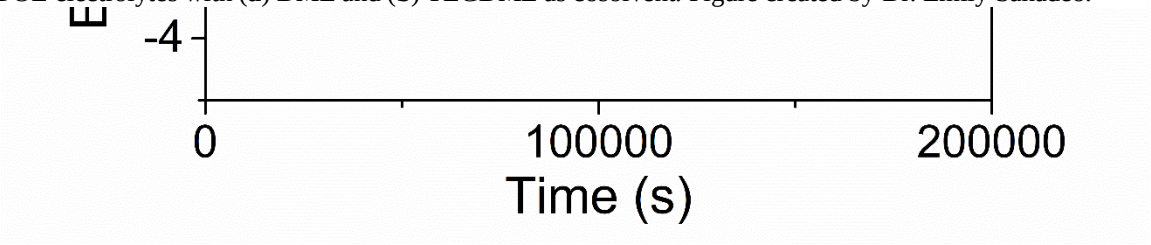

Figure 4-2 Galvanostatic charging and discharging profile of Mg-Mg symmetric cell using 0.35 M $Mg(TFSI)_2$ in DME/DOL as electrolyte.

To study the functions of using LiTFSI-DOL electrolytes in Mg-Mg symmetric cells to form the ASEI, we chose two ethers as cosolvent, DME and tetraethylene glycol dimethyl ether (TEGDME) which has been used as a measure to coordinate the deposition of Li^+ due to the increasing number of oxygen in glyme structure and it has shown improvement

in the suppression of Li dendrites.[202] Figure 4-3 shows the electrochemical cycling profiles comparing the two cosolvents. We chose three different hold times for every fifteen cycles of charge and discharge processes and we observed the stark contrast between the two cycling profiles. With DME as cosolvent as shown in Figure 4-3(a), the profile appears to show two plateaus at ±0.05 V and ±1.0 V, which strongly resemble the profile of full-cell batteries. On the other hand, with TEGDME as cosolvent as shown in Figure 4-3(b), it shows a standard symmetric cell stripping and plating profile at lower overpotential at ±0.5 V and the shape is similar to Figure 2-3(b) of Li-Li. The shape of the profile also indicates there is no dendritic Li formation on the surface of Mg metal.[131] The drastic difference between the profiles of two straight-chain ethers requires more understanding but it could be a result of the strong coordinating capability of TEGDME of cations that smoothened the stripping and plating process.[202]However, it cannot be ruled out that there could be some regional internal short-circuiting that caused the overpotential to decrease to ±0.5 V after 33 hours and completely short-circuited after 140 hours. Informatively, the two voltage plateaus at ±1 V and ±0.05 V of DME profile could be attributed to the stripping and plating process of Mg which has higher overpotential, and lithiation of the formed SEI which has very low overpotential. The ±0.5 V plateau of standard symmetric cell profile of TEGDME could be the combination of the behaviors, or some degree of soft short-circuiting where the overpotentials between SEIs are being measured while the direct

contact between Mg-Mg is still blocked. The overpotentials of both cycling profiles indicate Mg is participating in deposition and dissolution processes.

To study the surface chemistry after the electrochemical pretreatment with different cosolvents, XPS analysis was done and the high-resolution XPS spectra of C 1s are presented in Figure 4-4. By comparing with the XPS spectra of Li metal after pretreatment shown in Figure 2-6, there is O-C-O peak which strongly corresponds to poly-DOL structure in sample with DME as cosolvent, even though the peak ratio of C-O-R to O-C-O is less than 2:1. However, there is no O-C-O peak in sample with TEGDME as cosolvent, but only C-O-R peak. This result indicates some poly-DOL is formed on the surface of Mg where DME is used as cosolvent, but not with TEGDME solvent. This could be the result of TEGDME strongly solvates and interacts with Mg^{2+} ions than DME, which leads to lower activity of Mg^{2+} at the surface to catalyze the polymerization of DOL. Or it may be

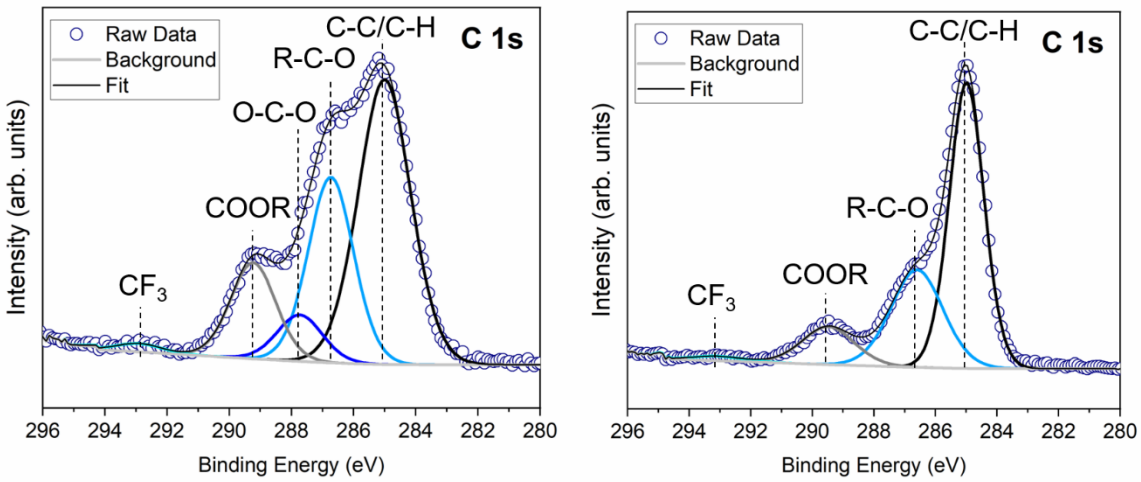

Figure 4-4 High-resolution XPS spectra of C 1s of Mg metal electrodes after being pretreated in LiTFSI in DOL electrolytes with DME (left) or TEGDME (right) as cosolvent. Figure created by Dr. Emily Sahadeo.

due to poly-DOL having a larger solubility in TEGDME that it is dissolved from the surface into the bulk electrolyte during formation process.[201] In addition, the layer formed on the

surface of TEGDME could contain polyethylene oxide structure CH_2CH_2O being formed, which is widely regarded as one possible component of SEI *in situ* formed in Li-S batteries during electrochemical cycling.[1, 4, 203] The slightly higher reduction potential of Mg over Li could have made the difference. This difference in surface chemistry by using different cosolvents may be the reason that DME and TEGDME show drastically different electrochemical cycling profiles. This requires more surface analysis study and different techniques for further investigation.

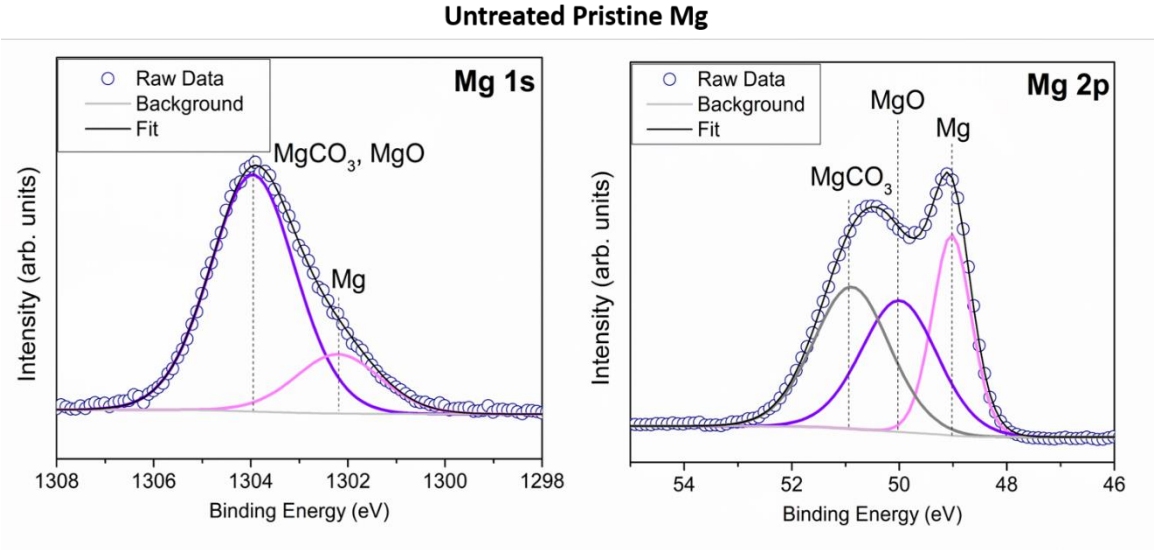

Figure 4-5 High-resolution XPS spectra of Mg 1s and Mg 2p of untreated pristine Mg metal.

Figure 4-5 shows the high-resolution XPS spectra of Mg 1s and Mg 2p of untreated Mg pristine metal. It can be seen that Mg metal, even after being polished, still has MgO on the surface. Mg 1s electrons have lower kinetic energy thus the Mg 1s spectrum is more prone to surface sensitivity. The appearance of Mg metal peak in Mg 1s spectrum demonstrates that though MgO is unavoidable on the surface, it is a thin layer.

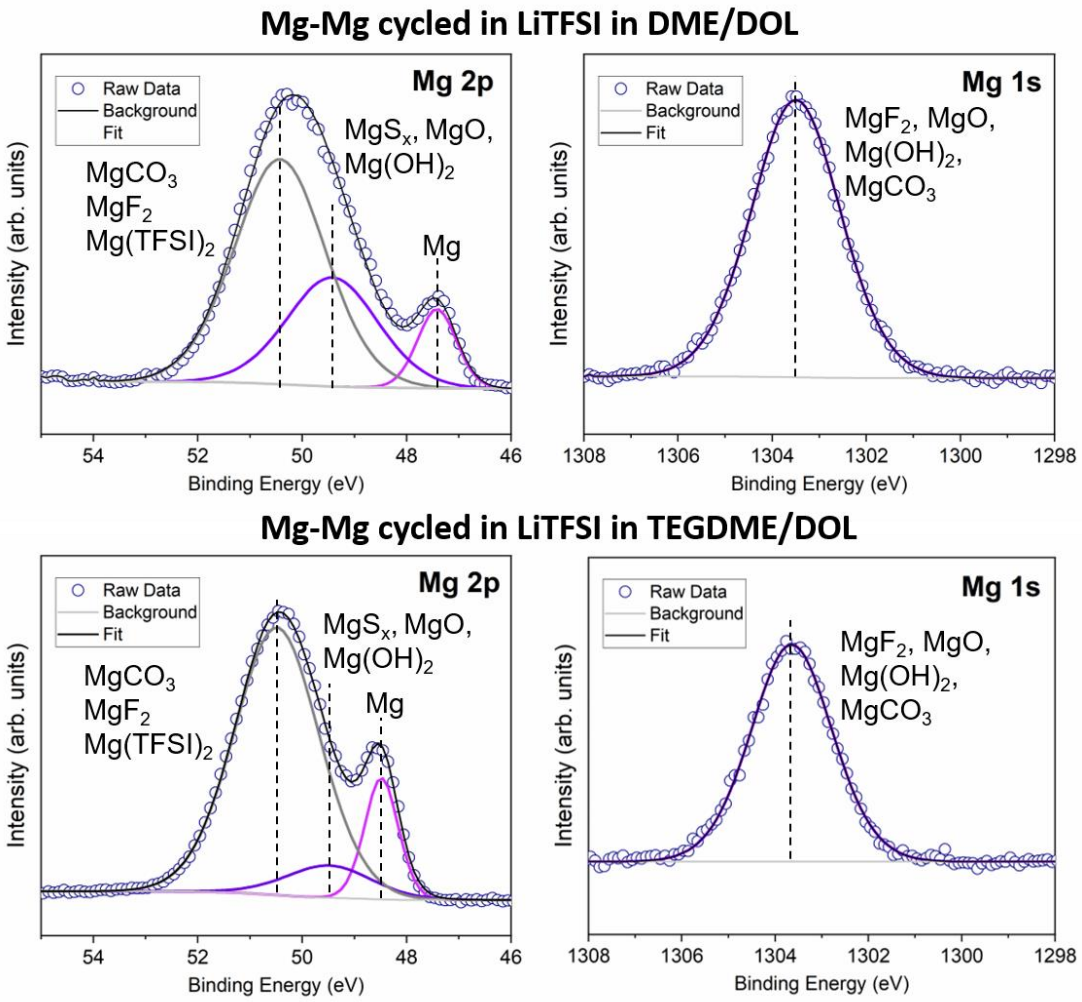

Figure 4-6 High-resolution XPS spectra of Mg 1s and Mg 2p of Mg metal electrodes after being pretreated in LiTFSI in DOL electrolytes with DME or TEGDME as cosolvent. Figure created by Dr. Emily Sahadeo.

Figure 4-6 shows the high-resolution XPS spectra of Mg 1s and Mg 2p with DME and TEGDME as cosolvents. In the more surface sensitive Mg 1s spectra, no Mg metal peak is visible compared to Figure 4-5 of untreated pristine Mg metal, it indicates a thicker layer is formed on the surface and the Mg metal is embedded beneath a surface layer that was formed by the electrochemical cycling of the Mg-Mg symmetric cells. Most importantly, this layer is more likely electronically insulating but ionically conductive for Mg which explains why Mg metal is depositing beneath the layer. This fits the crucial criteria of a

good ASEI. From Mg 2p spectra, the Mg metal peak is visible, in addition to peaks of MgO, $Mg(OH)_2$, $MgCO_3$ and MgF_2 due to the decomposition of electrolyte and an inevitable MgO layer. The slight peak shifting of Mg peak in two spectra may be caused by differential charging during XPS analysis, which is common. One difference is Mg metal peak in sample with TEGDME as cosolvent has larger peak area and stronger intensity than in DME, indicating that the layer formed in TEGDME electrolyte is thinner and Mg is less buried beneath of it. This is consistent with results shown in Figure 4-4, in which there is no poly-DOL peak in sample with TEGDME. The thinner layer on Mg pretreated in TEGDME may have confirmed that a poly-DOL layer is either dissolved or not formed at all.

4.3.3 Electrochemical Testing of Pretreated Mg Metal Anodes

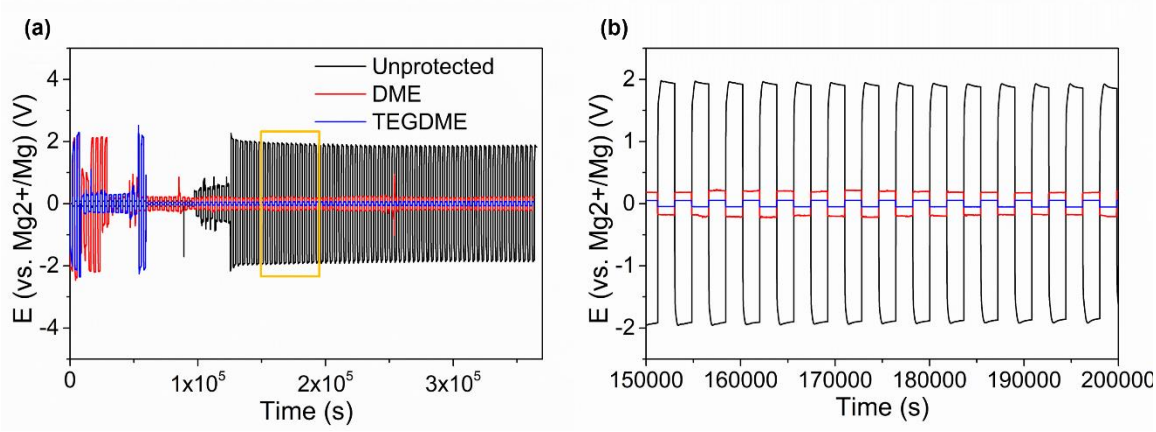

Figure 4-7 Galvanostatic charge and discharge profiles of untreated pristine Mg metal and Mg metal electrochemically pretreated in LiTFSI-DOL electrolytes with DME or TEGDME as cosolvents respectively.

To study if the pretreated Mg metal electrodes was effective, we open the symmetric cells with DME and TEGDME as cosolvents for pretreatment and assembled them in Mg-Mg coin cells with conventional 0.25 M $Mg(TFSI)_2$ in DME as electrolyte. The electrochemical cycling results are shown in Figure 4-7. All cells underwent large

overpotential at the first several cycles regardless if the Mg metal electrodes were pretreated. This is usually not a good sign because the large overpotential indicates a passivation layer needs to be broken down, which may have also broken down the ASEI that was formed on the surface. However, after the initial breakdown, the overpotential of untreated Mg metal quickly increased again and stayed at very high 2 V. The overpotential of two cells with pretreated Mg in different cosolvents went down and stayed stably at very low values. This result could be promising meaning that despite the breakdown or reorganizing of the surface layer, the ASEI was able to serve its purpose and protected Mg metal from further passivation and parasitic reactions. Nonetheless, it might also be the result of short-circuiting of the cells even though ±0.2 V does not fall in the range of voltage of short-circuited cells as of Li-Li symmetric cells. Unfortunately, there have been very few concrete data displaying the range of overpotentials of Mg-Mg symmetric cells and the results presented so far appear to show random values. More work is needed to understand the exact conditions of the cells.

4.4 Conclusion and Future Work

4.4.1 Conclusion

It needs to be stressed that this study, though groundbreaking and similar research has never been reported before, is still on its early stage and has a lot to be investigated. However, it can be concluded that by borrowing the electrochemical anode protection strategy for Li with some modifications of the method to address the issues of Mg, we were able to grow a layer on the surface of Mg metal electrodes and this layer seems to allow the transport of Mg^{2+} ions and does not fully passivate Mg. By cycling Mg-Mg symmetric cells using

LiTFSI/DOL electrolytes with two different cosolvents, DME and TEGDME, we were able to "activate" Mg to participate in the stripping and plating processes. We observed strikingly different galvanostatic charging and discharging profiles of two different cosolvents, which may be attributed to the stronger capability of TEGDME to coordinate the surface deposition of Mg^{2+} ions at the interface that resulted in smaller overpotential of cycling and stronger resemblance to the standard cycling profiles of Li-Li symmetric cell. The results of XPS indicate that in cells with DME as cosolvent, poly-DOL component with $CH_2CH_2OCH_2O$ structure was formed. But when TEGDME is cosolvent, only CH_2CH_2O structure was present. The difference in reaction products may explain the very different cycling profiles when using two different cosolvents. We observed significantly decreased overpotentials of cells with pretreated Mg metal electrodes in $Mg(TFSI)_2$ in DME electrolyte. However, it is still too early to say if the enhancement was due to the ASEI or the cells were internally short-circuited, especially considering the cells still underwent large overpotential at the first several cycles which were the breaking down of priorly formed surface layers.

4.4.2 Future Work

The first and most important work in the future is to use SEM with the help of focused ion beam technique to examine the surface and cross-sections of pretreated Mg to collect the most direct evidence that an ASEI is formed and can be manipulated by changing the pretreatment conditions. Preferably, though technology-wise very difficult, an operando SEM imaging of the Mg-Mg electrochemical pretreatment would allow much deeper insights into this process. Secondly, EIS will be used in combination with electrochemical cycling to monitor and understand the change of surface composition after every certain

number of cycles. Most importantly, it can help to rule out the possibility of short-circuiting of the cells that may result in smaller and desirable overpotentials.

There are several plans on agenda for the future of this project. First, the pretreatment conditions of Mg metal electrodes, including the type of the salt, the concentration of the salt, the ratio of DOL to cosolvent, current density, hold time for charge and discharge processes and cycle numbers which dictate the overall amount of charge. These conditions are in parallel with the ones for Li metal anode protection, but they also differ in a few ways. First, the SEI formed on the surface of Mg metal strongly passivates it so regardless of what conditions are used, the resulted ASEI must be thin enough to allow the transport of Mg^{2+} ions. Therefore, a lower concentration of salt is more suitable. Second, DME will be used as cosolvent along with DOL in future work due to poly-DOL component can grow in it by electrochemical pretreatment. However, it has been reported that polyethylene oxide with CH_2CH_2O structure, which was possibly electrochemically formed in both cells with different cosolvent, has also been used as an ASEI for Li anode protection, so this product deserves attention as well.[204, 205] In addition to the further exploration in search of application in liquid Mg rechargeable batteries, this strategy can also be for fabricating pseudo-solid-state electrolyte for Mg batteries, which are still at the stage of proof-of-concept. By serving as a Mg^{2+} ion conducting interlayer, this ASEI can be the key to overcome the technical obstacles in front of Mg rechargeable batteries. In summary, Mg rechargeable batteries system is a promising beyond Li technology that is full of research opportunities and principles to investigate.

5. Summary and Prospect

5.1 Summary

The overall goal of this study is to electrochemically pretreat Li metal anodes and to form an elastomeric artificial solid electrolyte interphase layer that have good Li^+ ionic conductivity, can suppress the growth of dendrites and accommodate the drastic volume change of Li metal during electrochemical cycling. The electrochemically pretreated Li metal anodes can be applied to solid-state batteries with $Li_{10}GeP_2S_{12}$ as solid-state electrolyte to serve as a protective layer. The electrochemical pretreatment method itself is applied to Mg anodes to solve its passivation issue with conventional electrolytes.

The main goals of this dissertation are:

(1) Use electrochemical method to fabricate an ASEI serving as the protective layer on Li metal anodes.

(2) Study and understand the surface chemistry and electrochemical impact of this ASEI and provide further guidance on the optimization of the ASEI layer and Li-S batteries system

(3) Develop the electrochemical methodology and apply it to solid-state batteries and Mg batteries systems.

In the second chapter, the electrochemical pretreatment of Li metal anode using conventional electrolytes of Li-S batteries were systematically studied. We found that an elastomeric inorganic-organic composite layer mainly consists of poly-DOL is formed on

the surface of Li metal anodes. The properties of this elastomer can be tuned and optimized by controlling the current density and cycle number that controls the total cycle time and amount of charge. It is found that at 20 μA cm^{-2} current density and being cycled for 50 cycles in electrochemical pretreatment, it has the most poly-DOL rich structure which contributes to the suppression of Li dendrites, retainment of surface conformality and enhancement of specific capacity and rate capability. With this elastomer, the Li metal anodes demonstrate almost 100% Coulombic efficiency which is the result of greatly mitigated polysulfides shuttle reactions.

In the third chapter, a sulfide superionic conductor $Li_{10}GeP_2S_{12}$ is studied as solid-state electrolyte for solid-state Li-S batteries. We first optimized the fabrication method of LGPS from commercialized powder by using high temperature pressing at high pressure. This hot press method greatly densifies the LGPS pellets which enhances its inner contact and reduces interfacial impedance at the interface with Li metal that improve the overall ionic conductivity. By pressing at 150 °C and 300 MPa, the obtained LGPS pellets have a Li^+ ionic conductivity of 4.25×10^{-3} S cm^{-1}, which is almost half of the theoretical value. LGPS has a narrow electrochemical stability window and is prone to degradation reactions with Li metal. Therefore, we applied 20-nm LiPON to both sides of LGPS using atomic layer deposition method. This LiPON layer enables extended electrochemical stability window of LGPS and it shows great stability in cyclic voltammetry and galvanostatic charging and discharging testing. It proves to mitigate the interfacial degradation reactions which result in a less than twice increase in electrochemical impedance than unprotected bare LGPS which has over 1000 times of increase in impedance. We also proposed that the electrochemically pretreated Li metal anodes described in Chapter 2 would be another great

ASEI between Li and LGPS due to its malleable feature and capabilities to suppress the growth of Li dendrites and the volume change which is more severe in a solid-state system. In the fourth chapter, the electrochemical pretreatment of Mg metal anodes was explored. Mg metal suffers from an impermeable passivation layer that entirely blocks electrochemical activities and transport of Mg^{2+} ions. We strived to transfer the method used for Li metal anodes to Mg metal anodes with $Mg(TFSI)_2$ in DME/DOL. We first found that Mg^{2+} can catalyze the polymerization of DOL, so we changed the salt to LiTFSI in Mg-Mg symmetric cells to "activate" the stripping and plating of Mg while also studying the cosolvent effect by comparing DME and TEGDME. Our results show that depending on the cosolvent used, DME and TEGDME can render drastically different electrochemical cycling profiles and Mg^{2+} ions participate in the stripping and plating in both cosolvents which also happen beneath the ASEI grown by electrochemical pretreatment. Differing from the ASEI grown on the surface of Li metal anodes that have poly-DOL structure, this ASEI on Mg metal is more similar in structure to polyethylene oxide CH_2CH_2O. The pretreated Mg metal anodes were assembled in Mg-Mg symmetric cells with $Mg(TFSI)_2$ in DME electrolyte and it showed much smaller overpotential than cell with untreated pristine Mg metal anodes in electrochemical cycling. However, more testing and characterizations are needed to validate this result.

5.2 Prospect

In this dissertation, electrochemical pretreatment of Li metal anodes was systematically studied in surface chemistry and electrochemical performances. This is a feasible, practical and simple method for Li metal anode protection and can be tuned by controlling different parameters of formation of the ASEI. This allows us to curtail the properties of the ASEI

to meet the demands of different cell types and configurations. It can be applied to any battery system that utilizes Li metal as anode including high energy density Li-ion batteries and solid-state batteries beyond conventional Li-S batteries system. This method could be transferred to Mg metal anodes and potentially more metal electrodes which will be important future technologies in place of Li chemistry today for much broader applications and greater impact. Though promising results have been obtained, there is still much left to be uncovered and investigated, including the detailed structure and composition of SEI and its formation process and the correlation between surface chemistry and the electrochemical performance. In the future, the necessity and demand for energy storage devices with high power, high energy density, long lifespan and reliable safety will only grow, and insightful study and fine engineering of those energy storage devices will be key to hit these targets.

Appendices

The following figures depict the work published in Sahadeo, E.; Wang, Y.; Lin, C.-F.; Li, Y.; Rubloff, G.; Lee, S. B., Mg2+ ion-catalyzed polymerization of 1,3-dioxolane in battery electrolytes. *Chemical Communications* **2020** and beriefly discussed in Chapter 4.3.1, which is about the polymerization of 1,3-dioxolane (DOL) catalyzed by Mg^{2+}. All three figures were made by Dr. Sahadeo.

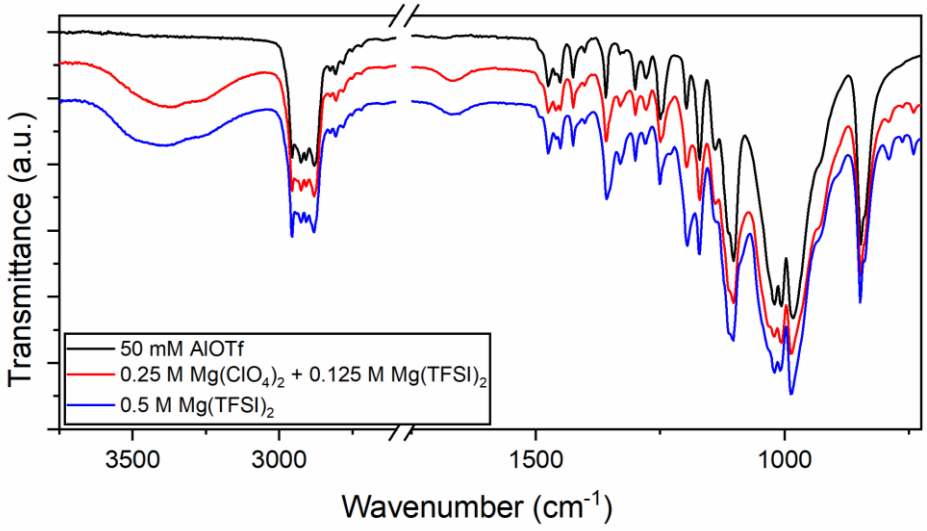

Appendix 1 FTIR spectrum of fully polymerized DOL with different amount of salt catalysts. Major C-H and C-O functional groups indicative of poly-DOL structure are visible around 2900 and 1000 cm^{-1}, respectively. The presence of the OH peak around 3400 cm^{-1} is apparent likely due to cleaning of the diamond window with ethanol and collecting the next spectra before it was dry, as all samples were air-exposed for similar times and the 50 mM AlOTf sample, collected first, does not show an -OH peak. The higher salt concentrations in the red and blue samples may also account for slightly more water.

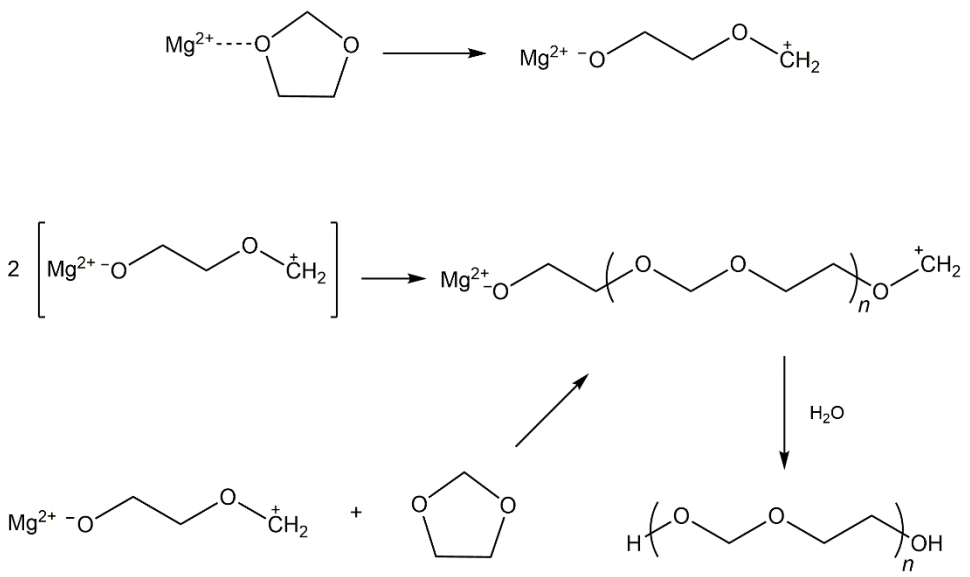

Appendix 3 Proposed reaction mechanism for Mg(TFSI)2 with DOL (TFSI- anions omitted for simplification).

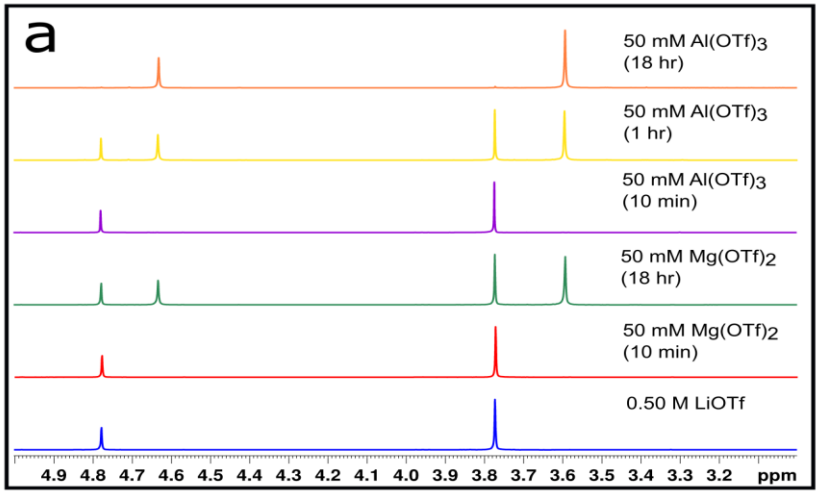

Appendix 2 H-NMR spectra of a) DOL samples with Al, Mg, and Li triflate salts after various reaction times.

Bibliography

1. Aurbach, D., Review of Selected Electrode-Solution Interactions Which Determine the Performance of Li and Li Ion Batteries. *J. Power Sources* **2000,** *89* (2), 206.
2. Johnson, R. W.; Hultqvist, A.; Bent, S. F., A Brief Review of Atomic Layer Deposition: From Fundamentals to Applications. *Mater. Today* **2014,** *17* (5), 236.
3. Kamaya, N.; Homma, K.; Yamakawa, Y.; Hirayama, M.; Kanno, R.; Yonemura, M.; Kamiyama, T.; Kato, Y.; Hama, S.; Kawamoto, K.; Mitsui, A., A lithium superionic conductor. *Nature Materials* **2011,** *10* (9), 682-686.
4. Rosenman, A.; Markevich, E.; Salitra, G.; Aurbach, D.; Garsuch, A.; Chesneau, F. F., Review on Li-Sulfur Battery Systems: an Integral Perspective. *Advanced Energy Materials* **2015,** *5* (16), 1500212-n/a.
5. Kozen, A. C.; Pearse, A. J.; Lin, C. F.; Noked, M.; Rubloff, G. W., Atomic Layer Deposition of the Solid Electrolyte LiPON. *Chem. Mater.* **2015,** *27* (15), 5324.
6. Lochala, J.; Liu, D.; Wu, B.; Robinson, C.; Xiao, J., Research Progress toward the Practical Applications of Lithium–Sulfur Batteries. *ACS Applied Materials & Interfaces* **2017,** *9* (29), 24407-24421.
7. Bruce, P. G.; Freunberger, S. A.; Hardwick, L. J.; Tarascon, J.-M., Li–O2 and Li–S batteries with high energy storage. *Nature Materials* **2011,** *11*, 19.
8. Xu, J.; Ma, J.; Fan, Q.; Guo, S.; Dou, S., Recent Progress in the Design of Advanced Cathode Materials and Battery Models for High-Performance Lithium-X (X = O2, S, Se, Te, I2, Br2) Batteries. *Advanced Materials* **2017,** *29* (28), 1606454-n/a.
9. Lin, D.; Liu, Y.; Cui, Y., Reviving the lithium metal anode for high-energy batteries. *Nature Nanotechnology* **2017,** *12*, 194.
10. Hamann, C.; Hamnett, A.; Vielstich, W., Galvanic Cells. In *Electrochemistry*, 2nd ed.; Wiley: 2007; p 550.
11. Huggins, R., Introductory Material. In *Advanced Batteries: Materials Science Aspects*, 1 ed.; Springer: 2009; p 474.
12. Nitta, N.; Wu, F.; Lee, J. T.; Yushin, G., Li-ion battery materials: present and future. *Materials Today* **2015,** *18* (5), 252-264.
13. Xu, W.; Wang, J.; Ding, F.; Chen, X.; Nasybulin, E.; Zhang, Y.; Zhang, J. G., Lithium Metal Anodes for Rechargeable Batteries. *Energy Environ. Sci.* **2014,** *7*, 513.
14. Kolosnitsyn, V. S.; Karaseva, E. V., Lithium-sulfur batteries: Problems and solutions. *Russian Journal of Electrochemistry* **2008,** *44* (5), 506-509.
15. Cao, R.; Xu, W.; Lv, D.; Xiao, J.; Zhang, J.-G., Anodes for Rechargeable Lithium-Sulfur Batteries. *Advanced Energy Materials* **2015,** *5* (16), 1402273-n/a.
16. Manthiram, A.; Fu, Y.; Chung, S.-H.; Zu, C.; Su, Y.-S., Rechargeable Lithium–Sulfur Batteries. *Chemical Reviews* **2014,** *114* (23), 11751-11787.
17. Verma, P.; Maire, P.; Novak, P., A Review of the Features and Analyses of the Solid Electrolyte Interphase in Li-Ion Batteries. *Electrochim. Acta* **2010,** *55* (22), 6332.
18. Wang, A.; Kadam, S.; Li, H.; Shi, S.; Qi, Y., Review on modeling of the anode solid electrolyte interphase (SEI) for lithium-ion batteries. *npj Computational Materials* **2018,** *4* (1), 15.

19. Li, L.; Wang, L.; Liu, R., Effect of Ether-Based and Carbonate-Based Electrolytes on the Electrochemical Performance of Li–S Batteries. *Arabian Journal for Science and Engineering* **2019,** *44* (7), 6361-6371.
20. Huang, F.; Gao, L.; Zou, Y.; Ma, G.; Zhang, J.; Xu, S.; Li, Z.; Liang, X., Akin solid–solid biphasic conversion of a Li–S battery achieved by coordinated carbonate electrolytes. *Journal of Materials Chemistry A* **2019,** *7* (20), 12498-12506.
21. Barghamadi, M.; Musameh, M.; Rüther, T.; Bhatt, A. I.; Hollenkamp, A. F.; Best, A. S., Electrolyte for Lithium–Sulfur Batteries. *Lithium–Sulfur Batteries* **2019**, 71-119.
22. Chu, H.; Noh, H.; Kim, Y.-J.; Yuk, S.; Lee, J.-H.; Lee, J.; Kwack, H.; Kim, Y.; Yang, D.-K.; Kim, H.-T., Achieving three-dimensional lithium sulfide growth in lithium-sulfur batteries using high-donor-number anions. *Nature Communications* **2019,** *10* (1), 188.
23. Raccichini, R.; Dibden, J. W.; Brew, A.; Owen, J. R.; García-Aráez, N., Ion Speciation and Transport Properties of LiTFSI in 1,3-Dioxolane Solutions: A Case Study for Li–S Battery Applications. *The Journal of Physical Chemistry B* **2018,** *122* (1), 267-274.
24. Mikhaylik, Y., Methods of charging lithium sulfur cells. Google Patents: 2006.
25. Zhang, S. S., Role of LiNO3 in rechargeable lithium/sulfur battery. *Electrochimica Acta* **2012,** *70* (Supplement C), 344-348.
26. Zhang, L.; Ling, M.; Feng, J.; Mai, L.; Liu, G.; Guo, J., The synergetic interaction between LiNO3 and lithium polysulfides for suppressing shuttle effect of lithium-sulfur batteries. *Energy Storage Materials* **2018,** *11*, 24-29.
27. Li, W.; Yao, H.; Yan, K.; Zheng, G.; Liang, Z.; Chiang, Y.-M.; Cui, Y., The synergetic effect of lithium polysulfide and lithium nitrate to prevent lithium dendrite growth. *Nature Communications* **2015,** *6*, 7436.
28. Liu, G.; Lu, W., A Model of Concurrent Lithium Dendrite Growth, SEI Growth, SEI Penetration and Regrowth. *Journal of The Electrochemical Society* **2017,** *164* (9), A1826-A1833.
29. Wang, Y.; Lin, C.-F.; Rao, J.; Gaskell, K.; Rubloff, G.; Lee, S. B., Electrochemically Controlled Solid Electrolyte Interphase Layers Enable Superior Li-S Batteries. *ACS applied materials & interfaces* **2018**.
30. Wang, Y.; Sahadeo, E.; Rubloff, G.; Lin, C.-F.; Lee, S. B., High-capacity lithium sulfur battery and beyond: a review of metal anode protection layers and perspective of solid-state electrolytes. *Journal of Materials Science* **2019,** *54* (5), 3671-3693.
31. Lee, J. T.; Eom, K.; Wu, F.; Kim, H.; Lee, D. C.; Zdyrko, B.; Yushin, G., Enhancing the Stability of Sulfur Cathodes in Li–S Cells via in Situ Formation of a Solid Electrolyte Layer. *ACS Energy Letters* **2016,** *1* (2), 373-379.
32. Guo, J.; Du, X.; Zhang, X.; Zhang, F.; Liu, J., Facile Formation of a Solid Electrolyte Interface as a Smart Blocking Layer for High-Stability Sulfur Cathode. *Advanced Materials* **2017,** *29* (26), 1700273-n/a.
33. Dharmasena, R.; Thapa, A. K.; Hona, R. K.; Jasinski, J.; Sunkara, M. K.; Sumanasekera, G. U., Mesoporous TiO2 coating on carbon–sulfur cathode for high capacity Li–sulfur battery. *RSC Advances* **2018,** *8* (21), 11622-11632.

34. Shin, W.; Lu, J.; Ji, X., ZnS coating of cathode facilitates lean-electrolyte Li-S batteries. *Carbon Energy* **2019,** *1* (2), 165-172.
35. Wu, F.; Thieme, S.; Ramanujapuram, A.; Zhao, E.; Weller, C.; Althues, H.; Kaskel, S.; Borodin, O.; Yushin, G., Toward in-situ protected sulfur cathodes by using lithium bromide and pre-charge. *Nano Energy* **2017,** *40* (Supplement C), 170-179.
36. Kwak, H. W.; Park, Y. J., Cathode coating using LiInO2-LiI composite for stable sulfide-based all-solid-state batteries. *Scientific Reports* **2019,** *9* (1), 8099.
37. Liu, J.; Qian, T.; Wang, M.; Liu, X.; Xu, N.; You, Y.; Yan, C., Molecularly Imprinted Polymer Enables High-Efficiency Recognition and Trapping Lithium Polysulfides for Stable Lithium Sulfur Battery. *Nano Letters* **2017,** *17* (8), 5064-5070.
38. Shaibani, M.; Hollenkamp, A. F.; Hill, M. R.; Majumder, M., Permselective membranes in lithium–sulfur batteries. *Current Opinion in Chemical Engineering* **2017,** *16* (Supplement C), 31-38.
39. Li, W.; Zhang, Q.; Zheng, G.; Seh, Z. W.; Yao, H.; Cui, Y., Understanding the Role of Different Conductive Polymers in Improving the Nanostructured Sulfur Cathode Performance. *Nano Lett.* **2013,** *13*, 5534.
40. Song, J.; Noh, H.; Lee, J.; Nah, I.-W.; Cho, W.-I.; Kim, H.-T., In situ coating of Poly(3,4-ethylenedioxythiophene) on sulfur cathode for high performance lithium–sulfur batteries. *Journal of Power Sources* **2016,** *332* (Supplement C), 72-78.
41. Kazazi, M.; Vaezi, M. R.; Kazemzadeh, A., Improving the self-discharge behavior of sulfur-polypyrrole cathode material by LiNO3 electrolyte additive. *Ionics* **2014,** *20* (9), 1291-1300.
42. Jin, J.; Wen, Z.; Ma, G.; Lu, Y.; Rui, K., Mesoporous carbon/sulfur composite with polyaniline coating for lithium sulfur batteries. *Solid State Ionics* **2014,** *262* (Supplement C), 170-173.
43. Song, Y.; Wang, H.; Ma, Q.; Li, D.; Wang, J.; Liu, G.; Yang, Y.; Dong, X.; Yu, W., 3D nitrogen-doped hierarchical porous carbon framework for protecting sulfur cathode in lithium–sulfur batteries. *New Journal of Chemistry* **2019,** *43* (24), 9641-9651.
44. Guo, Z.; Feng, X.; Li, X.; Zhang, X.; Peng, X.; Song, H.; Fu, J.; Ding, K.; Huang, X.; Gao, B., Nitrogen Doped Carbon Nanosheets Encapsulated in situ Generated Sulfur Enable High Capacity and Superior Rate Cathode for Li-S Batteries. *Frontiers in Chemistry* **2018,** *6*, 429.
45. Yang, C.-P.; Yin, Y.-X.; Ye, H.; Jiang, K.-C.; Zhang, J.; Guo, Y.-G., Insight into the Effect of Boron Doping on Sulfur/Carbon Cathode in Lithium–Sulfur Batteries. *ACS Applied Materials & Interfaces* **2014,** *6* (11), 8789-8795.
46. Xie, Y.; Meng, Z.; Cai, T.; Han, W.-Q., Effect of Boron-Doping on the Graphene Aerogel Used as Cathode for the Lithium–Sulfur Battery. *ACS Applied Materials & Interfaces* **2015,** *7* (45), 25202-25210.
47. Zhang, J.; You, C.; Wang, J.; Xu, H.; Zhu, C.; Guo, S.; Zhang, W.; Yang, R.; Xu, Y., Confinement of sulfur species into heteroatom-doped, porous carbon container for high areal capacity cathode. *Chemical Engineering Journal* **2019,** *368*, 340-349.
48. Ogoke, O.; Hwang, S.; Hultman, B.; Chen, M.; Karakalos, S.; He, Y.; Ramsey, A.; Su, D.; Alexandridis, P.; Wu, G., Large-diameter and heteroatom-doped graphene nanotubes decorated with transition metals as carbon hosts for lithium–sulfur batteries. *Journal of Materials Chemistry A* **2019,** *7* (21), 13389-13399.

49. Stoeckli, H. F., Microporous carbons and their characterization: The present state of the art. *Carbon* **1990,** *28* (1), 1-6.
50. Eftekhari, A.; Fan, Z., Ordered mesoporous carbon and its applications for electrochemical energy storage and conversion. *Materials Chemistry Frontiers* **2017,** *1* (6), 1001-1027.
51. Liang, C.; Li, Z.; Dai, S., Mesoporous Carbon Materials: Synthesis and Modification. *Angewandte Chemie International Edition* **2008,** *47* (20), 3696-3717.
52. Cheng, X.-B.; Huang, J.-Q.; Zhang, Q.; Peng, H.-J.; Zhao, M.-Q.; Wei, F., Aligned carbon nanotube/sulfur composite cathodes with high sulfur content for lithium–sulfur batteries. *Nano Energy* **2014,** *4*, 65-72.
53. Zeng, L.; Pan, F.; Li, W.; Jiang, Y.; Zhong, X.; Yu, Y., Free-standing porous carbon nanofibers–sulfur composite for flexible Li–S battery cathode. *Nanoscale* **2014,** *6* (16), 9579-9587.
54. Juhl, A. C.; Schneider, A.; Ufer, B.; Brezesinski, T.; Janek, J.; Fröba, M., Mesoporous hollow carbon spheres for lithium–sulfur batteries: distribution of sulfur and electrochemical performance. *Beilstein Journal of Nanotechnology* **2016,** *7*, 1229-1240.
55. Yu, M.; Wang, A.; Tian, F.; Song, H.; Wang, Y.; Li, C.; Hong, J.-D.; Shi, G., Dual-protection of a graphene-sulfur composite by a compact graphene skin and an atomic layer deposited oxide coating for a lithium-sulfur battery. *Nanoscale* **2015,** *7* (12), 5292-5298.
56. Karuppiah, S.; Kalimuthu, B.; Nazrulla, M. A.; Krishnamurty, S.; Nallathamby, K., An effective polysulfide trapping polar interlayer for high rate Li–S batteries. *Journal of Materials Chemistry A* **2019,** *7* (16), 10067-10076.
57. Zeng, P.; Chen, M.; Jiang, S.; Li, Y.; Xie, X.; Liu, H.; Hu, X.; Wu, C.; Shu, H.; Wang, X., Architecture and Performance of the Novel Sulfur Host Material Based on Ti2O3 Microspheres for Lithium–Sulfur Batteries. *ACS Applied Materials & Interfaces* **2019,** *11* (25), 22439-22448.
58. He, Y.; Qiao, Y.; Zhou, H., Recent advances in functional modification of separators in lithium–sulfur batteries. *Dalton Transactions* **2018,** *47* (20), 6881-6887.
59. Peng, Q.; Yu, F.; Wang, W.; Wang, A.; Wang, F.; Huang, Y., Ultralight polyethylenimine/porous carbon modified separator as an effective polysulfide-blocking barrier for lithium-sulfur battery. *Electrochimica Acta* **2019,** *299*, 749-755.
60. Cheng, X.-B.; Zhang, R.; Zhao, C.-Z.; Wei, F.; Zhang, J.-G.; Zhang, Q., A Review of Solid Electrolyte Interphases on Lithium Metal Anode. *Advanced Science* **2015,** *3* (3), 1500213.
61. Liu, Y.; Lin, D.; Liang, Z.; Zhao, J.; Yan, K.; Cui, Y., Lithium-coated polymeric matrix as a minimum volume-change and dendrite-free lithium metal anode. *Nature Communications* **2016,** *7*, 10992.
62. Yang, C.; Fu, K.; Zhang, Y.; Hitz, E.; Hu, L., Protected Lithium-Metal Anodes in Batteries: From Liquid to Solid. *Advanced Materials* **2017,** *29* (36), 1701169.
63. Tao, T.; Lu, S.; Fan, Y.; Lei, W.; Huang, S.; Chen, Y., Anode Improvement in Rechargeable Lithium–Sulfur Batteries. *Advanced Materials* **2017,** *29* (48), 1700542.
64. Lin, C.-F.; Qi, Y.; Gregorczyk, K.; Lee, S. B.; Rubloff, G. W., Nanoscale Protection Layers To Mitigate Degradation in High-Energy Electrochemical Energy Storage Systems. *Accounts of Chemical Research* **2018,** *51* (1), 97-106.

65. Wu, M.; Wen, Z.; Jin, J.; Chowdari, B. V. R., Trimethylsilyl Chloride-Modified Li Anode for Enhanced Performance of Li–S Cells. *ACS Applied Materials & Interfaces* **2016,** *8* (25), 16386-16395.
66. Zu, C.; Azimi, N.; Zhang, Z.; Manthiram, A., Insight into lithium-metal anodes in lithium-sulfur batteries with a fluorinated ether electrolyte. *Journal of Materials Chemistry A* **2015,** *3* (28), 14864-14870.
67. Qian, J.; Henderson, W. A.; Xu, W.; Bhattacharya, P.; Engelhard, M.; Borodin, O.; Zhang, J.-G., High rate and stable cycling of lithium metal anode. *Nature Communications* **2015,** *6*, 6362.
68. Park, M. S.; Ma, S. B.; Lee, D. J.; Im, D.; Doo, S.-G.; Yamamoto, O., A Highly Reversible Lithium Metal Anode. *Scientific Reports* **2014,** *4*, 3815.
69. Zhao, C.-Z.; Cheng, X.-B.; Zhang, R.; Peng, H.-J.; Huang, J.-Q.; Ran, R.; Huang, Z.-H.; Wei, F.; Zhang, Q., Li2S5-based ternary-salt electrolyte for robust lithium metal anode. *Energy Storage Materials* **2016,** *3*, 77-84.
70. Zhang, P.; Zhu, J.; Wang, M.; Imanishi, N.; Yamamoto, O., Lithium dendrite suppression and cycling efficiency of lithium anode. *Electrochemistry Communications* **2018,** *87*, 27-30.
71. Peng, Z.; Zhao, N.; Zhang, Z.; Wan, H.; Lin, H.; Liu, M.; Shen, C.; He, H.; Guo, X.; Zhang, J.-G.; Wang, D., Stabilizing Li/electrolyte interface with a transplantable protective layer based on nanoscale LiF domains. *Nano Energy* **2017,** *39*, 662-672.
72. Li, N. W.; Yin, Y. X.; Yang, C. P.; Guo, Y. G., An Artificial Solid Electrolyte Interphase Layer for Stable Lithium Metal Anodes. *Advanced Materials* **2015,** *28* (9), 1853-1858.
73. Liu, Q. C.; Xu, J. J.; Yuan, S.; Chang, Z. W.; Xu, D.; Yin, Y. B.; Li, L.; Zhong, H. X.; Jiang, Y. S.; Yan, J. M.; Zhang, X. B., Artificial Protection Film on Lithium Metal Anode toward Long-Cycle-Life Lithium–Oxygen Batteries. *Advanced Materials* **2015,** *27* (35), 5241-5247.
74. Adams, B. D.; Carino, E. V.; Connell, J. G.; Han, K. S.; Cao, R.; Chen, J.; Zheng, J.; Li, Q.; Mueller, K. T.; Henderson, W. A.; Zhang, J.-G., Long term stability of Li-S batteries using high concentration lithium nitrate electrolytes. *Nano Energy* **2017,** *40*, 607-617.
75. Liu, Y.; Cui, Y., Lithium Metal Anodes: A Recipe for Protection. *Joule 1* (4), 649-650.
76. Zheng, J.; Yan, P.; Mei, D.; Engelhard, M. H.; Cartmell, S. S.; Polzin, B. J.; Wang, C.; Zhang, J.-G.; Xu, W., Highly Stable Operation of Lithium Metal Batteries Enabled by the Formation of a Transient High-Concentration Electrolyte Layer. *Advanced Energy Materials* **2016,** *6* (8), 1502151-n/a.
77. Busche, M. R.; Drossel, T.; Leichtweiss, T.; Weber, D. A.; Falk, M.; Schneider, M.; Reich, M.-L.; Sommer, H.; Adelhelm, P.; Janek, J., Dynamic formation of a solid-liquid electrolyte interphase and its consequences for hybrid-battery concepts. *Nature Chemistry* **2016,** *8*, 426.
78. Li, N. W.; Yin, Y. X.; Li, J. Y.; Zhang, C. H.; Guo, Y. G., Passivation of Lithium Metal Anode via Hybrid Ionic Liquid Electrolyte toward Stable Li Plating/Stripping. *Advanced Science* **2016,** *4* (2), 1600400.

79. Huang, C.; Xiao, J.; Shao, Y.; Zheng, J.; Bennett, W. D.; Lu, D.; Laxmikant, S. V.; Engelhard, M.; Ji, L.; Zhang, J., Manipulating Surface Reactions in Lithium–Sulphur Batteries Using Hybrid Anode Structures. *Nat. Commun.* **2014,** *5*, 3015.
80. Choudhury, S.; Tu, Z.; Stalin, S.; Vu, D.; Fawole, K.; Gunceler, D.; Sundararaman, R.; Archer Lynden, A., Electroless Formation of Hybrid Lithium Anodes for Fast Interfacial Ion Transport. *Angewandte Chemie International Edition* **2017,** *56* (42), 13070-13077.
81. Manthiram, A.; Yu, X.; Wang, S., Lithium battery chemistries enabled by solid-state electrolytes. *Nature Reviews Materials* **2017,** *2*, 16103.
82. Hassoun, J.; Scrosati, B., Moving to a Solid-State Configuration: A Valid Approach to Making Lithium-Sulfur Batteries Viable for Practical Applications. *Advanced Materials* **2010,** *22* (45), 5198-5201.
83. Monroe, C.; Newman, J., The Impact of Elastic Deformation on Deposition Kinetics at Lithium/Polymer Interfaces. *Journal of The Electrochemical Society* **2005,** *152* (2), A396-A404.
84. Wang, Q.; Jin, J.; Wu, X.; Ma, G.; Yang, J.; Wen, Z., A shuttle effect free lithium sulfur battery based on a hybrid electrolyte. *Physical Chemistry Chemical Physics* **2014,** *16* (39), 21225-21229.
85. Yu, X.; Bi, Z.; Zhao, F.; Manthiram, A., Polysulfide-Shuttle Control in Lithium-Sulfur Batteries with a Chemically/Electrochemically Compatible NaSICON-Type Solid Electrolyte. *Advanced Energy Materials* **2016,** *6* (24), 1601392-n/a.
86. Fu, K.; Gong, Y.; Liu, B.; Zhu, Y.; Xu, S.; Yao, Y.; Luo, W.; Wang, C.; Lacey, S. D.; Dai, J.; Chen, Y.; Mo, Y.; Wachsman, E.; Hu, L., Toward garnet electrolyte–based Li metal batteries: An ultrathin, highly effective, artificial solid-state electrolyte/metallic Li interface. *Science Advances* **2017,** *3* (4).
87. Choudhury, S.; Mangal, R.; Agrawal, A.; Archer, L. A., A highly reversible room-temperature lithium metal battery based on crosslinked hairy nanoparticles. *Nature Communications* **2015,** *6*, 10101.
88. Zhao-Karger, Z.; Zhao, X.; Wang, D.; Diemant, T.; Behm, R. J.; Fichtner, M., Performance Improvement of Magnesium Sulfur Batteries with Modified Non-Nucleophilic Electrolytes. *Advanced Energy Materials* **2015,** *5* (3), 1401155.
89. Aurbach, D.; Suresh, G. S.; Levi, E.; Mitelman, A.; Mizrahi, O.; Chusid, O.; Brunelli, M., Progress in Rechargeable Magnesium Battery Technology. *Advanced Materials* **2007,** *19* (23), 4260-4267.
90. Canepa, P.; Sai Gautam, G.; Hannah, D. C.; Malik, R.; Liu, M.; Gallagher, K. G.; Persson, K. A.; Ceder, G., Odyssey of Multivalent Cathode Materials: Open Questions and Future Challenges. *Chemical Reviews* **2017,** *117* (5), 4287-4341.
91. Song, J.; Sahadeo, E.; Noked, M.; Lee, S. B., Mapping the Challenges of Magnesium Battery. *The Journal of Physical Chemistry Letters* **2016,** *7* (9), 1736-1749.
92. Muldoon, J.; Bucur, C. B.; Oliver, A. G.; Sugimoto, T.; Matsui, M.; Kim, H. S.; Allred, G. D.; Zajicek, J.; Kotani, Y., Electrolyte roadblocks to a magnesium rechargeable battery. *Energy & Environmental Science* **2012,** *5* (3), 5941-5950.
93. Yoo, H. D.; Shterenberg, I.; Gofer, Y.; Gershinsky, G.; Pour, N.; Aurbach, D., Mg rechargeable batteries: an on-going challenge. *Energy & Environmental Science* **2013,** *6* (8), 2265-2279.

94. Zhao, H.; Deng, N.; Yan, J.; Kang, W.; Ju, J.; Ruan, Y.; Wang, X.; Zhuang, X.; Li, Q.; Cheng, B., A review on anode for lithium-sulfur batteries: Progress and prospects. *Chemical Engineering Journal* **2018,** *347*, 343-365.
95. Chen, L.; Connell, J. G.; Nie, A.; Huang, Z.; Zavadil, K. R.; Klavetter, K. C.; Yuan, Y.; Sharifi-Asl, S.; Shahbazian-Yassar, R.; Libera, J. A.; Mane, A. U.; Elam, J. W., Lithium metal protected by atomic layer deposition metal oxide for high performance anodes. *Journal of Materials Chemistry A* **2017,** *5* (24), 12297-12309.
96. Wang, L.; Zhang, L.; Wang, Q.; Li, W.; Wu, B.; Jia, W.; Wang, Y.; Li, J.; Li, H., Long lifespan lithium metal anodes enabled by Al2O3 sputter coating. *Energy Storage Materials* **2018,** *10*, 16-23.
97. Kozen, A. C.; Lin, C. F.; Pearse, A. J.; Schroeder, M. A.; Han, X. G.; Hu, L. B.; Lee, S. B.; Rubloff, G. W.; Noked, M., Next-Generation Lithium Metal Anode Engineering via Atomic Layer Deposition. *ACS Nano* **2015,** *9* (6), 5884.
98. Cresce, A. v.; Russell, S. M.; Baker, D. R.; Gaskell, K. J.; Xu, K., In Situ and Quantitative Characterization of Solid Electrolyte Interphases. *Nano Letters* **2014,** *14* (3), 1405-1412.
99. Lin, D.; Liu, Y.; Chen, W.; Zhou, G.; Liu, K.; Dunn, B.; Cui, Y., Conformal Lithium Fluoride Protection Layer on Three-Dimensional Lithium by Nonhazardous Gaseous Reagent Freon. *Nano Letters* **2017,** *17* (6), 3731-3737.
100. Qian, J.; Xu, W.; Bhattacharya, P.; Engelhard, M.; Henderson, W. A.; Zhang, Y.; Zhang, J.-G., Dendrite-free Li deposition using trace-amounts of water as an electrolyte additive. *Nano Energy* **2015,** *15*, 135-144.
101. Kanamura, K.; Shiraishi, S.; Takehara, Z. i., Electrochemical Deposition of Very Smooth Lithium Using Nonaqueous Electrolytes Containing HF. *Journal of The Electrochemical Society* **1996,** *143* (7), 2187-2197.
102. Pang, Q.; Liang, X.; Shyamsunder, A.; Nazar, L. F., An In Vivo Formed Solid Electrolyte Surface Layer Enables Stable Plating of Li Metal. *Joule* **2017,** *1* (4), 871-886.
103. Lu, Y.; Gu, S.; Hong, X.; Rui, K.; Huang, X.; Jin, J.; Chen, C.; Yang, J.; Wen, Z., Pre-modified Li3PS4 based interphase for lithium anode towards high-performance Li-S battery. *Energy Storage Materials* **2018,** *11*, 16-23.
104. Li, N.-W.; Yin, Y.-X.; Yang, C.-P.; Guo, Y.-G., An Artificial Solid Electrolyte Interphase Layer for Stable Lithium Metal Anodes. *Advanced Materials* **2015,** *28* (9), 1853-1858.
105. Wang, L.; Wang, Q.; Jia, W.; Chen, S.; Gao, P.; Li, J., Li metal coated with amorphous Li3PO4 via magnetron sputtering for stable and long-cycle life lithium metal batteries. *Journal of Power Sources* **2017,** *342*, 175-182.
106. Ma, G.; Wen, Z.; Wu, M.; Shen, C.; Wang, Q.; Jin, J.; Wu, X., A lithium anode protection guided highly-stable lithium-sulfur battery. *Chemical Communications* **2014,** *50* (91), 14209-14212.
107. Umeda, G. A.; Menke, E.; Richard, M.; Stamm, K. L.; Wudl, F.; Dunn, B., Protection of lithium metal surfaces using tetraethoxysilane. *Journal of Materials Chemistry* **2011,** *21* (5), 1593-1599.
108. Cha, E.; Patel, M. D.; Park, J.; Hwang, J.; Prasad, V.; Cho, K.; Choi, W., 2D MoS2 as an efficient protective layer for lithium metal anodes in high-performance Li–S batteries. *Nature Nanotechnology* **2018,** *13* (4), 337-344.

109. Liu, S.; Li, G.-R.; Gao, X.-P., Lanthanum Nitrate As Electrolyte Additive To Stabilize the Surface Morphology of Lithium Anode for Lithium–Sulfur Battery. *ACS Applied Materials & Interfaces* **2016,** *8* (12), 7783-7789.
110. Yan, J.; Yu, J.; Ding, B., Mixed Ionic and Electronic Conductor for Li-Metal Anode Protection. *Advanced Materials* **2018,** *30* (7), 1705105.
111. Wei, S.; Choudhury, S.; Tu, Z.; Zhang, K.; Archer, L. A., Electrochemical Interphases for High-Energy Storage Using Reactive Metal Anodes. *Accounts of Chemical Research* **2018,** *51* (1), 80-88.
112. Lee, Y.-G.; Ryu, S.; Sugimoto, T.; Yu, T.; Chang, W.-s.; Yang, Y.; Jung, C.; Woo, J.; Kang, S. G.; Han, H. N.; Doo, S.-G.; Hwang, Y.; Chang, H.; Lee, J.-M.; Sun, J.-Y., Dendrite-Free Lithium Deposition for Lithium Metal Anodes with Interconnected Microsphere Protection. *Chemistry of Materials* **2017,** *29* (14), 5906-5914.
113. Zhu, B.; Jin, Y.; Hu, X.; Zheng, Q.; Zhang, S.; Wang, Q.; Zhu, J., Poly(dimethylsiloxane) Thin Film as a Stable Interfacial Layer for High-Performance Lithium-Metal Battery Anodes. *Advanced Materials* **2016,** *29* (2), 1603755.
114. Ma, G. Q.; Wen, Z. Y.; Wang, Q. S.; Shen, C.; Jin, J.; Wu, X. W., Enhanced Cycle Performance of a Li–S Battery Based on a Protected Lithium Anode. *J. Mater. Chem. A* **2014,** *2*, 19355.
115. Luo, J.; Fang, C.-C.; Wu, N.-L., High Polarity Poly(vinylidene difluoride) Thin Coating for Dendrite-Free and High-Performance Lithium Metal Anodes. *Advanced Energy Materials* **2017,** *8* (2), 1701482.
116. Li, N.-W.; Shi, Y.; Yin, Y.-X.; Zeng, X.-X.; Li, J.-Y.; Li, C.-J.; Wan, L.-J.; Wen, R.; Guo, Y.-G., A Flexible Solid Electrolyte Interphase Layer for Long-Life Lithium Metal Anodes. *Angewandte Chemie International Edition* **2017,** *57* (6), 1505-1509.
117. Zheng, G.; Wang, C.; Pei, A.; Lopez, J.; Shi, F.; Chen, Z.; Sendek, A. D.; Lee, H.-W.; Lu, Z.; Schneider, H.; Safont-Sempere, M. M.; Chu, S.; Bao, Z.; Cui, Y., High-Performance Lithium Metal Negative Electrode with a Soft and Flowable Polymer Coating. *ACS Energy Letters* **2016,** *1* (6), 1247-1255.
118. Liu, K.; Pei, A.; Lee, H. R.; Kong, B.; Liu, N.; Lin, D.; Liu, Y.; Liu, C.; Hsu, P.-c.; Bao, Z.; Cui, Y., Lithium Metal Anodes with an Adaptive "Solid-Liquid" Interfacial Protective Layer. *Journal of the American Chemical Society* **2017,** *139* (13), 4815-4820.
119. Kozen, A. C.; Lin, C.-F.; Zhao, O.; Lee, S. B.; Rubloff, G. W.; Noked, M., Stabilization of Lithium Metal Anodes by Hybrid Artificial Solid Electrolyte Interphase. *Chemistry of Materials* **2017,** *29* (15), 6298-6307.
120. Lee, H.; Lee, D. J.; Kim, Y.-J.; Park, J.-K.; Kim, H.-T., A simple composite protective layer coating that enhances the cycling stability of lithium metal batteries. *Journal of Power Sources* **2015,** *284*, 103-108.
121. Zhao, Y.; Goncharova Lyudmila, V.; Sun, Q.; Li, X.; Lushington, A.; Wang, B.; Li, R.; Dai, F.; Cai, M.; Sun, X., Robust Metallic Lithium Anode Protection by the Molecular-Layer-Deposition Technique. *Small Methods* **2018,** *2* (5), 1700417.
122. Liu, Y.; Lin, D.; Yuen Pak, Y.; Liu, K.; Xie, J.; Dauskardt Reinhold, H.; Cui, Y., An Artificial Solid Electrolyte Interphase with High Li-Ion Conductivity, Mechanical

Strength, and Flexibility for Stable Lithium Metal Anodes. *Advanced Materials* **2016,** *29* (10), 1605531.
123. Liu, W.; Li, W.; Zhuo, D.; Zheng, G.; Lu, Z.; Liu, K.; Cui, Y., Core–Shell Nanoparticle Coating as an Interfacial Layer for Dendrite-Free Lithium Metal Anodes. *ACS Central Science* **2017,** *3* (2), 135-140.
124. Yan, K.; Lee, H.-W.; Gao, T.; Zheng, G.; Yao, H.; Wang, H.; Lu, Z.; Zhou, Y.; Liang, Z.; Liu, Z.; Chu, S.; Cui, Y., Ultrathin Two-Dimensional Atomic Crystals as Stable Interfacial Layer for Improvement of Lithium Metal Anode. *Nano Letters* **2014,** *14* (10), 6016-6022.
125. Xu, R.; Zhang, X.-Q.; Cheng, X.-B.; Peng, H.-J.; Zhao, C.-Z.; Yan, C.; Huang, J.-Q., Artificial Soft–Rigid Protective Layer for Dendrite-Free Lithium Metal Anode. *Advanced Functional Materials* **2018,** *28* (8), 1705838.
126. Han, Y.; Duan, X.; Li, Y.; Huang, L.; Zhu, D.; Chen, Y., Improved cycling performances with high sulfur loading enabled by pre-treating lithium anode. *Ionics* **2016,** *22* (2), 151-157.
127. Gu, Y.; Wang, W.-W.; Li, Y.-J.; Wu, Q.-H.; Tang, S.; Yan, J.-W.; Zheng, M.-S.; Wu, D.-Y.; Fan, C.-H.; Hu, W.-Q.; Chen, Z.-B.; Fang, Y.; Zhang, Q.-H.; Dong, Q.-F.; Mao, B.-W., Designable ultra-smooth ultra-thin solid-electrolyte interphases of three alkali metal anodes. *Nature Communications* **2018,** *9* (1), 1339.
128. Ma, L.; Kim, M. S.; Archer, L. A., Stable Artificial Solid Electrolyte Interphases for Lithium Batteries. *Chemistry of Materials* **2017,** *29* (10), 4181-4189.
129. Cheng, X.-B.; Yan, C.; Chen, X.; Guan, C.; Huang, J.-Q.; Peng, H.-J.; Zhang, R.; Yang, S.-T.; Zhang, Q., Implantable Solid Electrolyte Interphase in Lithium-Metal Batteries. *Chem* **2017,** *2* (2), 258-270.
130. Aurbach, D.; Pollak, E.; Elazari, R.; Salitra, G.; Kelley, C. S.; Affinito, J., On the Surface Chemical Aspects of Very High Energy Density, Rechargeable Li-Sulfur Batteries. *J. Electrochem. Soc.* **2009,** *156* (8), A694.
131. Wood, K. N.; Kazyak, E.; Chadwick, A. F.; Chen, K. H.; Zhang, J. G.; Thornton, K.; Dasgupta, N. P., Dendrites and Pits: Untangling the Complex Behavior of Lithium Metal Anodes Through Operando Video Microscopy. *ACS Cent. Sci.* **2016,** *2* (11), 790.
132. Kong, L.; Xing, Y.; Pecht, M. G., In-Situ Observations of Lithium Dendrite Growth. *IEEE Access* **2018,** *6*, 8387-8393.
133. Frenck, L.; Sethi, G. K.; Maslyn, J. A.; Balsara, N. P., Factors That Control the Formation of Dendrites and Other Morphologies on Lithium Metal Anodes. *Frontiers in Energy Research* **2019,** *7*, 115.
134. Zainuddin; Albinska, J.; Ulański, P.; Rosiak, J. M., Radiation-induced degradation and crosslinking of poly(ethylene oxide) in solid state. *Journal of Radioanalytical and Nuclear Chemistry* **2002,** *253* (3), 339-344.
135. Emami Shahriar, H.; Salovey, R.; Hogen-Esch Thieo, E., Peroxide-mediated crosslinking of poly(ethylene oxide). *Journal of Polymer Science Part A: Polymer Chemistry* **2002,** *40* (17), 3021-3026.
136. Dampier, F. W.; Brummer, S. B., The cycling behavior of the lithium electrode in LiAsF6/methyl acetate solutions. *Electrochimica Acta* **1977,** *22* (12), 1339-1345.
137. Guan, X.; Wang, A.; Liu, S.; Li, G.; Liang, F.; Yang, Y.-W.; Liu, X.; Luo, J., Controlling Nucleation in Lithium Metal Anodes. *Small* **2018,** *14* (37), 1801423.

138. Suo, L.; Hu, Y. S.; Li, H.; Armand, M.; Chen, L., A New Class of Solvent-in-Salt Electrolyte for High-Energy Rechargeable Metallic Lithium Batteries. *Nat. Commun.* **2013,** *4*, 1481.
139. Qu, C.; Chen, Y.; Yang, X.; Zhang, H.; Li, X.; Zhang, H., LiNO3-free electrolyte for Li-S battery: A solvent of choice with low Ksp of polysulfide and low dendrite of lithium. *Nano Energy* **2017,** *39*, 262-272.
140. Huang, F.; Ma, G.; Wen, Z.; Jin, J.; Xu, S.; Zhang, J., Enhancing metallic lithium battery performance by tuning the electrolyte solution structure. *Journal of Materials Chemistry A* **2018,** *6* (4), 1612-1620.
141. Hu, J. J.; Long, G. K.; Liu, S.; Li, G. R.; Gao, X. P., A LiFSI–LiTFSI Binary-Salt Electrolyte to Achieve High Capacity and Cycle Stability for a Li–S Battery. *Chem. Commun.* **2014,** *50*, 14647.
142. Zheng, J.; Ji, G.; Fan, X.; Chen, J.; Li, Q.; Wang, H.; Yang, Y.; DeMella, K. C.; Raghavan, S. R.; Wang, C., High-Fluorinated Electrolytes for Li–S Batteries. *Advanced Energy Materials* **2019,** *9* (16), 1803774.
143. Meisner, Q. J.; Rojas, T.; Dietz Rago, N. L.; Cao, J.; Bareño, J.; Glossmann, T.; Hintennach, A.; Redfern, P. C.; Pahls, D.; Zhang, L.; Bloom, I. D.; Ngo, A. T.; Curtiss, L. A.; Zhang, Z., Lithium–sulfur battery with partially fluorinated ether electrolytes: Interplay between capacity, coulombic efficiency and Li anode protection. *Journal of Power Sources* **2019,** *438*, 226939.
144. Drvarič Talian, S.; Jeschke, S.; Vizintin, A.; Pirnat, K.; Arčon, I.; Aquilanti, G.; Johansson, P.; Dominko, R., Fluorinated Ether Based Electrolyte for High-Energy Lithium–Sulfur Batteries: Li+ Solvation Role Behind Reduced Polysulfide Solubility. *Chemistry of Materials* **2017,** *29* (23), 10037-10044.
145. Li, R.; Sun, X.; Zou, J.; He, Q., Lithium fluoride as an efficient additive for improved electrochemical performance of Li-S batteries. *Colloids and Surfaces A: Physicochemical and Engineering Aspects* **2020**, 124737.
146. Zhu, Y.; He, X.; Mo, Y., Origin of Outstanding Stability in the Lithium Solid Electrolyte Materials: Insights from Thermodynamic Analyses Based on First-Principles Calculations. *ACS Applied Materials & Interfaces* **2015,** *7* (42), 23685-23693.
147. Zhao, C.-Z.; Zhao, B.-C.; Yan, C.; Zhang, X.-Q.; Huang, J.-Q.; Mo, Y.; Xu, X.; Li, H.; Zhang, Q., Liquid phase therapy to solid electrolyte–electrode interface in solid-state Li metal batteries: A review. *Energy Storage Materials* **2020,** *24*, 75-84.
148. Hayashi, A.; Ohtomo, T.; Mizuno, F.; Tadanaga, K.; Tatsumisago, M., All-solid-state Li/S batteries with highly conductive glass–ceramic electrolytes. *Electrochemistry Communications* **2003,** *5* (8), 701-705.
149. Yang, X.; Luo, J.; Sun, X., Towards high-performance solid-state Li–S batteries: from fundamental understanding to engineering design. *Chemical Society Reviews* **2020,** *49* (7), 2140-2195.
150. Han, F.; Westover, A. S.; Yue, J.; Fan, X.; Wang, F.; Chi, M.; Leonard, D. N.; Dudney, N. J.; Wang, H.; Wang, C., High electronic conductivity as the origin of lithium dendrite formation within solid electrolytes. *Nature Energy* **2019,** *4* (3), 187-196.
151. Mo, Y.; Ong, S. P.; Ceder, G., First Principles Study of the Li10GeP2S12 Lithium Super Ionic Conductor Material. *Chemistry of Materials* **2012,** *24* (1), 15-17.
152. Han, F.; Gao, T.; Zhu, Y.; Gaskell, K. J.; Wang, C., A Battery Made from a Single Material. *Advanced Materials* **2015,** *27* (23), 3473-3483.

153. Cao, Y.; Zuo, P.; Lou, S.; Sun, Z.; Li, Q.; Huo, H.; Ma, Y.; Du, C.; Gao, Y.; Yin, G., A quasi-solid-state Li–S battery with high energy density, superior stability and safety. *Journal of Materials Chemistry A* **2019,** *7* (11), 6533-6542.
154. Philip, M. A.; Sullivan, P. T.; Zhang, R.; Wooley, G. A.; Kohn, S. A.; Gewirth, A. A., Improving Cell Resistance and Cycle Life with Solvate-Coated Thiophosphate Solid Electrolytes in Lithium Batteries. *ACS Applied Materials & Interfaces* **2019,** *11* (2), 2014-2021.
155. Choi, S.-J.; Lee, S.-H.; Ha, Y.-C.; Yu, J.-H.; Doh, C.-H.; Lee, Y.; Park, J.-W.; Lee, S.-M.; Shin, H.-C., Synthesis and Electrochemical Characterization of a Glass-Ceramic Li7P2S8I Solid Electrolyte for All-Solid-State Li-Ion Batteries. *Journal of The Electrochemical Society* **2018,** *165* (5), A957-A962.
156. Park, K. H.; Bai, Q.; Kim, D. H.; Oh, D. Y.; Zhu, Y.; Mo, Y.; Jung, Y. S., Design Strategies, Practical Considerations, and New Solution Processes of Sulfide Solid Electrolytes for All-Solid-State Batteries. *Advanced Energy Materials* **2018,** *8* (18), 1800035.
157. Jung, Y. S.; Oh, D. Y.; Nam, Y. J.; Park, K. H., Issues and Challenges for Bulk-Type All-Solid-State Rechargeable Lithium Batteries using Sulfide Solid Electrolytes. *Israel Journal of Chemistry* **2015,** *55* (5), 472-485.
158. Kim, K.; Park, J.; Jeong, G.; Yu, J.-S.; Kim, Y.-C.; Park, M.-S.; Cho, W.; Kanno, R., Rational Design of a Composite Electrode to Realize a High-Performance All-Solid-State Battery. *ChemSusChem* **2019,** *12* (12), 2637-2643.
159. Lau, J.; DeBlock, R. H.; Butts, D. M.; Ashby, D. S.; Choi, C. S.; Dunn, B. S., Sulfide Solid Electrolytes for Lithium Battery Applications. *Advanced Energy Materials* **2018,** *8* (27), 1800933.
160. Fitzhugh, W.; Wu, F.; Ye, L.; Su, H.; Li, X., Strain-Stabilized Ceramic-Sulfide Electrolytes. *Small* **2019,** *15* (33), 1901470.
161. Fei, Y.; Song, S.; Wu, F.; Yan, Z.; Yuan, D.; Fu, C.; Shi, J.; Zhang, X.; Xiang, Y., Effects of Sintering Temperatures on the Crystallinity and Electrochemical Properties of the Li10GeP2S12 via Solid-State Sintering Method. *IOP Conference Series: Materials Science and Engineering* **2018,** *394*, 022038.
162. Davaasuren, B.; Tietz, F., Impact of sintering temperature on phase formation, microstructure, crystallinity and ionic conductivity of Li1.5Al0.5Ti1.5(PO4)3. *Solid State Ionics* **2019,** *338*, 144-152.
163. Xue, W.; Yang, Y.; Yang, Q.; Liu, Y.; Wang, L.; Chen, C.; Cheng, R., The effect of sintering process on lithium ionic conductivity of Li6.4Al0.2La3Zr2O12 garnet produced by solid-state synthesis. *RSC Advances* **2018,** *8* (24), 13083-13088.
164. Seino, Y.; Ota, T.; Takada, K.; Hayashi, A.; Tatsumisago, M., A sulphide lithium super ion conductor is superior to liquid ion conductors for use in rechargeable batteries. *Energy & Environmental Science* **2014,** *7* (2), 627-631.
165. Awotunde, M. A.; Adegbenjo, A. O.; Obadele, B. A.; Okoro, M.; Shongwe, B. M.; Olubambi, P. A., Influence of sintering methods on the mechanical properties of aluminium nanocomposites reinforced with carbonaceous compounds: A review. *Journal of Materials Research and Technology* **2019,** *8* (2), 2432-2449.
166. Pham, V. T.; Bui, H. T.; Tran, B. T.; Nguyen, V. T.; Le, D. Q.; Than, X. T.; Nguyen, V. C.; Doan, D. P.; Phan, N. M., The effect of sintering temperature on the mechanical properties of a Cu/CNT nanocomposite prepared via a powder metallurgy

method. *Advances in Natural Sciences: Nanoscience and Nanotechnology* **2011,** *2* (1), 015006.
167. Bron, P.; Roling, B.; Dehnen, S., Impedance characterization reveals mixed conducting interphases between sulfidic superionic conductors and lithium metal electrodes. *Journal of Power Sources* **2017,** *352*, 127-134.
168. Chen, B.; Ju, J.; Ma, J.; Zhang, J.; Xiao, R.; Cui, G.; Chen, L., An insight into intrinsic interfacial properties between Li metals and Li10GeP2S12 solid electrolytes. *Physical Chemistry Chemical Physics* **2017,** *19* (46), 31436-31442.
169. Wenzel, S.; Randau, S.; Leichtweiß, T.; Weber, D. A.; Sann, J.; Zeier, W. G.; Janek, J., Direct Observation of the Interfacial Instability of the Fast Ionic Conductor Li10GeP2S12 at the Lithium Metal Anode. *Chemistry of Materials* **2016,** *28* (7), 2400-2407.
170. Sang, L.; Haasch, R. T.; Gewirth, A. A.; Nuzzo, R. G., Evolution at the Solid Electrolyte/Gold Electrode Interface during Lithium Deposition and Stripping. *Chemistry of Materials* **2017,** *29* (7), 3029-3037.
171. Zhang, W.; Richter, F. H.; Culver, S. P.; Leichtweiss, T.; Lozano, J. G.; Dietrich, C.; Bruce, P. G.; Zeier, W. G.; Janek, J., Degradation Mechanisms at the Li10GeP2S12/LiCoO2 Cathode Interface in an All-Solid-State Lithium-Ion Battery. *ACS Applied Materials & Interfaces* **2018,** *10* (26), 22226-22236.
172. Li, X.; Ren, Z.; Norouzi Banis, M.; Deng, S.; Zhao, Y.; Sun, Q.; Wang, C.; Yang, X.; Li, W.; Liang, J.; Li, X.; Sun, Y.; Adair, K.; Li, R.; Hu, Y.; Sham, T.-K.; Huang, H.; Zhang, L.; Lu, S.; Luo, J.; Sun, X., Unravelling the Chemistry and Microstructure Evolution of a Cathodic Interface in Sulfide-Based All-Solid-State Li-Ion Batteries. *ACS Energy Letters* **2019,** *4* (10), 2480-2488.
173. Zhang, Z.; Chen, S.; Yang, J.; Wang, J.; Yao, L.; Yao, X.; Cui, P.; Xu, X., Interface Re-Engineering of Li10GeP2S12 Electrolyte and Lithium anode for All-Solid-State Lithium Batteries with Ultralong Cycle Life. *ACS Applied Materials & Interfaces* **2018,** *10* (3), 2556-2565.
174. Zhang, H.; Li, X.; Hao, S.; Zhang, X.; Lin, J., Inducing interfacial progress based on a new sulfide-based composite electrolyte for all-solid-state lithium batteries. *Electrochimica Acta* **2019,** *325*, 134943.
175. Yoon, K.; Kim, J.-J.; Seong, W. M.; Lee, M. H.; Kang, K., Investigation on the interface between Li10GeP2S12 electrolyte and carbon conductive agents in all-solid-state lithium battery. *Scientific Reports* **2018,** *8* (1), 8066.
176. Gao, Y.; Wang, D.; Li, Y. C.; Yu, Z.; Mallouk, T. E.; Wang, D., Salt-Based Organic–Inorganic Nanocomposites: Towards A Stable Lithium Metal/Li10GeP2S12 Solid Electrolyte Interface. *Angewandte Chemie International Edition* **2018,** *57* (41), 13608-13612.
177. Wang, C.; Adair, K. R.; Liang, J.; Li, X.; Sun, Y.; Li, X.; Wang, J.; Sun, Q.; Zhao, F.; Lin, X.; Li, R.; Huang, H.; Zhang, L.; Yang, R.; Lu, S.; Sun, X., Solid-State Plastic Crystal Electrolytes: Effective Protection Interlayers for Sulfide-Based All-Solid-State Lithium Metal Batteries. *Advanced Functional Materials* **2019,** *29* (26), 1900392.
178. Dewald, G. F.; Ohno, S.; Kraft, M. A.; Koerver, R.; Till, P.; Vargas-Barbosa, N. M.; Janek, J.; Zeier, W. G., Experimental Assessment of the Practical Oxidative Stability of Lithium Thiophosphate Solid Electrolytes. *Chemistry of Materials* **2019,** *31* (20), 8328-8337.

179. Emslie, D. J. H.; Chadha, P.; Price, J. S., Metal ALD and pulsed CVD: Fundamental reactions and links with solution chemistry. *Coordination Chemistry Reviews* **2013,** *257* (23), 3282-3296.
180. Puurunen, R. L., Surface chemistry of atomic layer deposition: A case study for the trimethylaluminum/water process. *Journal of Applied Physics* **2005,** *97* (12), 121301.
181. Nisula, M.; Shindo, Y.; Koga, H.; Karppinen, M., Atomic Layer Deposition of Lithium Phosphorus Oxynitride. *Chemistry of Materials* **2015,** *27* (20), 6987-6993.
182. Pearse, A. J.; Schmitt, T. E.; Fuller, E. J.; El-Gabaly, F.; Lin, C.-F.; Gerasopoulos, K.; Kozen, A. C.; Talin, A. A.; Rubloff, G.; Gregorczyk, K. E., Nanoscale Solid State Batteries Enabled by Thermal Atomic Layer Deposition of a Lithium Polyphosphazene Solid State Electrolyte. *Chemistry of Materials* **2017,** *29* (8), 3740-3753.
183. Irvine, J. T. S.; Sinclair, D. C.; West, A. R., Electroceramics: Characterization by Impedance Spectroscopy. *Advanced Materials* **1990,** *2* (3), 132-138.
184. Sahu, G.; Lin, Z.; Li, J.; Liu, Z.; Dudney, N.; Liang, C., Air-stable, high-conduction solid electrolytes of arsenic-substituted Li4SnS4. *Energy & Environmental Science* **2014,** *7* (3), 1053-1058.
185. Ohtomo, T.; Hayashi, A.; Tatsumisago, M.; Kawamoto, K., Glass Electrolytes with High Ion Conductivity and High Chemical Stability in the System LiI-Li₂O-Li₂S-P₂S₅. *Electrochemistry* **2013,** *81* (6), 428-431.
186. Gao, T.; Hou, S.; Huynh, K.; Wang, F.; Eidson, N.; Fan, X.; Han, F.; Luo, C.; Mao, M.; Li, X.; Wang, C., Existence of Solid Electrolyte Interphase in Mg Batteries: Mg/S Chemistry as an Example. *ACS Applied Materials & Interfaces* **2018,** *10* (17), 14767-14776.
187. Lu, Z.; Schechter, A.; Moshkovich, M.; Aurbach, D., On the electrochemical behavior of magnesium electrodes in polar aprotic electrolyte solutions. *Journal of Electroanalytical Chemistry* **1999,** *466* (2), 203-217.
188. Arthur, T. S.; Glans, P.-A.; Singh, N.; Tutusaus, O.; Nie, K.; Liu, Y.-S.; Mizuno, F.; Guo, J.; Alsem, D. H.; Salmon, N. J.; Mohtadi, R., Interfacial Insight from Operando XAS/TEM for Magnesium Metal Deposition with Borohydride Electrolytes. *Chemistry of Materials* **2017,** *29* (17), 7183-7188.
189. Ha, S.-Y.; Lee, Y.-W.; Woo, S. W.; Koo, B.; Kim, J.-S.; Cho, J.; Lee, K. T.; Choi, N.-S., Magnesium(II) Bis(trifluoromethane sulfonyl) Imide-Based Electrolytes with Wide Electrochemical Windows for Rechargeable Magnesium Batteries. *ACS Applied Materials & Interfaces* **2014,** *6* (6), 4063-4073.
190. Shterenberg, I.; Salama, M.; Yoo, H. D.; Gofer, Y.; Park, J.-B.; Sun, Y.-K.; Aurbach, D., Evaluation of (CF3SO2)2N−(TFSI) Based Electrolyte Solutions for Mg Batteries. *Journal of The Electrochemical Society* **2015,** *162* (13), A7118-A7128.
191. Yoo, H. D.; Han, S.-D.; Bolotin, I. L.; Nolis, G. M.; Bayliss, R. D.; Burrell, A. K.; Vaughey, J. T.; Cabana, J., Degradation Mechanisms of Magnesium Metal Anodes in Electrolytes Based on (CF3SO2)2N– at High Current Densities. *Langmuir* **2017,** *33* (37), 9398-9406.
192. Wetzel, D. J.; Malone, M. A.; Haasch, R. T.; Meng, Y.; Vieker, H.; Hahn, N. T.; Gölzhäuser, A.; Zuo, J.-M.; Zavadil, K. R.; Gewirth, A. A.; Nuzzo, R. G., Passivation Dynamics in the Anisotropic Deposition and Stripping of Bulk Magnesium

Electrodes During Electrochemical Cycling. *ACS Applied Materials & Interfaces* **2015,** *7* (33), 18406-18414.
193. Ding, M. S.; Diemant, T.; Behm, R. J.; Passerini, S.; Giffin, G. A., Dendrite Growth in Mg Metal Cells Containing Mg(TFSI)2/Glyme Electrolytes. *Journal of The Electrochemical Society* **2018,** *165* (10), A1983-A1990.
194. Kuwata, H.; Matsui, M.; Imanishi, N., Passivation Layer Formation of Magnesium Metal Negative Electrodes for Rechargeable Magnesium Batteries. *Journal of The Electrochemical Society* **2017,** *164* (13), A3229-A3236.
195. Gao, T.; Noked, M.; Pearse, A. J.; Gillette, E.; Fan, X.; Zhu, Y.; Luo, C.; Suo, L.; Schroeder, M. A.; Xu, K.; Lee, S. B.; Rubloff, G. W.; Wang, C., Enhancing the Reversibility of Mg/S Battery Chemistry through Li+ Mediation. *Journal of the American Chemical Society* **2015,** *137* (38), 12388-12393.
196. Wang, P.; Buchmeiser, M. R., Rechargeable Magnesium–Sulfur Battery Technology: State of the Art and Key Challenges. *Advanced Functional Materials* **2019,** *29* (49), 1905248.
197. Zhao-Karger, Z.; Fichtner, M., Beyond Intercalation Chemistry for Rechargeable Mg Batteries: A Short Review and Perspective. *Frontiers in Chemistry* **2019,** *6*, 656.
198. Vinayan, B. P.; Euchner, H.; Zhao-Karger, Z.; Cambaz, M. A.; Li, Z.; Diemant, T.; Behm, R. J.; Gross, A.; Fichtner, M., Insights into the electrochemical processes of rechargeable magnesium–sulfur batteries with a new cathode design. *Journal of Materials Chemistry A* **2019,** *7* (44), 25490-25502.
199. Li, X.; Gao, T.; Han, F.; Ma, Z.; Fan, X.; Hou, S.; Eidson, N.; Li, W.; Wang, C., Reducing Mg Anode Overpotential via Ion Conductive Surface Layer Formation by Iodine Additive. *Advanced Energy Materials* **2018,** *8* (7), 1701728.
200. Son, S.-B.; Gao, T.; Harvey, S. P.; Steirer, K. X.; Stokes, A.; Norman, A.; Wang, C.; Cresce, A.; Xu, K.; Ban, C., An artificial interphase enables reversible magnesium chemistry in carbonate electrolytes. *Nature Chemistry* **2018,** *10* (5), 532-539.
201. Sahadeo, E.; Wang, Y.; Lin, C.-F.; Li, Y.; Rubloff, G.; Lee, S. B., Mg2+ ion-catalyzed polymerization of 1,3-dioxolane in battery electrolytes. *Chemical Communications* **2020**.
202. Yang, H.; Yin, L.; Shi, H.; He, K.; Cheng, H.-M.; Li, F., Suppressing lithium dendrite formation by slowing its desolvation kinetics. *Chemical Communications* **2019,** *55* (88), 13211-13214.
203. Briggs, D.; Brewis, D. M.; Dahm, R. H.; Fletcher, I. W., Analysis of the surface chemistry of oxidized polyethylene: comparison of XPS and ToF-SIMS. *Surface and Interface Analysis* **2003,** *35* (2), 156-167.
204. Assegie, A. A.; Cheng, J.-H.; Kuo, L.-M.; Su, W.-N.; Hwang, B.-J., Polyethylene oxide film coating enhances lithium cycling efficiency of an anode-free lithium-metal battery. *Nanoscale* **2018,** *10* (13), 6125-6138.
205. Zhang, C.; Lan, Q.; Liu, Y.; Wu, J.; Shao, H.; Zhan, H.; Yang, Y., A dual-layered artificial solid electrolyte interphase formed by controlled electrochemical reduction of LiTFSI/DME-LiNO3 for dendrite-free lithium metal anode. *Electrochimica Acta* **2019,** *306*, 407-419.